ELECTROMAGNETIC ANALYSIS OF STATOR GROUND FAULTS IN SYNCHRONOUS GENERATORS

A Dissertation

by

KHALED ALI MOHAMMED ALI AL JAAFARI

Submitted to the Office of Graduate and Professional Studies of
Texas A&M University
in partial fulfillment of the requirements for the degree of

DOCTOR OF PHILOSOPHY

Chair of Committee,	Hamid Toliyat
Committee Members,	Mehrdad Ehsani
	Shankar P. Bhattacharyya
	Alan Palazzolo
Head of Department,	Miroslav Begovic

August 2016

Major Subject: Electrical Engineering

ABSTRACT

There are many stator ground faults protection schemes available in the industry. These schemes relatively perform well in detecting the faults in the stator winding. The protection of the neutral point vicinity is the challenge because of the low voltage induced in that area. The 100% stator protection concept has been around for a long time. However, these schemes sometimes have limitations. The fact that stator ground fault detection in generators depends on many factors like the generator design, the generator loading, and the equivalent capacitance of the generator's windings and the apparatus connected to it, occasionally caused these schemes to fail to detect the winding faults near the neutral or to miss-operate during normal system disturbance. In this dissertation, an electromagnetic analysis of the synchronous generators stator winding ground faults is presented. A mathematical model for the synchronous generator under stator winding fault is being derived. In addition, a study is conducted using 2D FEA simulation and verified using experimental testing on the third harmonic ratio under-voltage protection scheme. Another study focuses on finding a unique signature for the stator ground fault using wavelet transform. This analysis is an attempt to understand this phenomenon from the machine design point of view by looking at the generator terminal and neutral voltages. The analysis presented in this dissertation shows that the protection schemes perform positively in detecting stator ground fault. However, it does not show reliable performance under system disturbances. On the other hand, the wavelet method shows better performance and it reflects robustness against these disturbances.

DEDICATION

To my father, mother, wife, brother and sister. Without whom none of my success would be possible.

ACKNOWLEDGEMENTS

I would like to thank all the committee members for their help and support. Also, I would like to express my special appreciation to the chair of my committee, Professor Hamid Toliyat, for his continuous assistance and advice.

Thanks also go to my friends and colleagues and the department faculty and staff for making my time at Texas A&M University a great experience Finally, thanks to my wife for her encouragement, patience and love.

TABLE OF CONTENTS

Page

LIST OF FIGURES

LIST OF TABLES

Page

1. INTRODUCTION AND LITERATURE REVIEW

1.1 Introduction

The purpose of this literature review is fourfold. First, synchronous generators will be briefly discussed, with an emphasis on the principles as well as physical characteristics of these machines. Second, types of faults in synchronous generators originating from ground faults will be evaluated. Third, methods of protecting against ground faults in various components of synchronous generators (in particular, the windings and stator) will be discussed. Fourth, a meta-analysis of statistical data pertaining to ground faults will be presented. A brief conclusion will summarize the findings of the literature review.

The protection of generators from internal ground faults, as well as from damage originating from other points of fault, is an important concern in the engineering literature [1]. Many faults as well as protection mechanisms have been described [2]. Recently, particular attention has been paid to hybrid grounding approaches as a promising means of reducing ground fault damage to synchronous generators [3]. Because of the promise of hybrid approaches [4], they will receive particular attention in the literature review, but other protective approaches will be considered as well.

Finally, several independent works regarding protective relaying for power generation systems and the advantages and disadvantages of third-harmonic schemes will be examined in-depth. These articles explain just how these schemes work, as well as their

technical limitations. By analyzing these articles, it is possible to understand, with greater precision, the applications of some of these systems.

1.2 Brief overview of synchronous generators

A synchronous generator takes its name from the relationship between mechanical rotational speed and the electrical frequency produced [5]. The relevant formula is as follows:

$$fe = \frac{p}{120}\, n_m \tag{1.1}$$

Where:

f_e = supply frequency, Hz

n_m = rotor speed of the machine

p = number of poles

The equation can be rewritten as:

$$n_m = \frac{(120) f_e}{p} \tag{1.2}$$

In a synchronous generator with a given number of poles, the relationship between f_e and n_m is perfectly linear.

A synchronous generator is thus a machine in which mechanical input is used to generate electrical output based on the formula presented above. A synchronous machine can also function as a motor if electrical input is converted to mechanical output [6]. In either case, the machine is synchronous if it obeys the formula presented above.

There are numerous components in a synchronous generator [7]. Figure 1.1 below depicts a two-pole synchronous generator with common components.

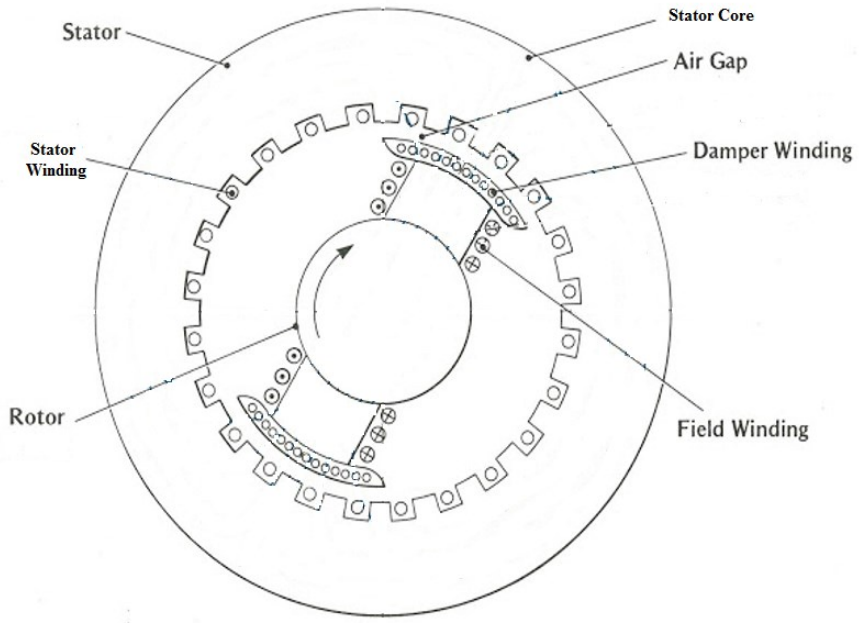

Figure 1.1. Components of a 2-pole synchronous generator.

This depiction of a synchronous generator is particularly useful in envisioning some of the ground fault damage and component-specific protection scenarios discussed later in the literature review.

Figure 1.2 shows that synchronous generators became much more widespread in the middle of the 20th century. As a result, the amount of power generated from them increased almost exponentially during this period as the following graph will help to demonstrate. Today, nearly all power is generated via synchronous generators.

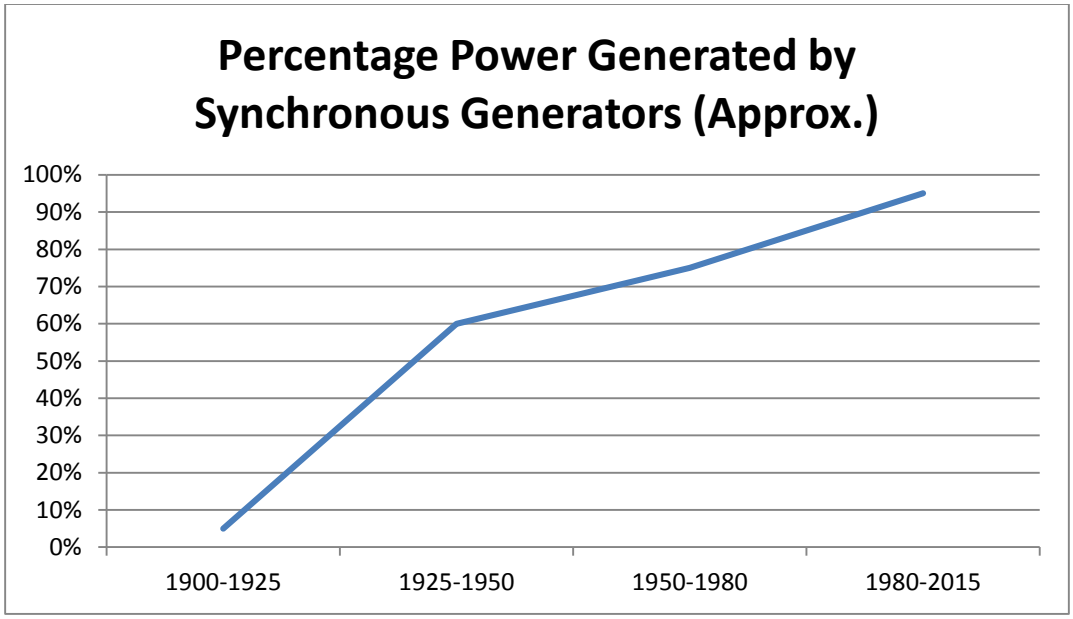

Figure 1.2. Percentage power generated by synchronous generators

One feature of synchronous generators is that they can operate in parallel, which is why they are often found in interconnected power systems [8, 9]. This feature of synchronous generators is particularly important when considering grounding faults that can affect interlinked systems [10]. However, when they operate as stand-alone units, synchronous generators remain vulnerable to ground faults in numerous ways [11].

Having provided a brief overview of synchronous generators, it remains to consult the literature on (a) ground faults and (b) means of protecting the components of synchronous machines from ground faults.

1.3 Overview of grounding faults and issues

Grounding is capable of causing anywhere from mild to irreparable damage to synchronous generators [12]. In order to understand how these damages can occur, it is necessary to provide a systematic overview of both the phenomenon of grounding and of the specific approaches to grounding. There is some conceptual overlap between discussing grounding approaches and examining means of protecting synchronous generators from grounding flaws, the topic of the third section of the literature review. However, while some means of protecting synchronous generators can be inferred from the second section of the literature review, the third section will contain a more focused discussion of issues related to generator design.

1.3.1 Ground faults

A ground fault occurs when, rather than traveling across its intended path, electricity travels to the ground [13]. There are various faults that can arise from the way in which a system is grounded or ungrounded.

1.3.2 Low-resistance grounding

A low-resistance grounded system is one in which resistors keep the ground fault current within a limit, often in the range of 200-600 A [14]. When the ground fault current

is low, total fault damage is limited. Such an approach is oftentimes utilized when working with common bus-connected generators [15]. Fault current magnitudes can be kept high enough for relaying with feeders and also bus-tie breakers but low enough to keep over-voltages and associated damages limited [16]. The low-resistance grounded approach also allows other sources to be added into the system with much added complexity or cost. Low-resistance grounding approaches not only reduce damage at the point of system fault but also reduce the destructive power of stray currents and reduce heat-related and mechanical stress on equipment [17].

Low-resistance grounded systems can have disadvantages that can result in flaws. One problem is that, if there are multiple sources, the total ground fault current becomes higher, which in turn creates the potential for more damage if the sources are not appropriately managed (as with the use of the right kinds of surge arresters) [18]. If, for example, each generator in a 4-generator system has a maximum ground fault current of 500 A, then the maximum fault current is actually 2,000 A [19].

Another, more specific problem that can arise in low-resistance grounded systems is the burning out of generator stator iron laminations in the presence of ground fault currents of sufficient magnitude [20]. Once there is a ground fault inside a generator's stator winding, the generator will persist in feeding the ground fault until the field excitation of the generator dwindles [21]. In such a scenario, the generator will become substantially damaged. Additionally, when there are variations in fault current, there can be coordination problems within the system [22].

1.3.3 Single-point grounding

Single-point grounding involves the grounding of only one source. Such an approach does not require only one generator in the system. Existence of a single ground source is a natural limit on ground fault current which will be much higher in scenarios of multiple point grounding. Single-point grounding eases the process of relay coordination by reducing ground current variation. Regardless of how many generators there are, single-point grounding can draw upon neutral isolators to connect only one resistor to the system at a given time [23]. This approach to single-point grounding has its own disadvantages. The use of isolator switches can add complexity to the system, and transferring can also be difficult [24].

Another approach to single-point grounding is to connect neutrals to each other, meaning that there is a single return path for the ground fault [25]. In this approach, complexity arises when third harmonic currents have to be circulated through the neutrals [26]. Because connection of the neutrals raises their potential, regardless of whether a generator is connected or otherwise, safety issues can arise. The use of an artificial neutral can alleviate these concerns [27]. However, some general limitations and risks of single-point grounding remain. Perhaps the main disadvantage of single-point grounding is the vulnerability of the system to the single grounded power source.

1.3.4 Multiple-point grounding

Multiple-point grounding is often utilized in conjunction with low-resistance grounding. In multiple-point grounding, the neutral terminals of transformers and generators alike are grounded separately through resistors. In this scenario, control can be exercised over the ground fault current associated with each source [28]. Combined with low-resistance grounding, a multiple-point ground is a viable means of ensuring that a system remains perpetually grounded, which in turn means the elimination of an important safety hazard [29].

However, multiple-point grounding also presents several challenges. One challenge of multiple-point grounding is that choosing resistors can be complicated, another challenge involves the stator winding of the generator. If the point of fault is within the stator winding, a fault current continuing uninterrupted can lead to substantial damages in the windings of the stator [30].

1.3.5 High-impedance grounded system

In a high-impedance grounded system, the neutral terminal of the generator is connected to the ground through an impedance. In such a system, there is much lower current at the point of fault than in other systems [31]. High-impedance systems also allow for operational continuity [32]. However, to achieve these benefits, a high-impedance grounded system must be able to detect ground faults at a high level of sensitivity. High-

impedance grounded systems can also be unsuited to an environment with many generators.

1.3.6 Hybrid approach

In a hybrid system, high- and low-impedance systems are merged. This system is particularly relevant in light of damage to a generator as the point of fault because it is based on deploying low resistance for external ground faults and deploying a high-impedance grounded system in case the point of fault is the generator [33].

If a ground fault takes place within the generator's stator winding, then the hybrid system could limit the ground fault current until isolating the generator from the supply. At this point, the generator would shut down while the ground fault would be limited to a very low level such as 10 A. As the generator remains in a high-impedance state, any damage to the generator's stator windings is reduced [34].

A best practice in hybrid design would be to configure the system so that maximum ground fault current never exceeds the magnitude of 400A or thereabouts even if there are many generators connected to the system. In doing so, the system's ground fault current would be reduced.

1.4 Methods of protection

There are numerous ways in which stators and the larger systems in which they inhere can be protected against ground faults. Some of the major methods will be discussed here.

In conventional fault protection, an overvoltage relay detects faults and protects between 90 and 95% of the stator winding [32]. The bottom 5 to 10% of the stator winding is not protected by the conventional method of stator ground fault protection [35]. This method has the clear disadvantage of not being able to protect the entire stator winding. Conventional fault protection depends on the combination of the following components [36]:

- Percentage phase differential protection (device 87)
- Ground differential protection (device 87GN)
- Ground time-overcurrent protection (device 51G)
- Instantaneous ground overcurrent protection (device 50G)
- Wye-broken-delta ground overvoltage protection (device 59G)
- Stator winding zero-sequence neutral overvoltage protection (device 59GN)

The output voltage of generators is not perfectly sinusoidal. Harmonic components distort the output voltage. The third harmonic voltage is greater than other stages in the triple harmonic, leading to certain regularities. For example, when ground faults occur at points that are close to neutral, the third harmonic voltage at the terminal point is the total of the third harmonic generator yield [35]. On the other hand, when a ground fault unfolds

at or near the terminal point in the generator, the third harmonic voltage at the neutral point equals the sum of the third harmonic voltage produced by the generator [35]. Knowledge about the third harmonic voltage can be used to protect against ground faults.

The third harmonic neutral under voltage approach involves detection of the absence of third harmonic voltage at the neutral of the generator, which in turn suggests that there is a ground fault close to the neutral. For this approach to work fully, however, the 59G relay must pick up [37].

In the book "Protective Relaying for Power Control Systems," by Donald Reimert, the concept of these third-harmonic schemes are examined in depth [38]. According to him, harmonic voltage is divided between the neutral end and the terminal end shunt impedances according to the zero-sequence network. One of the keys here is that, at some point during the stator winding, third-harmonic voltage is equal to zero. The generator harmonics model is used to approximate the value of the voltage harmonics at the neutral and at the generator terminals. Most of the available 100% stator protection schemes are working based on that approximation. The author in [38] explains the split capacitance model of the generator stator windings (shown in Figure 1.3). Where C_s represents the stator winding capacitance, which is the largest element of the system capacitance. C_t represents all the shunt capacitance at the generator terminals including the capacitance of the primary windings of the connected transformer. Splitting the impedances causes the voltage harmonics to split between the terminals and the neutral (Figure 1.3). When the ground faults happen close to neutral, the capacitive impedance close to the neutral and the neutral impedance Z_g are shorted, the 3rd harmonic voltage in the same area will

reduce. Therefore, all voltage harmonics will appear at the terminals. In contrast, when the ground faults occur close to terminal, the capacitive impedance close to the terminal is shorted and the 3rd harmonic voltage in the same area will reduce. Therefore, all voltage harmonics will appear at the neutral. In summary, the change in the harmonics ratio between the neutral and the terminals is the base where the relay senses the fault.

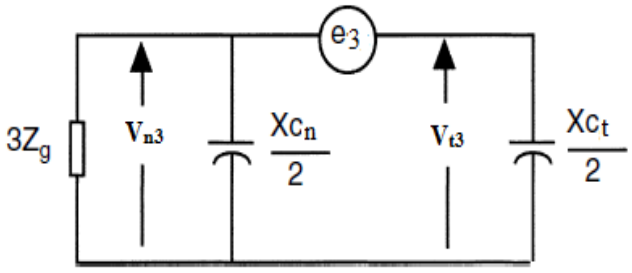

Figure 1.3. Split capacitance model of synchronous generator.

The article [38] also stresses the importance of third-harmonic voltage created by the generator and the operations presented by the book necessitate the use of these voltages. The article finds that, across all load levels and operation modes, about 1 percent, as a minimum, of third-harmonic voltage is produced by the protected machine. However, the third-harmonic voltage produced is tied directly to the design of the generator itself, meaning that these values have the potential to vary greatly, usually between 1 and 10 percent.

Another key method of protective relaying is the voltage ratio scheme. Essentially, this voltage ratio scheme involves the division of the third-harmonic voltage produced by the generator between the terminals. Furthermore, the impedances of the zero-sequence

circuit, in theory, alleviates that ratio of third-harmonic terminal voltage allowing it to maintain neutral voltage during normal operation.

The key benefit of this particular voltage ratio scheme is that it allows the detection of ground faults at the neutral, as well as at the terminal end of the stator winding. To accomplish this, a 60 Hz 59GN overvoltage relay is utilized, providing fault detection near the null points in the stator winding.

Finally, the neutral injection scheme is another key method of providing 100 percent ground fault protection. However, one difficulty with this method is that the individual designs of the neutral injection scheme tend to vary between manufacturers. The basics, however, are that an AC voltage signal is applied at the neutral using an injection transformer along with the grounding transformer. The signal, which is encoded, creates a 15 Hz current which is monitored by an overcurrent element at the secondary of the injection transformer. If a stator ground fault manages to make it through the winding capacitance, the current will be increased, tripping the device. In some references this method is called the sub-harmonic injection method and is based on the early detection of stator ground faults through the use of an injection module that generates a square wave pulse of 20 Hz (and a magnitude of +/- 26V) straight into the stator winding [40, 41]. As the injection module tracks the magnitude and the frequency of the signal that it generates, it can determine whether a ground fault has occurred in the stator winding and take advantage of a critical-fail relay.

1.5 Meta-analysis of literature

The meta-analysis of the literature was carried out in studies of stator winding faults from the engineering literature. The inclusion criteria for the meta-analysis were as follows (Note: Original graphic based on meta-analysis of literature.):

- Publication date: 2000-2015.
- Source: Peer-reviewed journal or accredited industry publication.
- Content: Stator fault descriptions, system fault descriptions, cost of failure data.
- Total cost data, meaning costs that take business causes into account.

1.5.1 Costs of failure

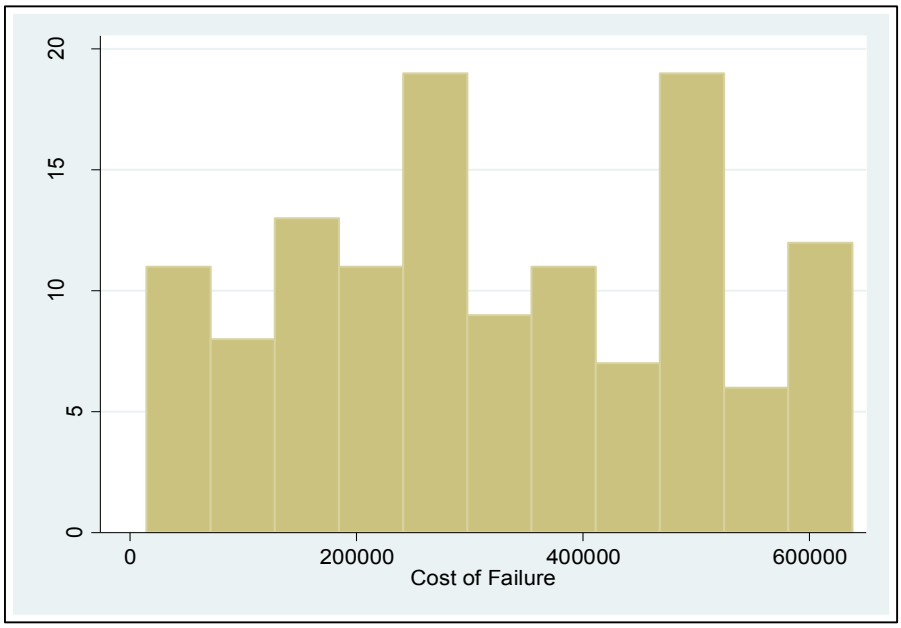

Figure 1.4. Cost of system failure associated with stator failure.

Figure 1.4 shows the mean cost of a stator failure that was associated with a system failure was $326,470.5 (SD = $176,479). Figures 1.5 and 1.6 indicate that the failure costs of Roebel bar stator types was highest, followed by the failure costs of hybrid stator types. In addition, single-point and low-resistance systems had the highest associated costs.

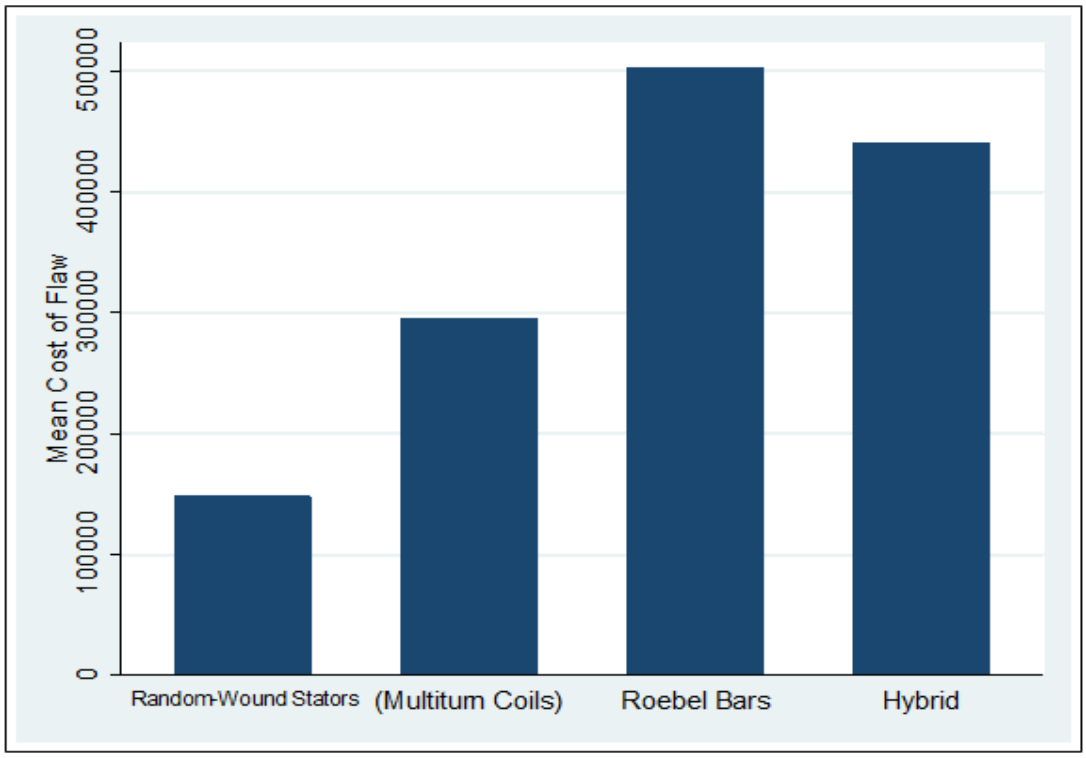

Figure 1.5. Cost of system failure associated with specific stator types.

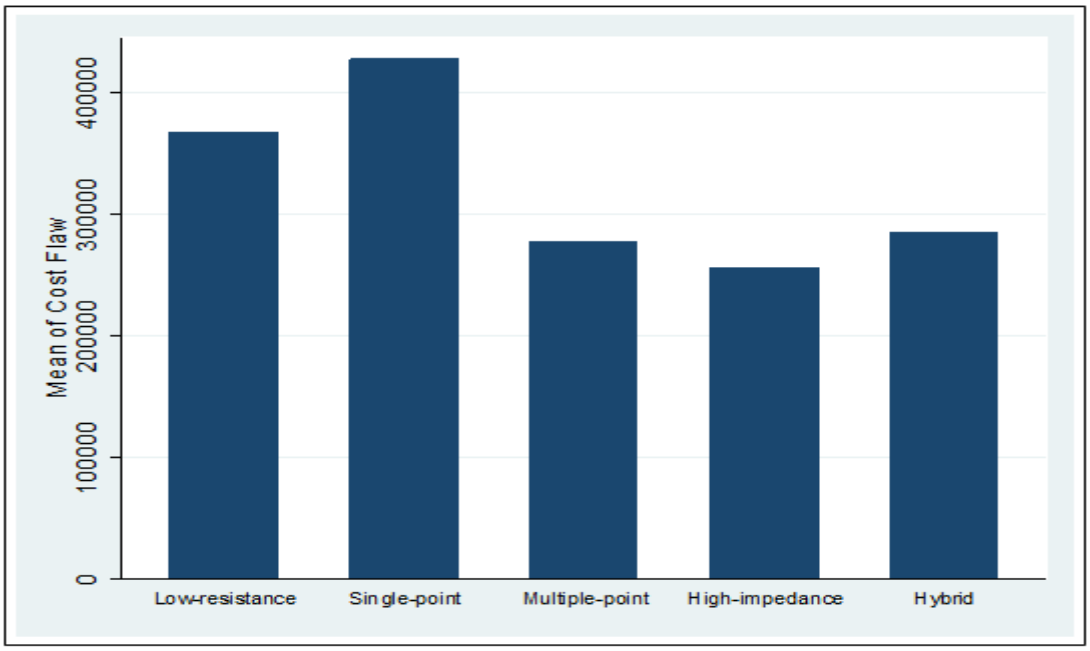

Figure 1.6. Cost of system failure associated with specific system grounding.

1.5.2 Causes of stator failure and nature of system failures

Causes of stator failures were examined in two ways. First, the meta-analysis disclosed the respective percentages of stator failures ascribable to insulation failure, unknown short-circuit causes, and polarization failure (Figure 1.7). Next, by dividing the prevalence of stator types by system faults, the adjusted contribution of stator types to system faults was derived (Figure1.8), which indicates that both random-wound stators and hybrid stators make a disproportionate contribution to system failures. On the other hand, most system failures were multiple-point in nature (Figure 1.9).

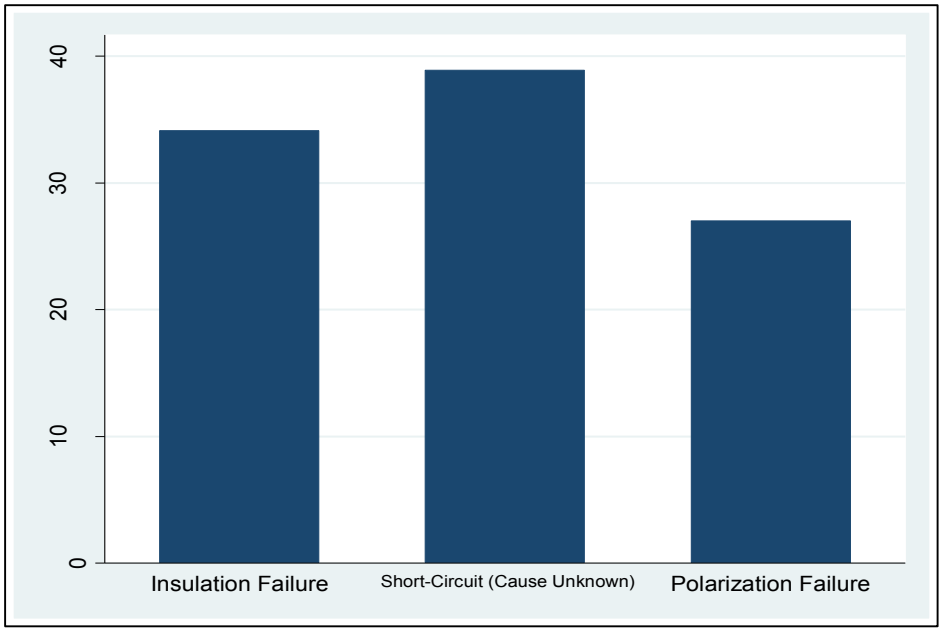

Figure 1.7. Stator failures as contributors to system failure.

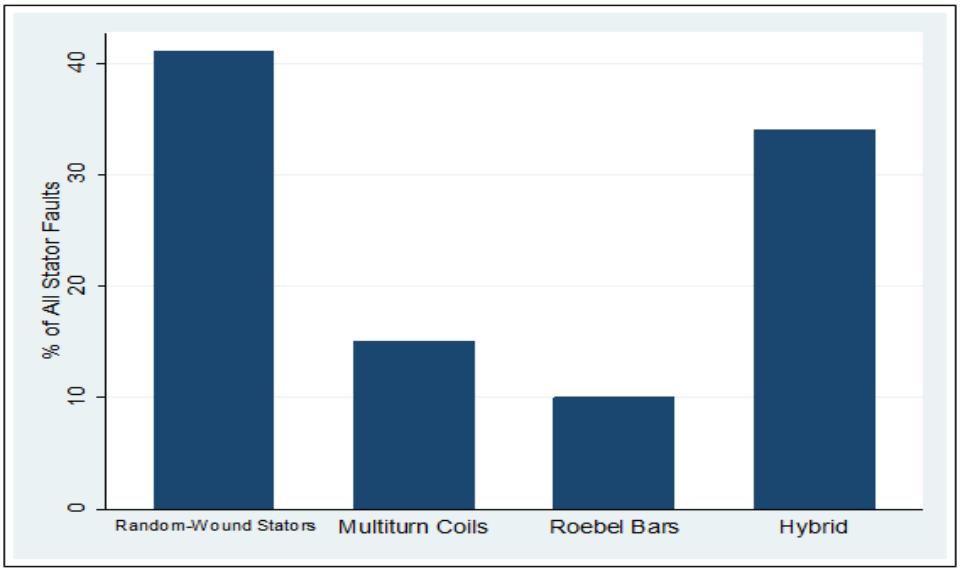

Figure 1.8. Stator types as contributors to system failure.

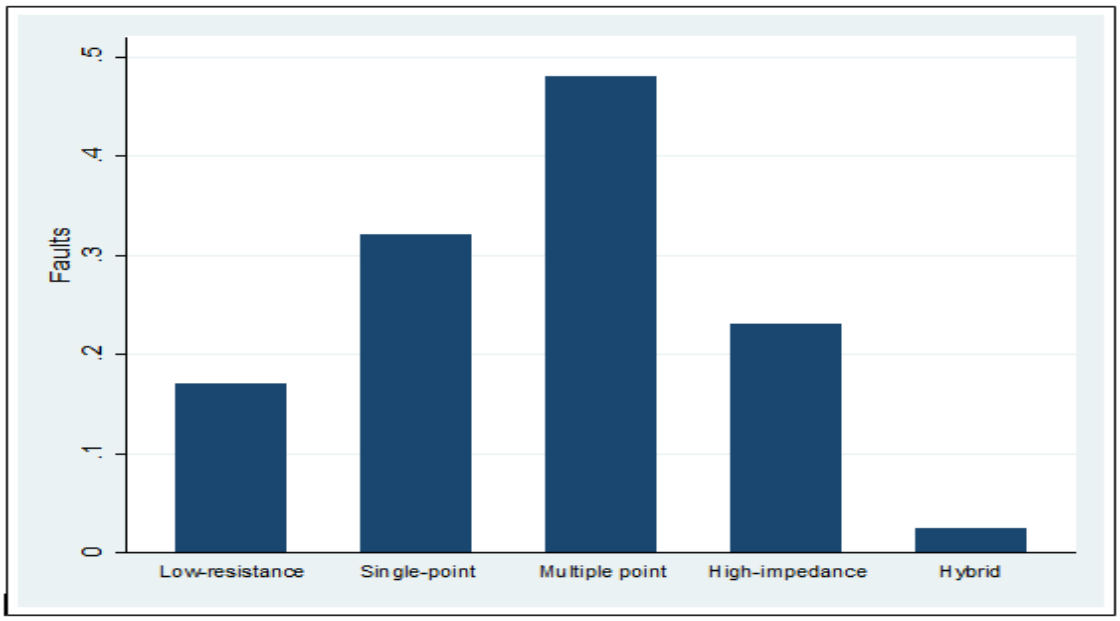

Figure 1.9. Adjusted contribution of stator type to system failure.

1.6 Motivation and proposed work

From the previous section, we can say that synchronous generators are an important element of the power system as they are the main source of power that feeds both the residential sector and industrial sector. As a result, the reliability of its protection scheme against faults is a major issue these days. In this thesis, we will focus more on internal faults in high-impedance grounded (HIG) systems, especially the stator ground fault which can occur due to electro-mechanical stresses and deterioration of the stator windings insulation [38].

The 100% stator protection schemes utilizing third-harmonic schemes are used in many places but are most widely used in the United States, largely as a means of providing

stator ground fault protection within the stator winding. However, it should be noted that these third-harmonic schemes have a number of drawbacks that keep them from reaching complete salience, even within the United States. There are many reports showing that the 100% stator protection schemes are not secure enough. Many incidents of false tripping and other issues have been reported for such schemes. There is an article which cites some of the critical elements of these 100% stator ground fault protection schemes [39]. The author of this article stated that third-harmonic schemes are utilized predominantly in stator windings that have a great deal of third-harmonic that is actually present. That is to say, generators which have very little third-harmonic are not used as predominantly. Third-harmonic schemes are also heavily used when the greater the MW and MVAR output of the generator is in question. Essentially, an increased MW load in a generator necessitates third-harmonic schemes because the third-harmonic voltage generally increases along with it, meaning that higher power necessitates third-harmonic schemes to a greater degree. Similarly, reactive generator output is also directly correlated with the third-harmonic; the unpredictability of this is another key application of third-harmonic schemes.

It is worthwhile to mention that third-harmonic schemes work most effectively in stator ground fault protection that is not 100%. That is to say, implementing third-harmonic schemes into stator ground fault protection that is 100% will cause the third-harmonic schemes either to not function altogether or have severe drawbacks that more than outweigh the advantages of using them in the first place.

Another important drawback of third-harmonic schemes which is considered a disadvantage that makes their implementation, on a more widespread basis less practical, is a tendency for false tripping during load rejection. Essentially, this means that when a hydro unit is rejected at full load, it is possible for the generator to increase speed up to twice the normal rate. The key problem here is that this causes the generator's terminal frequency to be increased by the same amount, potentially doubling it as well. This will cause the third harmonic in the generator neutral to have a value that is double the 180Hz traditional value. This will cause a false-operation because the neutral overvoltage of third harmonic relays are designed to detect at the normal 180 Hz frequency, causing a failure to trip.

Another drawback to third-harmonic schemes is that they have severe limitations when applied to the operation of synchronous condensers. More specifically, the level of third harmonic in a synchronous condenser must be determined via field measurements for the operating mode. This means that, in many cases, the27TN element had to be blocked due to too low a level of third-harmonic, preventing a secure setting for the operating mode. This precludes the generation of 100% stator ground fault protection.

On a similar note, performance of third harmonic schemes on parallel generators is lacking as well. That is to say, creating a secure 27TN setting between two generators operating in parallel using third harmonic schemes is extremely difficult. As a result, protections for these would, in some cases, have to be blocked when both of these generators are operating simultaneously, and potentially jeopardizing safety.

From the perspective of cross compound and large generator applications of third harmonic schemes, the key disadvantage here deals with the detection of faults in areas outside of the winding. More simply, there are areas of winding in cross compound steam units, common in nuclear plants with parallel stator windings, that are missed by using the 27TN relay. As a result, this creates "gaps" in the ability of third harmonic schemes to effectively detect ground faults in the stator winding.

Another drawback of these schemes lies in their application within gas turbines. The primary drawback here is a discrepancy between calculated values and measured values in regard to third harmonic voltage at the generator neutral level. The drop, between 20 to 30 MW, can cause the 27TN to falsely operate, leading to potential errors. Furthermore, this problem persists in other gas turbines as well, with third harmonic dropping dramatically at specific VAR outputs leading to false tripping. As a result, implementation of third harmonic schemes within these gas turbines necessitates a thorough field study be conducted on the gas turbine generator first, increasing the time and cost involved in implementation.

Thus, in this dissertation the problem has been looked at from the machine electromagnetic prospective. The machine voltages will be analyzed searching for a unique signature of the stator winding faults.

1.7 Conclusion

Synchronous generators provide power for many applications and are indispensable applications of technology in the modern world. Nonetheless, synchronous generators remain vulnerable to ground faults. While there are many viable means of defending stator windings against the damage created by ground faults, generators are complex machinery that can fail at various points. Indeed, the literature has documented various failures of generators originating in ground fault damage to the stator windings. Such failures are complex in that they can represent an inherent weakness in the stator windings themselves, a failure of detection and protection mechanisms, or both.

Stator winding damage is expensive. Failures require the purchases of new hardware, the dedication of man-hours for replacement and analysis, and, perhaps most importantly, the disruption of larger, more expensive systems such as power plants. When all the costs are taken into account, ground faults that impact stator windings are very expensive indeed.

The main contribution of this literature review was the identification and meta-analysis of data related to ground fault damage of stator windings. The meta-analysis resulted in a number of relevant insights:

- The mean cost of a stator failure that was associated with a system failure was $326,470.5.
- The failure costs of Roebel bar stator types was highest, followed by the failure costs of hybrid stator types.

- Single-point and low-resistance systems had the highest associated costs.
- Most system failures were multiple-point in nature.
- Both random-wound stators and hybrid stators make a disproportionately high contribution to system failures.
- Low-resistance ground failures were more expensive than multiple-point grounding failures.
- Single-point ground failures were more expensive than high-impedance grounded failures.
- Single-point ground failures were more expensive than hybrid grounded failures.

These findings offer some insight into the nature of ground protection involving stator findings. First, random-wound and hybrid stators appear to be particularly vulnerable to ground faults. Replacement with other types of stators might be appropriate. Second, multiple-point systems appear to be the most vulnerable to failure. Hybrid systems were the least susceptible to failure. A best practice in protecting stator windings from ground faults might be to take advantage of the protection methods noted earlier in the literature review while also giving extra thought to (a) the design of the larger system in which the stator operates and (b) the stator winding types used within the stator. Taking a top-down as well as bottom-up approach to stator windings could be effective.

Furthermore, the reviewed literature cast a more realistic light upon the capabilities and drawbacks of many of these technologies. Most importantly, third-harmonic schemes have been examined and written about numerous times by various sources, and this one

in particular states that third-harmonic schemes have a number of limitations. Learning and adapting to these limitations is key for the long-term success of these technologies. Understanding the intricacies of protective relaying for power generation systems is also crucial. Ultimately, understanding the details of these machines allows for the creation of new and improved ways to maintain and operate them. It also allows for the creation of more effective safety measures, particularly in regard to third-harmonic schemes.

2. MODELING LARGE SYNCHRONOUS GENERATORS

2.1 Introduction

One of the very important features of this work is the existence of a lab prototype emulating real plants. Very high costs associated with real data collection in high power stations and unwillingness of generating units to lend their facilities even for a short period of time, always create the challenge of providing field data for protection schemes. In order to overcome this issue, an experimental test bed containing the required synchronous machine was modified to model a real generation unit which consists of transmission and distribution transformers, stator windings terminal and neutral measurement potential transformers (PTs), data collection unit, load, etc. In this Section, a detailed explanation is provided for the experimental test bed and a comparison between the experimental results and the 2-D finite element analysis (FEA) for the same synchronous generator.

2.2 Generator design and parameters

The generator characteristics are shown in Table 2.1. Figure 2.1 shows the stator core after removing the winding from its slots, the outer frame, rotor and rotor winding of the synchronous generator. The detailed generator characteristics are shown in the Appendix.

Table 2.1. Synchronous generator parameters

Rated power	5 kVA
Number of poles	4
Rated voltage	240 V
Rated current	12 A
Power factor	0.8
Number of winding layers per stator slot	2
Number of turns per coil	24
Number of coils per phase	4

Figure 2.1. Synchronous generator stator and rotor.

The generator windings consist of 4 coils connected in series for each phase. Each coil has 24 turns which create a 96 turn coil per phase. The turns contain 4 strands of

copper wire gauge #17. The winding layout is shown in Figure 2.2. It is clear that the phase belt of the stator winding is equal to 4 and the coil span is equal to 9 which affects the harmonics content of stator windings. That effect will be discussed more in Section 4.

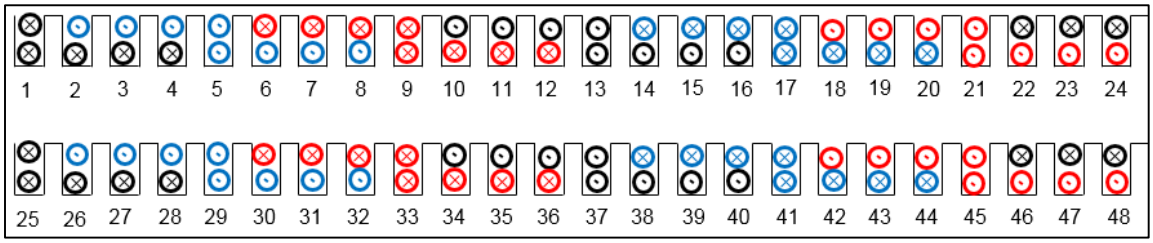

Figure 2.2. Stator winding layout.

On the other hand, the rotor winding includes four coils connected in series with 560 turns per coil (i.e. per pole). The pole arc of the rotor is equal to 73°.

2.3 Stator winding tabs layout

The original stator windings were pulled out of the slots and rewound to host certain tabs at different positions across the winding where the manual faults are applied (see Figure 2.3).

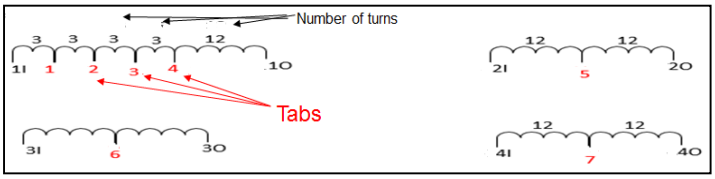

Figure 2.3. Stator windings' tabs.

In the vicinity of neutral, tabs are placed every 3 turns whereas towards the terminal end, tabs are used in every 12 turns. This is due to higher priority given to the study of faults at or in the vicinity of neutral point. Figure 2.4 shows the tabs connections in the stator windings. At the fault location, which is after specific turns (3 turns here), the wire is simply twisted and marked. After laying all the stator windings in the appropriate slots, the tabs leads are soldered to the twisted area and brought out of the machine. The machine stator was varnished after windings and tabs were placed to increase the coupling capacitance of the machine. This capacitance plays a major role in the third harmonic ratio protection scheme as we will discuss in Section 4.

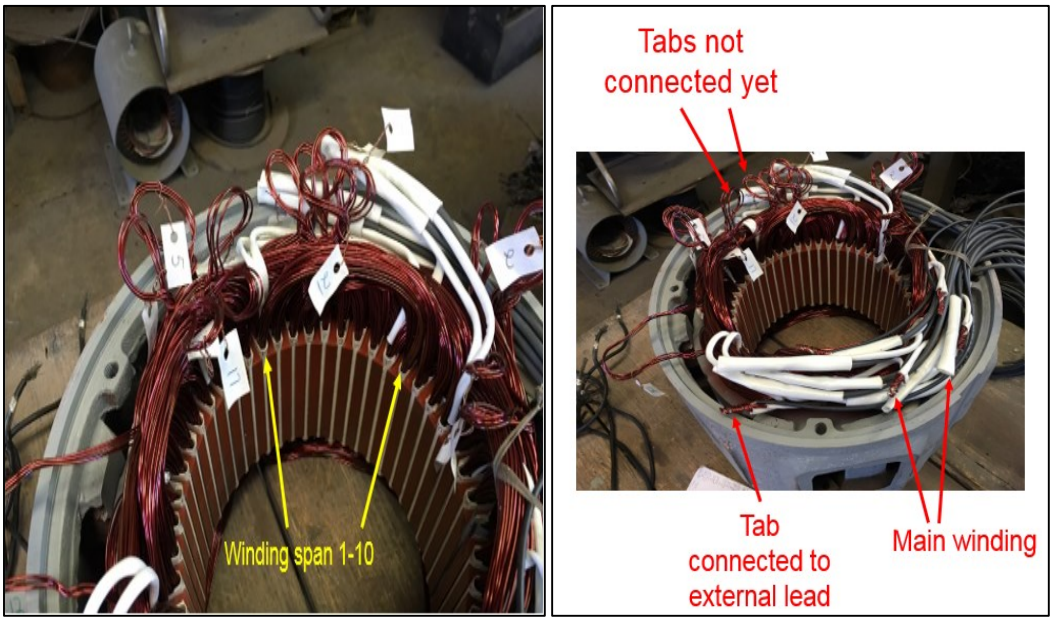

Figure 2.4. Main windings and tabs connection.

2.4 Experimental set-up

The experimental test bed contains synchronous machine, transmission and distribution transformers, stator windings terminal and neutral measurement PTs, data collection unit, and resistive load. An overview of such system is shown in Figure 2.5.

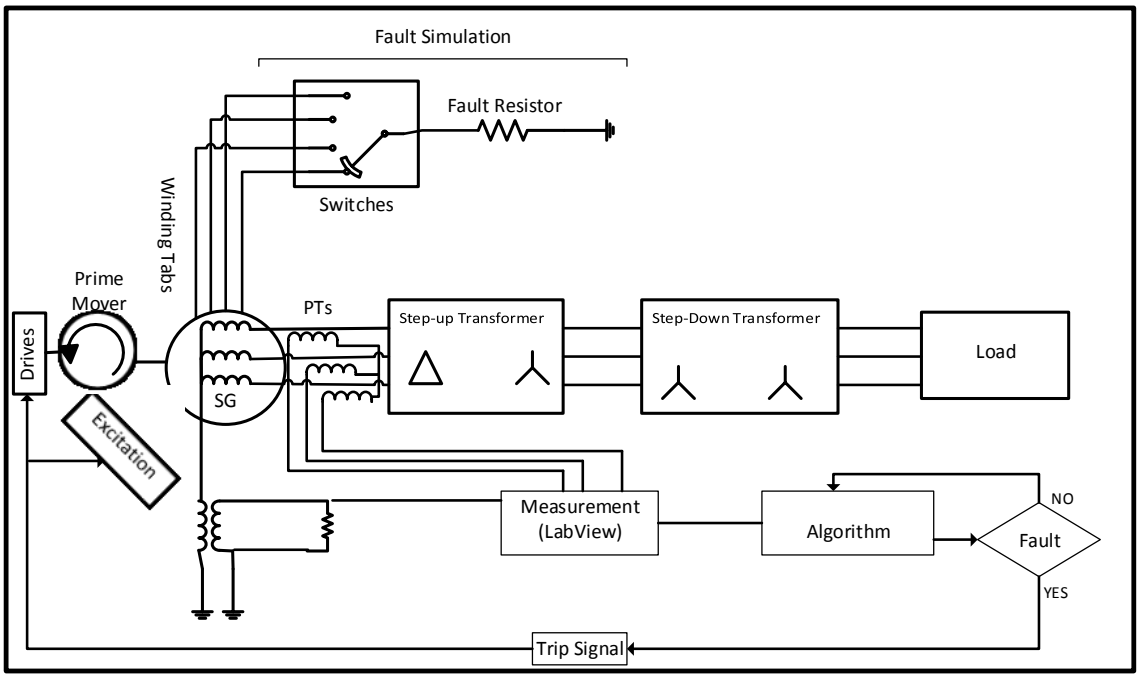

Figure 2.5. Overall system schematic.

The setup can be divided into three categories - power system apparatus, measurement devices and fault simulation components. The power system apparatus includes the prime mover which is a DC motor, the synchronous generator with its excitation DC power supply, 240/120 V generator neutral distribution transformer, 240 VΔ/480 V Y step up transformer, 480 VY/240 VY step down transformer and the load.

The measurement devices include the 240 VY/5 VY potential transformers (PT's), voltage sensors, and LABVIEW platform. The fault simulation components include fault resistors and the switches that connect the inserted winding tabs to the fault resistors and after that to the ground. Figure 2.6 shows the power system apparatus and the fault simulation components. The silver box in the left bottom corner is the system ground point. Figure 2.7 shows the measurement devices. The sensor circuit is designed to produce output voltage of range ± 1.5 V which suits both the LABVIEW and DSP controller. Figure 2.8 is an example of the terminal and neutral voltages of the generator displayed by the LABVIEW interface.

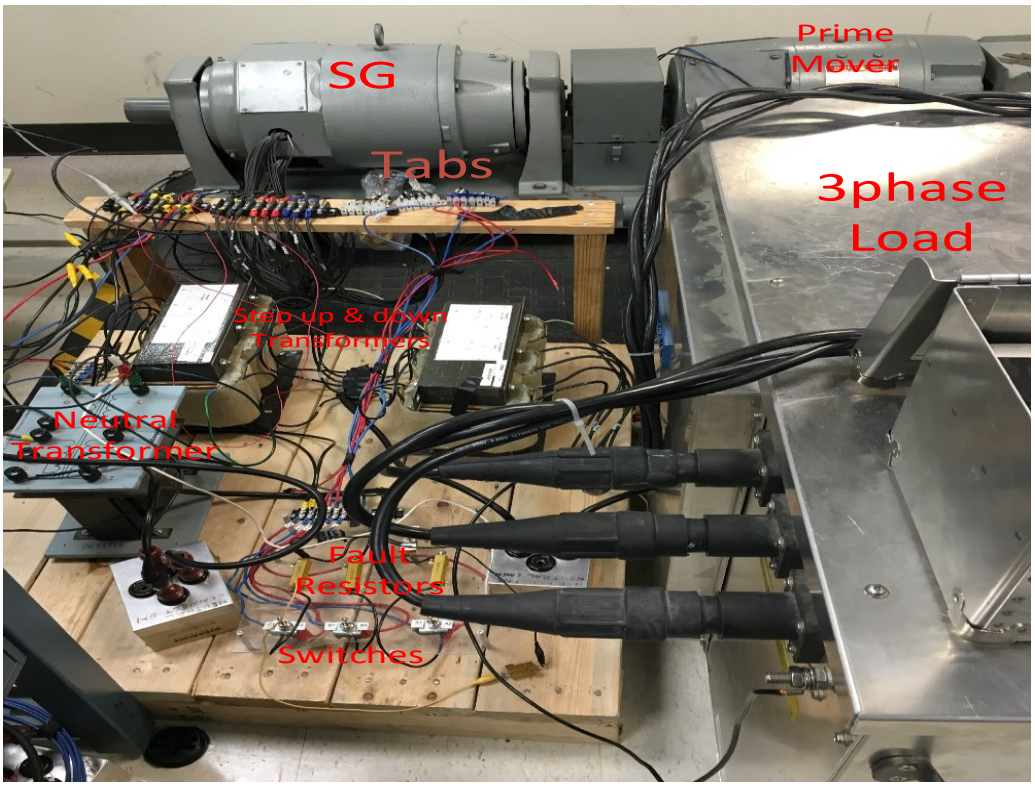

Figure 2.6. Power system and fault simulation circuit.

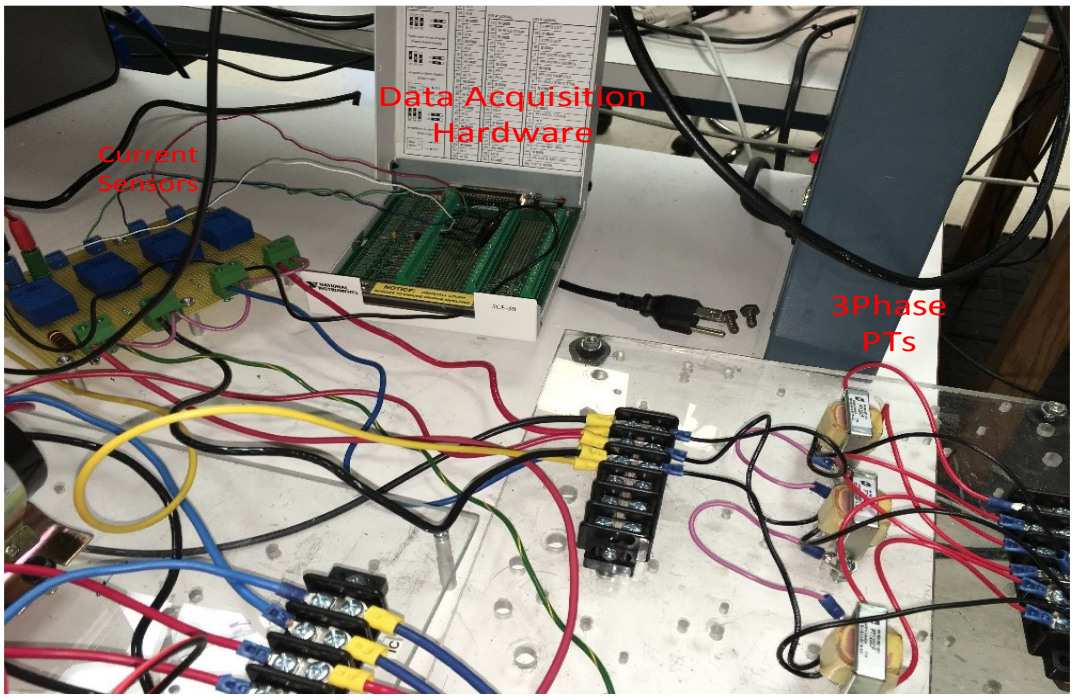

Figure 2.7. Measurement devices.

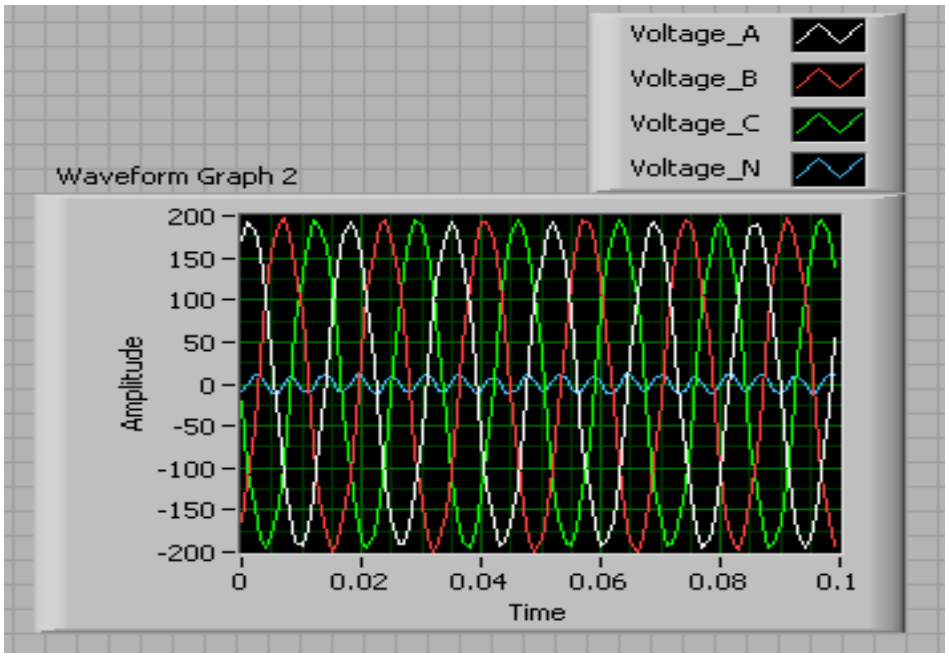

Figure 2.8. Generator voltages waveforms.

2.5 Finite element modeling of synchronous generators

Finite Element Analysis (FEA) software packages are very effective tools to study different types of electrical machines. These software packages enable the users to understand the transient and steady state behaviors of these machines by solving the electromagnetic equations that describe their dynamics. In order to explore the behavior of the synchronous generator under stator winding faults, a 2D transient model of the salient pole synchronous generator was created as shown in Figure 2.9.

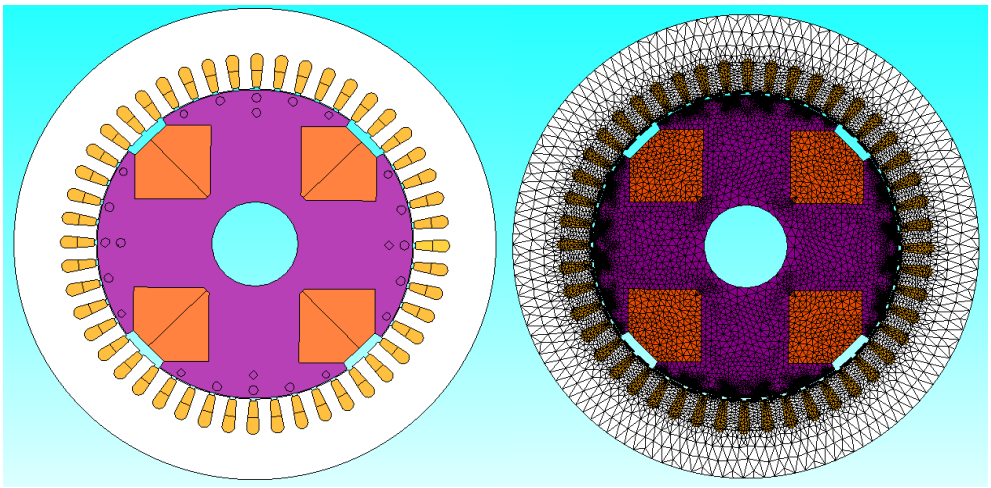

Figure 2.9. FEA model of the SG's stator and rotor with mesh loops.

In FEA software we assigned every slot layer to a coil so every slot layer has 6 turns. Thus, in total we have 96 turns per phase. In addition, the coupling capacitance between the windings and the ground was added to the machine model circuit. In order to

simulate the ground fault, the fault location is shorted through a resistor of 50Ω (see Figure 2.10).

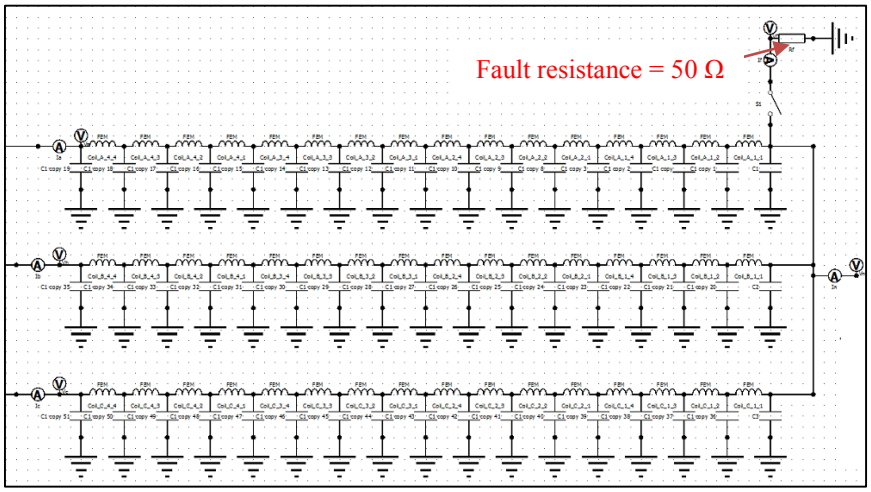

Figure 2.10. Circuit model coupled with FEA simulation.

The generator is simulated under full resistive load (12A) and the fault was applied at t_f = 0.062 s on phase 'a'. The three phase and neutral output voltages of the simulated machine operating at rated conditions are shown in Figure 2.11.

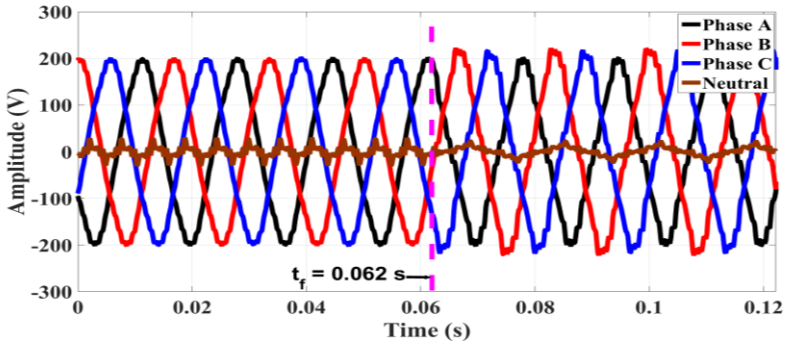

Figure 2.11. Three phase and neutral voltages before and after fault.

Figure 2.12 shows phase ‘a’ voltage of a simulated generator and an actual one. It is clear that both waveforms are very close to each other. The only difference is the presence of high order harmonics in the simulated waveform. That is because the 2-D model of the generator is not accounting for the rotor skew (7.5 degrees) which eliminates higher order voltage harmonics.

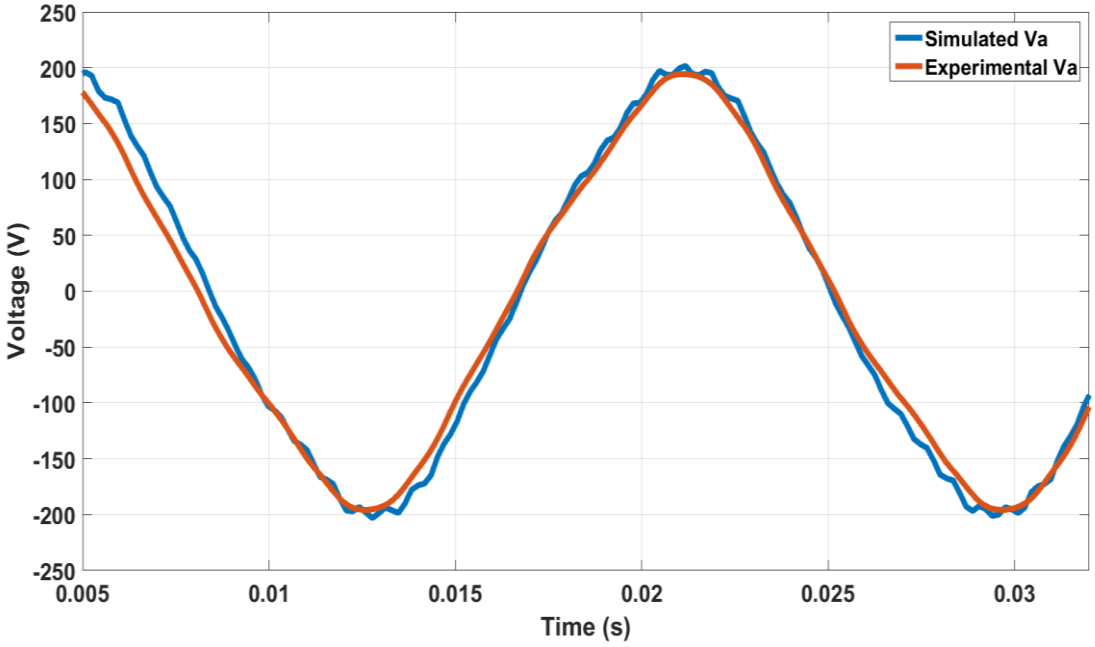

Figure 2.12. Simulated and experimental voltage of synchronous generator.

3. SYNCHRONOUS GENERATOR MATHEMATICAL MODEL

3.1 Introduction

Machines are tools to convert energy based on magnetic fields interaction between stationary windings placed on stator and the rotating windings placed on rotor. This interaction creates a rotating magnetic field distribution in the air gap that separates the stator from the rotor [42]. It is easier to simplify the problem of machine modeling by considering a coupled magnetic circuits approach instead of a magnetic fields approach which is used in FEA software. This approach is called Modified Winding Function (MWF) and is described by the authors in [42]. This approach is based on calculating the machine winding inductance considering the winding physical layout, the saliency of the rotor and considering the rotating flux of the machine. In this Section, self and mutual inductances of a synchronous machine mentioned in Table 1 will be calculated for both healthy machine and machine under stator winding ground fault. This calculation includes the saturation effects and slot harmonic effects of the air gap function of the machine.

3.2 Inductance calculations

The steps needed to calculate the magnetizing and mutual inductances of the machine are mentioned in [42]. They can be summarized as follows:

1. Reference mechanical angle φ should be chosen and according to the turn functions of the stator phases and the rotor can be expressed in Fourier series using (3.1) to (3.6).
2. With same reference mechanical angle the inverse air gap function of the machine can be expressed in Fourier series using (3.7) to (3.9).
3. Finally, (3.10) and (3.11) are used to compute the windings magnetizing and mutual inductances.

According to the stator winding distribution shown in Figure 2.2 the turn functions of the three phases n_a, n_b and n_c can be found from (3.1) to (3.4).

$$n_a = \sum_{h=odd}^{n} N_h * \cos\left(\frac{p}{2} * h * (\theta - \varphi)\right) \tag{3.1}$$

$$n_b = \sum_{h=odd}^{n} N_h * \cos\left(\frac{p}{2} * h * \left(\theta - \varphi - \frac{\pi}{3}\right)\right) \tag{3.2}$$

$$n_c = \sum_{h=odd}^{n} N_h * \cos\left(\frac{p}{2} * h * \left(\theta - \varphi + \frac{\pi}{3}\right)\right) \tag{3.3}$$

$$N_h = (-1)^{\frac{h-1}{2}} * \frac{4N_t}{p\pi h} * k_h \tag{3.4}$$

Where: p is number of poles and it equals 4 here, N_t is total number of turns in each stator phase winding (96 in this case), k_h is the harmonic winding factor. For our stator winding layout, the harmonic winding factor is shown below:

$$k_h = \frac{\sin\left(\frac{hq\gamma}{2} * \frac{p}{2}\right)}{q \sin\left(\frac{h\gamma}{2} * \frac{p}{2}\right)} * \cos\left[h(q-1)\frac{\gamma}{2} * \frac{p}{2}\right] \quad (3.5)$$

Where: q is phase belt and it equals 4 here, γ is stator slot pitch which equals 7.5°. Figure 3.1 shows the turn functions of the stator windings in our machine.

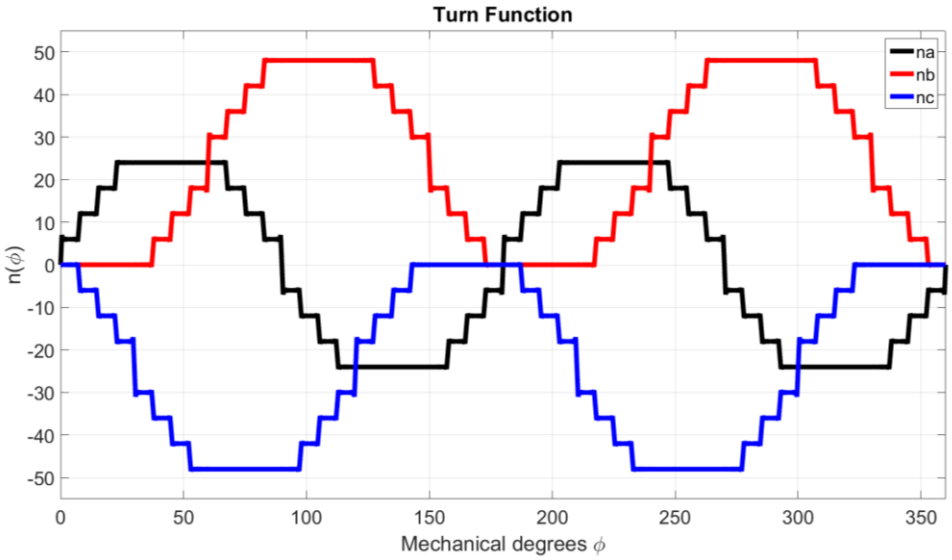

Figure 3.1. Stator windings turn functions.

Figure 3.2 shows the winding functions of the machine which are calculated by simply subtracting the turn function averages. Turns average of phase a is zero, turns average of phase b is Nt/p, and turns average of phase c is –Nt/p.

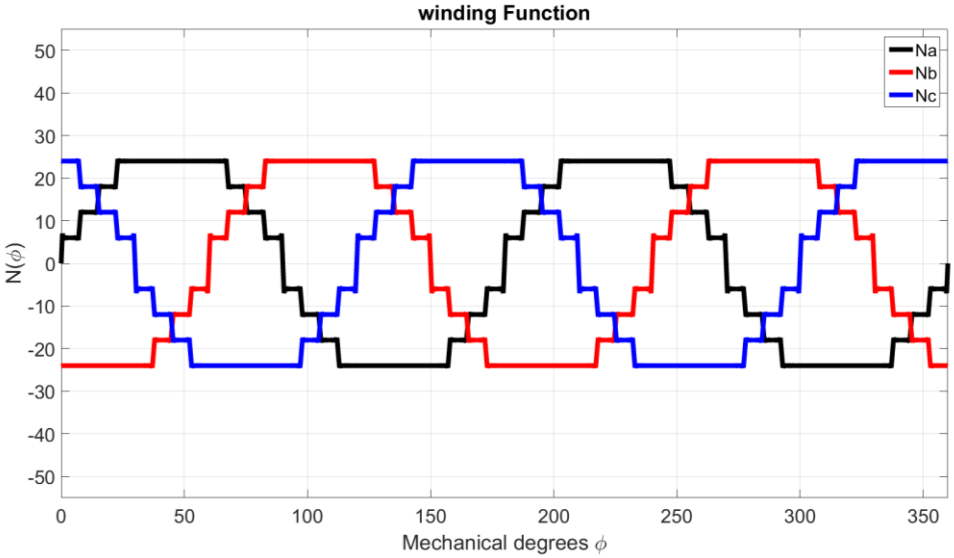

Figure 3.2. Stator windings functions.

Similarly, the rotor field turns function Fourier series can be calculated, as shown in (3.6). However, rotor winding is moving with respect to the stator reference angle. Therefore, rotor turn function will shift on the mechanical angle axes θ_m as the rotor is turning.

$$n_f = \sum_{h=odd*2}^{n} \frac{N_f}{2 * \pi * h} * \sin\left(h * \frac{\beta}{2}\right) * \cos\left(h * (\theta - \theta_m)\right) \qquad (3.6)$$

Where N_f is the rotor number of turns (560 turns) and β is rotor half pole arc (36.5°). Figure 3.3 shows the rotor turn and winding functions at $\theta_m = 0.0$.

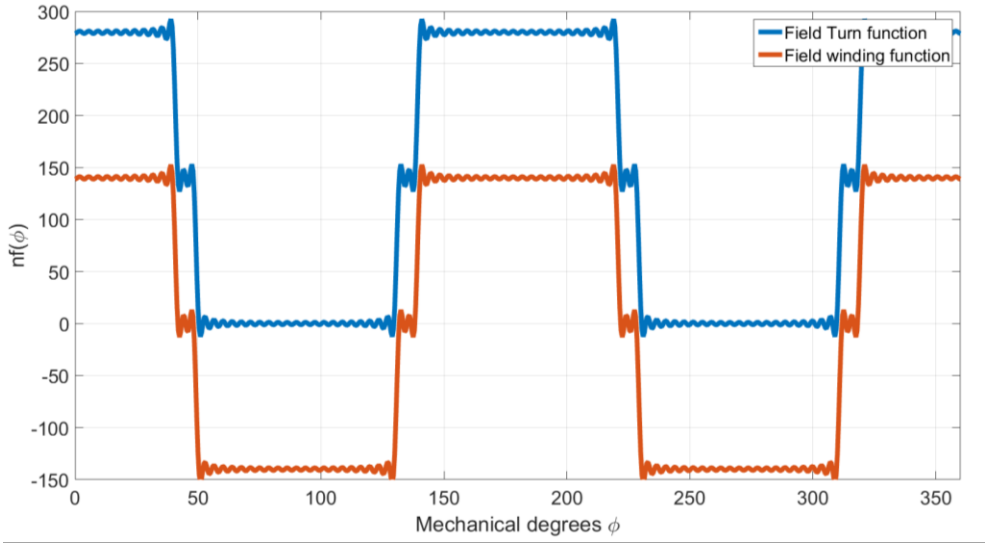

Figure 3.3. Rotor turn and winding functions.

The inverse air gap function of the salient synchronous machine can be expressed in Fourier series as follows:

$$g^{-1}(\varphi,\theta_m) = a_{0g} + \sum_{h=even*2}^{n} k_{gh} * \cos\left(\frac{p}{2} * h * (\varphi - \theta_m)\right) \tag{3.7}$$

$$a_{0g} = \frac{2}{\pi}\left(\frac{1}{g_{min}} * \theta_{min} + \frac{1}{g_{max}} * \theta_{max}\right) \tag{3.8}$$

$$k_{gh} = \frac{4 * \left(\frac{1}{g_{max}} - \frac{1}{g_{min}}\right)}{\pi h} * (-1)^{\frac{h+4}{2}} * \sin(h\theta_{max}) \tag{3.9}$$

Where g_{min} and g_{max} are the minimum and maximum effective air gap due to saliency (g_{min} = 0.5 mm, g_{max} = 5.5 mm). θ_{min} and θ_{max} are the arc angles associated with

the minimum and maximum effective air gap. The air gap function waveform is shown in Figure 3.4.

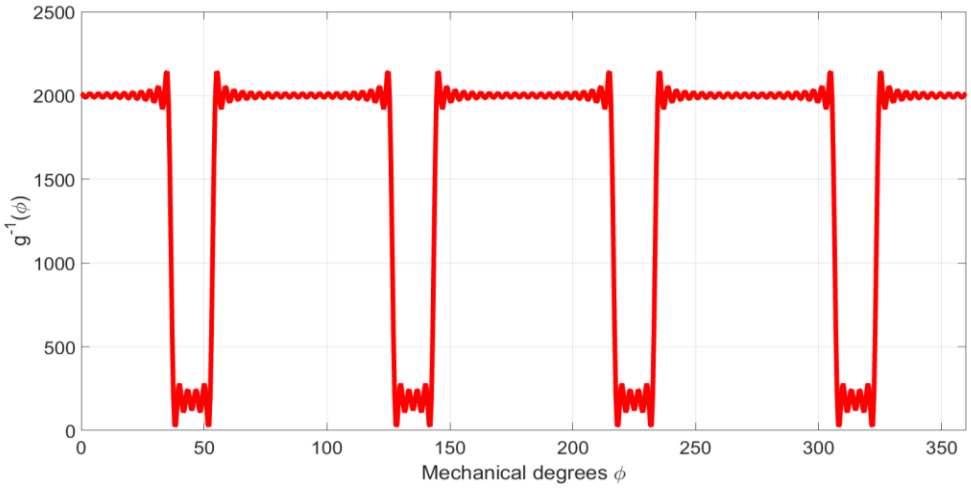

Figure 3.4. Air gap function.

After finding the windings functions and the air gap functions, we can calculate the magnetizing inductances and mutual inductances using (3.10) and (3.11) respectively.

$$L_{jj}(\varphi,\theta_m) = \mu r l * \frac{2\pi}{N}\sum_{n=1}^{N}(N_j(\varphi))^2 * g^{-1}(\varphi,\theta_m) \tag{3.10}$$

$$L_{ij}(\varphi,\theta_m) = \mu r l * \frac{2\pi}{N}\sum_{n=1}^{N} N_i(\varphi) * N_j(\varphi) * g^{-1}(\varphi,\theta_m) \tag{3.11}$$

Where μ is air permeability, r is stator inner radius (87.5 mm), and l is the stack length (97.35 mm). Figures 3.5 to 3.8 show the magnetizing inductances of the three

phases, the mutual inductances between the stator phases, the mutual inductances between the stator and rotor windings, and finally the rotor magnetizing inductance.

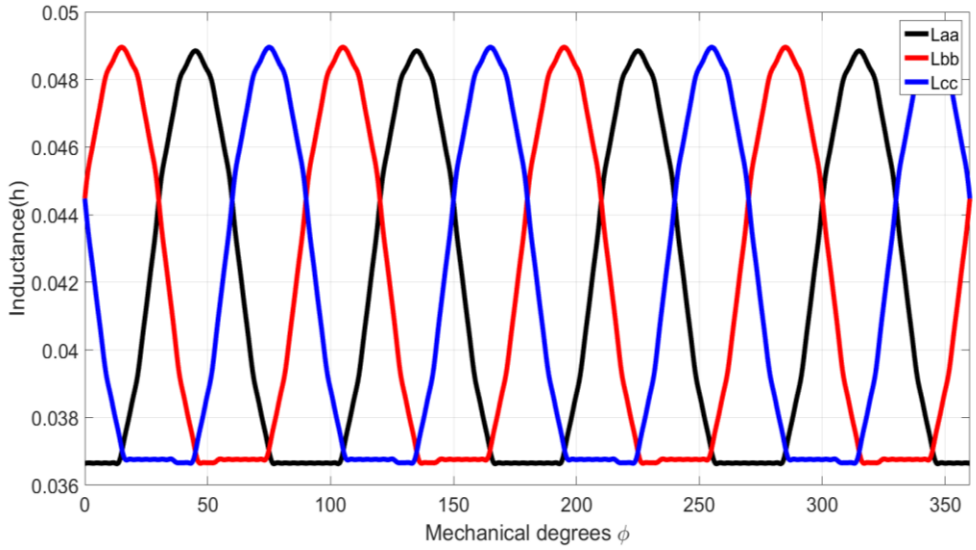

Figure 3.5. Stator windings magnetizing inductance.

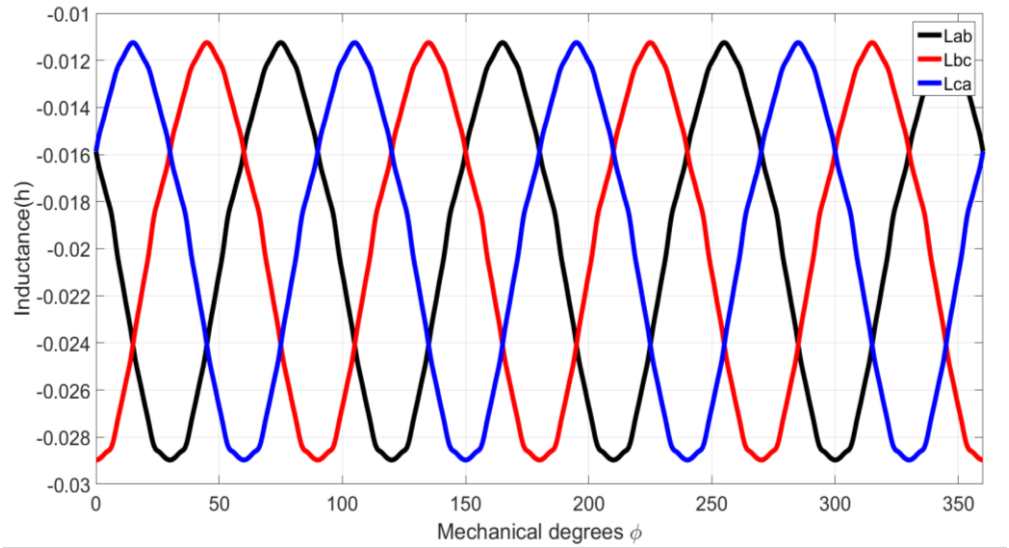

Figure 3.6. Stator mutual inductances.

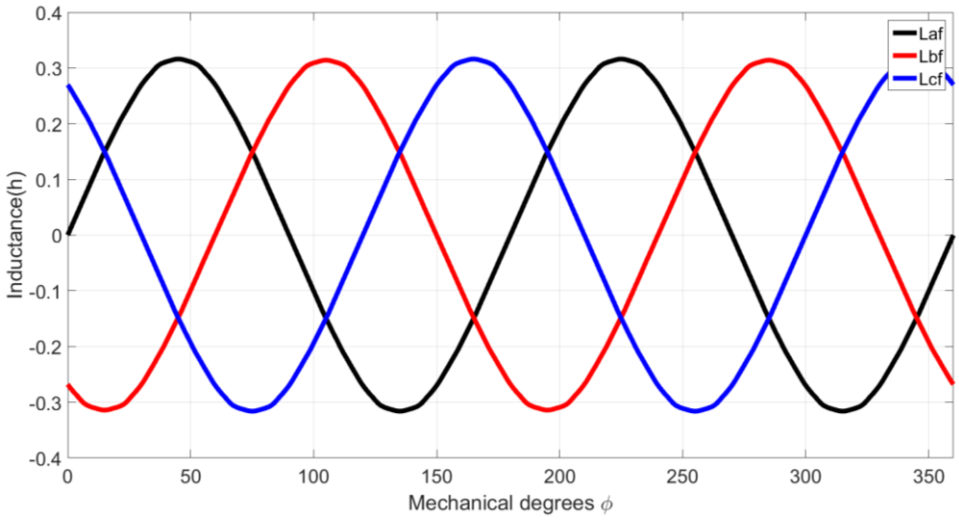

Figure 3.7. Stator winding to rotor winding mutual inductances.

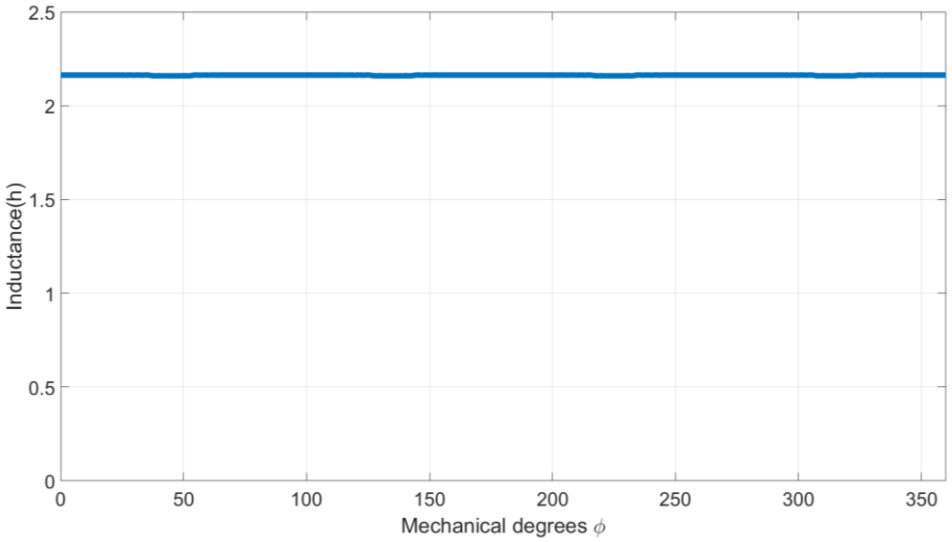

Figure 3.8. Rotor windings magnetizing inductances.

The inductances waveforms shown are calculated without accounting for the saturation. The saturation effects are discussed in the coming section.

3.3 Saturation effects modeling

Saturation is a well-known feature in electrical machines which affects their performance. Because of the saturation, harmonics start to show up in the machine flux. As a result, harmonic currents are induced in the stator windings. Even though they are small, their effects show up in the developed torque and increase the machine losses [43]. The main parts of the machine that saturate are stator and rotor core and slot teeth. However, since the core has more iron than teeth, the saturation appears more on the teeth [43]. For our model here, the core saturation is ignored and most of the saturation calculation is focused on teeth. The implementation of saturation effects in the generator model is done by modifying the air gap function to accommodate the change in the air gap flux due to the teeth saturation. Teeth saturation leads to the reduction of the iron path permeability and, as a result, the teeth reluctances increase which alter the air gap flux. This variation can be represented as an air gap reluctance variation, hence air gap length variation [43].

Based on the authors in [44] the air gap function of salient pole machine under Saturation can be represented by the following equation:

$$g_{sat}(\varphi, \theta_m) = g(\varphi, \theta_m) + g_{min} * (K_{sat} - 1) * \cos\big(p * (\varphi - \theta_m)\big) \qquad (3.12)$$

Where K_{sat} is the saturation factor and it equal to the ratio between full-load air gap voltage and no-load air gap voltage [45] (here $K_{sat} = 1.026$). Figure 3.9 is showing the inverse air gap function with and without the saturation effect.

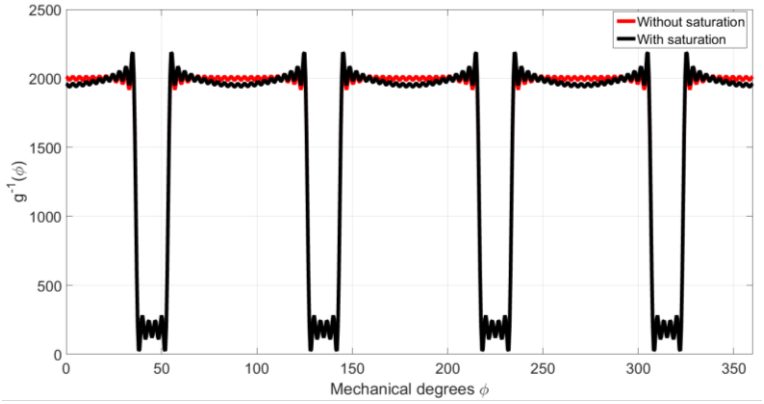

Figure 3.9. Inverse air gap function with and without saturation.

Since saturation increases the reluctance of the flux path which reduces the flux on that path, we expect the inductances to decrease. That occurred in this model and Figure 3.10 shows how the magnetizing inductance of phase 'a' decreases due to saturation.

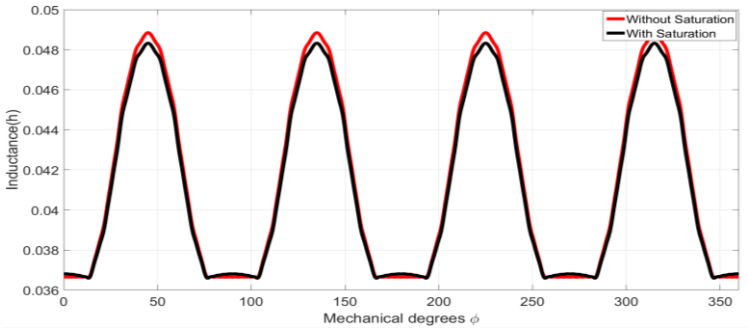

Figure 3.10. Magnetizing inductance with and without saturation.

3.4 Stator slot harmonics effects

The sources of Stator slot harmonics in ac machines are from the MMF harmonics induced in the stator, the variation of stator slot permeance and the inherent machine asymmetry [46]. The level of these harmonics is highly dependent on the saturation and, as a result, the air gap function. Slot harmonics order in the machine is based on the number of stator slots and number of poles. Usually the rotor or stator are skewed to some degree to reduce the amplitude of these harmonics, especially the higher order harmonics. Stator slot harmonics order in any machine can be found using the following equation:

$$h_{slot} = 1 + 2 * m * q * c \quad , \quad c = 0, \pm 1, \pm 2, \pm 3, \dots \dots \tag{3.13}$$

Where m is the number of phases (here m=3) and q is the machine slot per pole per phase (here q= 4). For the machine under study the positive harmonics order available are 25, 49, 73, 97, 121, 145, etc.

Since slot harmonics depends on saturation, the slot effects are modeled by multiplying the permeance variation caused by the slots by the inverse air gap function as shown below [47]:

$$g_{slot}^{-1}(\varphi, \theta_m) = a_{0g}\left[g^{-1}(\varphi, \theta_m) * \left(\frac{1}{k_{cs}} + G_{slot}\right)\right] \tag{3.14}$$

$$G_{slot} = -\sum_{h=1,2,3,\ldots}^{N} \beta * \left(\frac{4}{h\pi} * \left(0.5 + \frac{\left(\frac{h*O}{t_d}\right)^2}{0.78 - 2*\left(\frac{h*O}{t_d}\right)^2} \right) * \sin\left(1.6 * \pi * \frac{h*O}{t_d}\right) \right)$$

$$* \cos(h * S * \varphi) \qquad (3.15)$$

Where K_{cs} is the slot Carter's Coefficient (here K_{cs} = 1.07), t_d is the tooth width (11.5 mm), O is the slot opening (3 mm), β is a flux density factor, see [47], and S is number of stator slots (48 slots). Figure 3.11 shows the inverse air gap function with and without the slot harmonics effect.

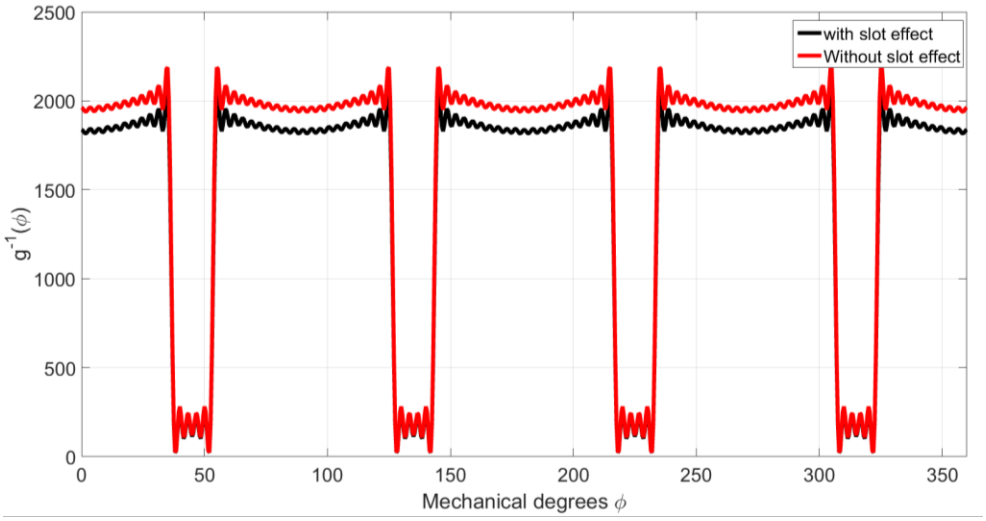

Figure 3.11. Inverse air gap function with and without slot effect.

This slot effect created ripples in the mutual inductance between the rotor and stator. Figure 3.12 shows the slot effect on mutual inductance between phase 'a' and field winding.

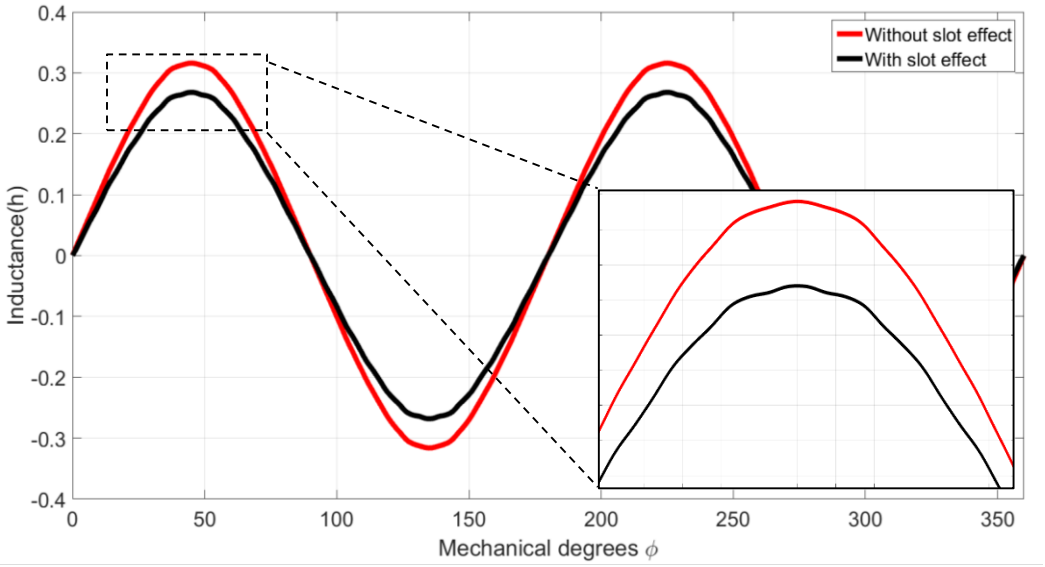

Figure 3.12. Rotor and phase 'a' mutual inductance with and without slot effect.

The slot effect on the generator under study is very minimal because of the rotor being skewed by one slot with respect to the stator (skewed by 7.5^{o}). This skewing eliminates slot harmonics of 49 and above.

3.5 Stator winding ground fault modeling

Modeling AC machines with internal faults is not similar to modeling them under external faults. Internal faults create imbalance in the winding of the machine. This imbalance in windings will lead to imbalance in the mutual and magnetizing inductances of the machine [48]. Hence, the balance of the generator terminal voltage will be altered leading to an increase in neutral voltage. According to the fault location in the stator phase winding, the turn function of that phase should be changed. The faulted winding will be

split into two windings - faulty winding and unfaulty winding. Since the focus of the work here is on faults close to neutral, a 6% fault is adopted here. Figures 3.13 and 3.14 show the faulted winding physical location and how the faulted windings look in vector space, respectively.

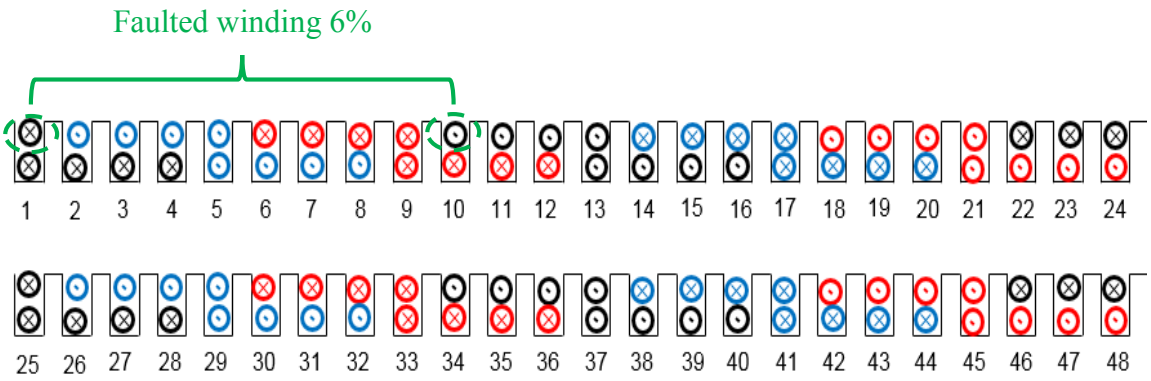

Figure 3.13. Faulted winding location.

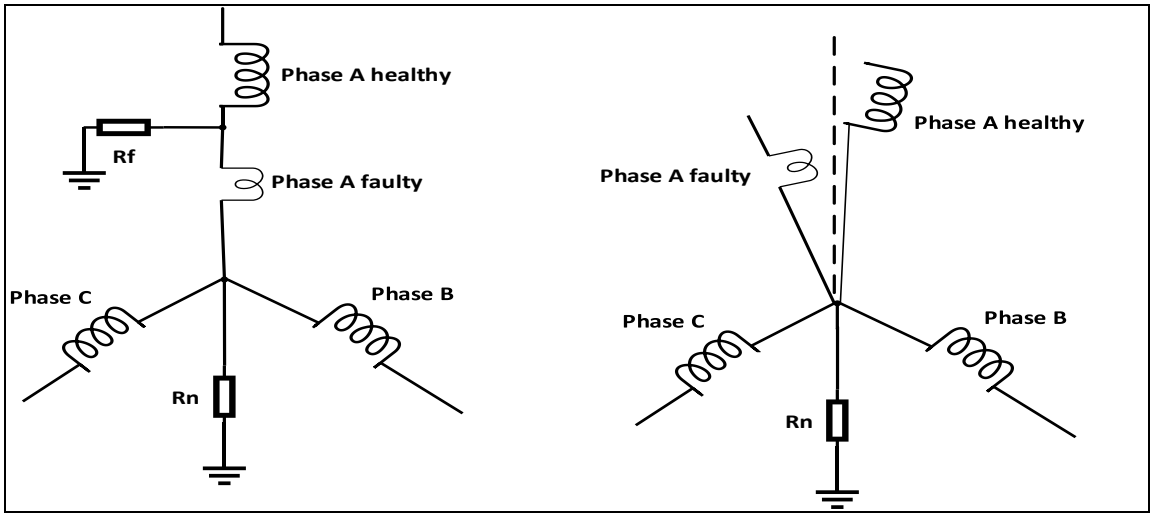

Figure 3.14. Machine stator phases vectors.

It is clear from the previous figure that the faulted portion of phase ‘a’ has its own turns function. That function vector is shifted due to the faulted winding physical location. The phase ‘a’ faulted and healthy winding turn functions are shown in Figure 3.15.

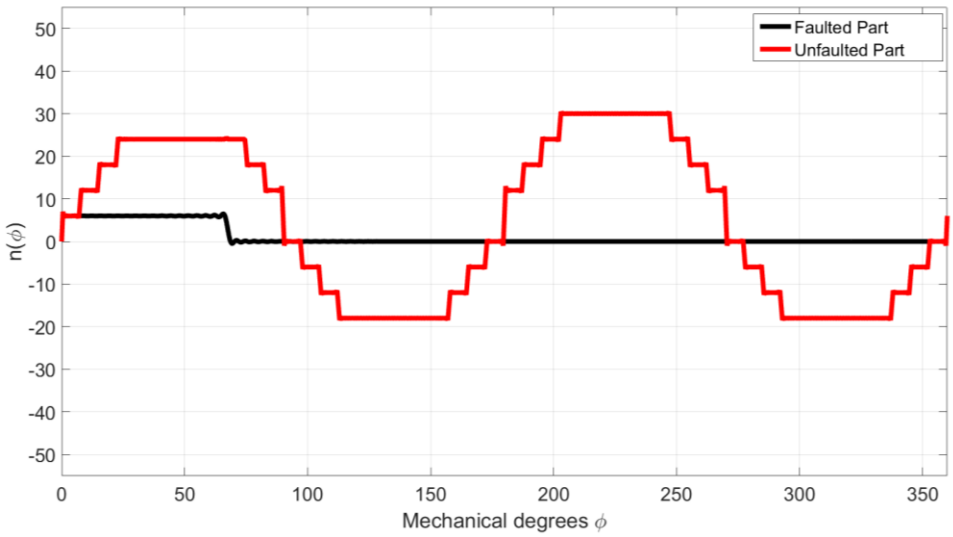

Figure 3.15. Phase a faulted and un-faulted turns functions.

The calculation of inductances is carried as before, except we are introducing a new winding (faulted winding) which increases the number of windings in the system to 5 instead of 4 in a healthy machine. With the adjustment in the phase ‘a’ turns function after the fault the 5 windings are: phase ‘a’ un-faulted, phase ‘a’ faulted, phase ‘b’, phase ‘c’, and the field windings. In Figure 3.16, it can be noticed that the mutual inductance between phase ‘a’ and phase ‘b’ dropped after fault due to the reduction in the phase ‘a’ turns function average. In the same manner, other inductances will be affected by the change in phase ‘a’. That change will be reflected in the voltage balance of the generator

output which will produce the familiar stator winding fault characteristics. The machine dynamic model under fault and machine voltage output will be discussed in next section.

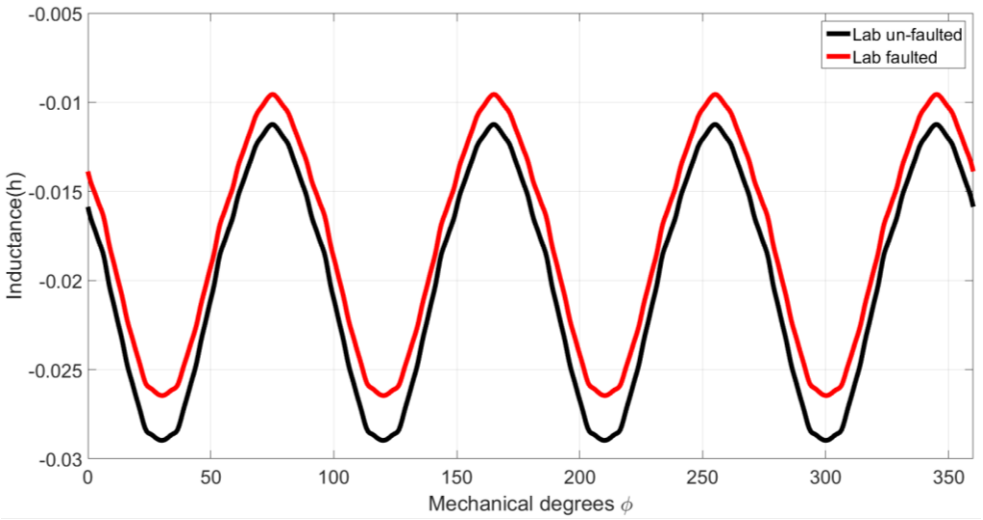

Figure 3.16. Mutual inductance between phase a and b before and after fault.

3.6 Dynamic model of synchronous generator under stator ground fault

In this section, the inductances of the salient pole synchronous generator, developed by MWF calculations, will be used to calculate the generator terminal and neutral voltages for both cases - healthy and under stator winding ground fault. Using the stator and rotor circuit voltage loops, the differential equations of the machine voltages will be developed. From [42], for a healthy case, the generator terminal voltages can be expressed as shown in (3.16). The only change made is replacing the currents by the division of voltage over the path resistance in order to solve for the voltages.

$$\begin{bmatrix} V_a \\ V_b \\ V_c \\ V_F \end{bmatrix} = \begin{bmatrix} \frac{-R_a-\omega_{rm}(\frac{dL_{aa}}{d\theta_r})}{R_L} & \frac{-\omega_{rm}\frac{dL_{ab}}{d\theta_r}}{R_L} & \frac{-\omega_{rm}\frac{dL_{ac}}{d\theta_r}}{R_L} & \frac{\omega_{rm}\frac{dL_{aF}}{d\theta_r}}{R_F} \\ \frac{-\omega_{rm}(\frac{dL_{ba}}{d\theta_r})}{R_L} & \frac{-R_b-\omega_{rm}\frac{dL_{bb}}{d\theta_r}}{R_L} & \frac{-\omega_{rm}\frac{dL_{bc}}{d\theta_r}}{R_L} & \frac{\omega_{rm}\frac{dL_{bF}}{d\theta_r}}{R_F} \\ \frac{-\omega_{rm}(\frac{dL_{ca}}{d\theta_r})}{R_L} & \frac{-\omega_{rm}\frac{dL_{cb}}{d\theta_r}}{R_L} & \frac{-R_c-\omega_{rm}\frac{dL_{cc}}{d\theta_r}}{R_L} & \frac{\omega_{rm}\frac{dL_{cF}}{d\theta_r}}{R_F} \\ \frac{-\omega_{rm}(\frac{dL_{Fa}}{d\theta_r})}{R_L} & \frac{-\omega_{rm}\frac{dL_{Fb}}{d\theta_r}}{R_L} & \frac{-\omega_{rm}\frac{dL_{Fc}}{d\theta_r}}{R_L} & \frac{R_F+\omega_{rm}\frac{dL_{FF}}{d\theta_r}}{R_F} \end{bmatrix} * \begin{bmatrix} V_a \\ V_b \\ V_c \\ V_F \end{bmatrix} +$$

$$\begin{bmatrix} \frac{-L_{aa}}{R_L} & \frac{-L_{ab}}{R_L} & -\frac{L_{ac}}{R_L} & \frac{L_{aF}}{R_F} \\ \frac{-L_{ba}}{R_L} & \frac{-L_{bb}}{R_L} & \frac{-L_{bc}}{R_L} & \frac{L_{bF}}{R_F} \\ \frac{-L_{ca}}{R_L} & \frac{-L_{cb}}{R_L} & \frac{-L_{cc}}{R_L} & \frac{L_{cF}}{R_F} \\ \frac{-L_{Fa}}{R_L} & \frac{-L_{Fb}}{R_L} & \frac{-L_{Fc}}{R_L} & \frac{L_{FF}}{R_F} \end{bmatrix} * \begin{bmatrix} \frac{dV_a}{dt} \\ \frac{dV_b}{dt} \\ \frac{dV_c}{dt} \\ \frac{dV_F}{dt} \end{bmatrix} - \begin{bmatrix} 1 \\ 1 \\ 1 \\ 0 \end{bmatrix} V_n \tag{3.16}$$

$$V_n = \frac{R_n}{R_L}V_a + \frac{R_n}{R_L}V_b + \frac{R_n}{R_L}V_c \tag{3.17}$$

Where R_a, R_b, and R_c are the phases resistances (R=0.6). R_F is the field resistance (28 Ω), R_L is the load resistance (30Ω). R_n is the neutral resistance (1 kΩ). V_n is neutral voltage. V_F is the field voltage which equals 60 V. ω_{rm} is the mechanical angular velocity in rad/s which at synchronous speed equals 1/p synchronous speed.

In case of the faulted machine, KVL for the faulted phase will be different from the other phases. Figure 3.17 illustrates the faulted phase circuit. (3.18) and (3.19) are the KVL of that circuit.

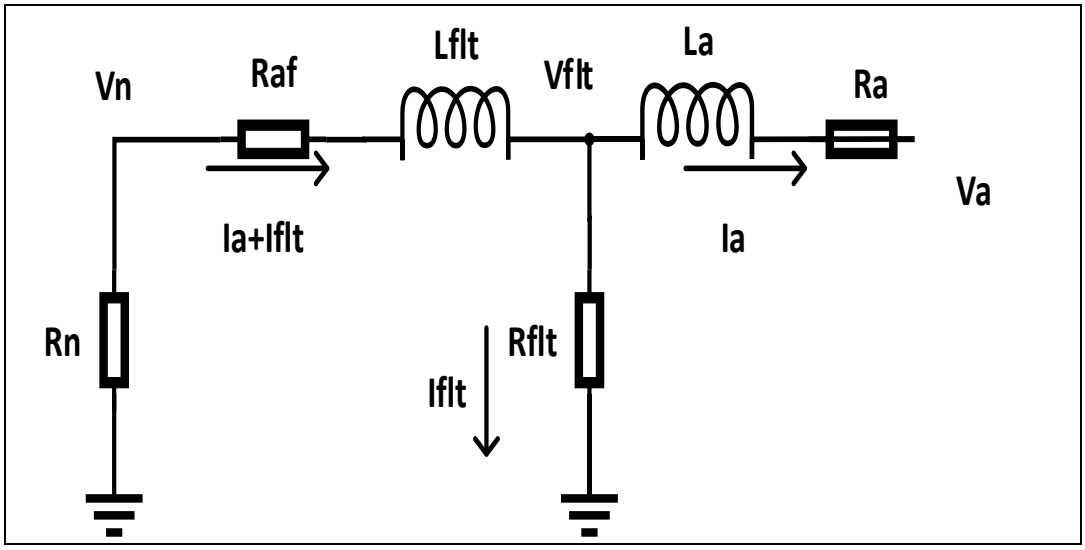

Figure 3.17. Faulted phase circuit.

$$V_n + R_{af}\left(I_a + I_{flt}\right) + \frac{d\lambda_{flt}}{dt} + V_{flt} = 0 \tag{3.18}$$

$$V_{flt} + R_a I_a + \frac{d\lambda_a}{dt} + V_a = 0 \tag{3.19}$$

$$V_{flt} = -V_n - R_{af}\left(I_a + I_{flt}\right) - \frac{d\lambda_{flt}}{dt} \tag{3.20}$$

$$V_a = -R_a I_a - \frac{d\lambda_a}{dt} - V_{flt} \tag{3.21}$$

Substituting (3.20) and (3.21) in (3.16) yields:

$$\begin{bmatrix} V_a \\ V_b \\ V_c \\ V_F \\ V_{flt} \end{bmatrix} = \begin{bmatrix} \frac{-R_a-\omega_{rm}\left(\frac{dL_{aa}}{d\theta_r}+\frac{dL_{aflt}}{d\theta_r}\right)}{R_L} & \frac{-\omega_{rm}\frac{dL_{ab}}{d\theta_r}}{R_L} & \frac{-\omega_{rm}\frac{dL_{ac}}{d\theta_r}}{R_L} & \frac{\omega_{rm}\frac{dL_{aF}}{d\theta_r}}{R_F} & \frac{-\omega_{rm}\frac{dL_{aflt}}{d\theta_r}}{R_{flt}} \\ \frac{-\omega_{rm}\left(\frac{dL_{ba}}{d\theta_r}+\frac{dL_{bflt}}{d\theta_r}\right)}{R_L} & \frac{-R_b-\omega_{rm}\frac{dL_{bb}}{d\theta_r}}{R_L} & \frac{-\omega_{rm}\frac{dL_{bc}}{d\theta_r}}{R_L} & \frac{\omega_{rm}\frac{dL_{bF}}{d\theta_r}}{R_F} & \frac{-\omega_{rm}\frac{dL_{bflt}}{d\theta_r}}{R_{flt}} \\ \frac{-\omega_{rm}\left(\frac{dL_{ca}}{d\theta_r}+\frac{dL_{cflt}}{d\theta_r}\right)}{R_L} & \frac{-\omega_{rm}\frac{dL_{cb}}{d\theta_r}}{R_L} & \frac{-R_c-\omega_{rm}\frac{dL_{cc}}{d\theta_r}}{R_L} & \frac{\omega_{rm}\frac{dL_{cF}}{d\theta_r}}{R_F} & \frac{-\omega_{rm}\frac{dL_{cflt}}{d\theta_r}}{R_{flt}} \\ \frac{-\omega_{rm}\left(\frac{dL_{Fa}}{d\theta_r}+\frac{dL_{Fflt}}{d\theta_r}\right)}{R_L} & \frac{-\omega_{rm}\frac{dL_{Fb}}{d\theta_r}}{R_L} & \frac{-\omega_{rm}\frac{dL_{Fc}}{d\theta_r}}{R_L} & \frac{R_F+\omega_{rm}\frac{dL_{FF}}{d\theta_r}}{R_F} & \frac{-\omega_{rm}\frac{dL_{Fflt}}{d\theta_r}}{R_{flt}} \\ \frac{-R_{af}-\omega_{rm}\left(\frac{dL_{flta}}{d\theta_r}+\frac{dL_{fltflt}}{d\theta_r}\right)}{R_L} & \frac{-\omega_{rm}\frac{dL_{fltb}}{d\theta_r}}{R_L} & \frac{-\omega_{rm}\frac{dL_{fltc}}{d\theta_r}}{R_L} & \frac{\omega_{rm}\frac{dL_{fltF}}{d\theta_r}}{R_F} & \frac{-R_{af}-R_{flt}-\omega_{rm}\frac{dL_{fltflt}}{d\theta_r}}{R_{flt}} \end{bmatrix} *$$

$$\begin{bmatrix} V_a \\ V_b \\ V_c \\ V_F \\ V_{flt} \end{bmatrix} + \begin{bmatrix} \frac{-L_{aa}-L_{aflt}}{R_L} & \frac{-L_{ab}}{R_L} & -\frac{L_{ac}}{R_L} & \frac{L_{aF}}{R_F} & \frac{-L_{aflt}}{R_f} \\ \frac{-L_{ba}-L_{bflt}}{R_L} & \frac{-L_{bb}}{R_L} & \frac{-L_{bc}}{R_L} & \frac{L_{bF}}{R_F} & \frac{-L_{bflt}}{R_f} \\ \frac{-L_{ca}-L_{cflt}}{R_L} & \frac{-L_{cb}}{R_L} & \frac{-L_{cc}}{R_L} & \frac{L_{cF}}{R_F} & \frac{-L_{cflt}}{R_f} \\ \frac{-L_{Fa}-L_{Fflt}}{R_L} & \frac{-L_{Fb}}{R_L} & \frac{-L_{Fc}}{R_L} & \frac{L_{FF}}{R_F} & \frac{-L_{Fflt}}{R_f} \\ \frac{-L_{fa}-L_{fltflt}}{R_L} & \frac{-L_{fltb}}{R_L} & \frac{-L_{fltc}}{R_L} & \frac{L_{fltF}}{R_F} & \frac{-L_{fltflt}}{R_f} \end{bmatrix} * \begin{bmatrix} \frac{dV_a}{dt} \\ \frac{dV_b}{dt} \\ \frac{dV_c}{dt} \\ \frac{dV_F}{dt} \\ \frac{dV_{flt}}{dt} \end{bmatrix} - \begin{bmatrix} 0 \\ 1 \\ 1 \\ 0 \\ 1 \end{bmatrix} V_n - \begin{bmatrix} 1 \\ 0 \\ 0 \\ 0 \\ 0 \end{bmatrix} V_{flt} \tag{3.22}$$

Rearranging the equations to solve for the machine voltages yields:

$$\begin{bmatrix} \frac{dV_a}{dt} \\ \frac{dV_b}{dt} \\ \frac{dV_c}{dt} \\ \frac{dI_F}{dt} \\ \frac{dV_{flt}}{dt} \end{bmatrix} = (L)^{-1} * \left(\left(A * eye(5)\right) * \begin{bmatrix} V_a \\ V_b \\ V_c \\ V_F \\ V_{flt} \end{bmatrix} + \begin{bmatrix} 0 \\ 1 \\ 1 \\ 0 \\ 1 \end{bmatrix} V_n + \begin{bmatrix} 1 \\ 0 \\ 0 \\ 0 \\ 0 \end{bmatrix} V_{flt} \right) \tag{3.23}$$

Where:

$$L = \begin{bmatrix} \frac{-L_{aa}-L_{aflt}}{R_L} & \frac{-L_{ab}}{R_L} & -\frac{L_{ac}}{R_L} & \frac{L_{aF}}{R_F} & \frac{-L_{aflt}}{R_f} \\ \frac{-L_{ba}-L_{bflt}}{R_L} & \frac{-L_{bb}}{R_L} & \frac{-L_{bc}}{R_L} & \frac{L_{bF}}{R_F} & \frac{-L_{bflt}}{R_f} \\ \frac{-L_{ca}-L_{cflt}}{R_L} & \frac{-L_{cb}}{R_L} & \frac{-L_{cc}}{R_L} & \frac{L_{cF}}{R_F} & \frac{-L_{cflt}}{R_f} \\ \frac{-L_{Fa}-L_{Fflt}}{R_L} & \frac{-L_{Fb}}{R_L} & \frac{-L_{Fc}}{R_L} & \frac{L_{FF}}{R_F} & \frac{-L_{Fflt}}{R_f} \\ \frac{-L_{fa}-L_{fltflt}}{R_L} & \frac{-L_{fltb}}{R_L} & \frac{-L_{fltc}}{R_L} & \frac{L_{fltF}}{R_F} & \frac{-L_{fltflt}}{R_f} \end{bmatrix} \tag{3.24}$$

$$A = \begin{bmatrix} \frac{-R_a-\omega_{rm}\left(\frac{dL_{aa}}{d\theta_r}+\frac{dL_{aflt}}{d\theta_r}\right)}{R_L} & \frac{-\omega_{rm}\frac{dL_{ab}}{d\theta_r}}{R_L} & \frac{-\omega_{rm}\frac{dL_{ac}}{d\theta_r}}{R_L} & \frac{\omega_{rm}\frac{dL_{aF}}{d\theta_r}}{R_F} & \frac{-\omega_{rm}\frac{dL_{aflt}}{d\theta_r}}{R_{flt}} \\ \frac{-\omega_{rm}\left(\frac{dL_{ba}}{d\theta_r}+\frac{dL_{bflt}}{d\theta_r}\right)}{R_L} & \frac{-R_b-\omega_{rm}\frac{dL_{bb}}{d\theta_r}}{R_L} & \frac{-\omega_{rm}\frac{dL_{bc}}{d\theta_r}}{R_L} & \frac{\omega_{rm}\frac{dL_{bF}}{d\theta_r}}{R_F} & \frac{-\omega_{rm}\frac{dL_{bflt}}{d\theta_r}}{R_{flt}} \\ \frac{-\omega_{rm}\left(\frac{dL_{ca}}{d\theta_r}+\frac{dL_{cflt}}{d\theta_r}\right)}{R_L} & \frac{-\omega_{rm}\frac{dL_{cb}}{d\theta_r}}{R_L} & \frac{-R_c-\omega_{rm}\frac{dL_{cc}}{d\theta_r}}{R_L} & \frac{\omega_{rm}\frac{dL_{cF}}{d\theta_r}}{R_F} & \frac{-\omega_{rm}\frac{dL_{cflt}}{d\theta_r}}{R_{flt}} \\ \frac{-\omega_{rm}\left(\frac{dL_{Fa}}{d\theta_r}+\frac{dL_{Fflt}}{d\theta_r}\right)}{R_L} & \frac{-\omega_{rm}\frac{dL_{Fb}}{d\theta_r}}{R_L} & \frac{-\omega_{rm}\frac{dL_{Fc}}{d\theta_r}}{R_L} & \frac{R_F+\omega_{rm}\frac{dL_{FF}}{d\theta_r}}{R_F} & \frac{-\omega_{rm}\frac{dL_{Fflt}}{d\theta_r}}{R_{flt}} \\ \frac{-R_{af}-\omega_{rm}\left(\frac{dL_{flta}}{d\theta_r}+\frac{dL_{fltflt}}{d\theta_r}\right)}{R_L} & \frac{-\omega_{rm}\frac{dL_{fltb}}{d\theta_r}}{R_L} & \frac{-\omega_{rm}\frac{dL_{fltc}}{d\theta_r}}{R_L} & \frac{\omega_{rm}\frac{dL_{fltF}}{d\theta_r}}{R_F} & \frac{-R_{af}-R_{flt}-\omega_{rm}\frac{dL_{fltflt}}{d\theta_r}}{R_{flt}} \end{bmatrix} \tag{3.25}$$

$$V_n = \frac{R_n}{R_L}V_a + \frac{R_n}{R_f}V_f + \frac{R_n}{R_L}V_b + \frac{R_n}{R_L}V_c \tag{3.26}$$

The differential equations in (3.23) were solved in Matlab Simulink using code script linked to an integrator in a SIMULINK environment. The step size was set to be very small to assure the convergence of the integrator output. The generator model output voltages are shown in Figure 3.18. Figures 3.19 to 3.22 show a comparison between the results obtained from FEA and results of the coupled magnetic circuit (CMC) model.

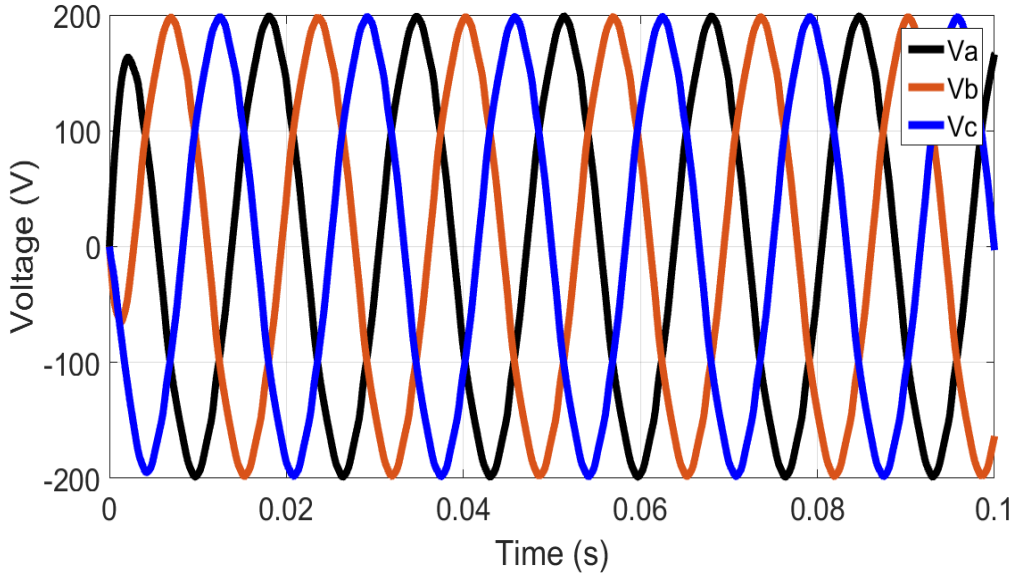

Figure 3.18. Generator voltages using CMC model.

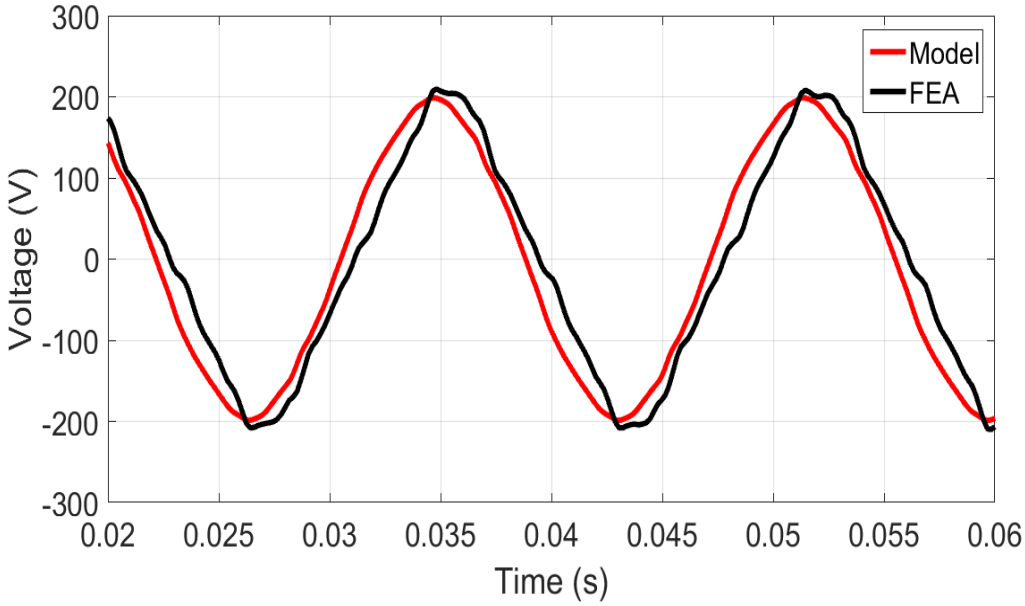

Figure 3.19. Phase a voltage in CMC model and FEA.

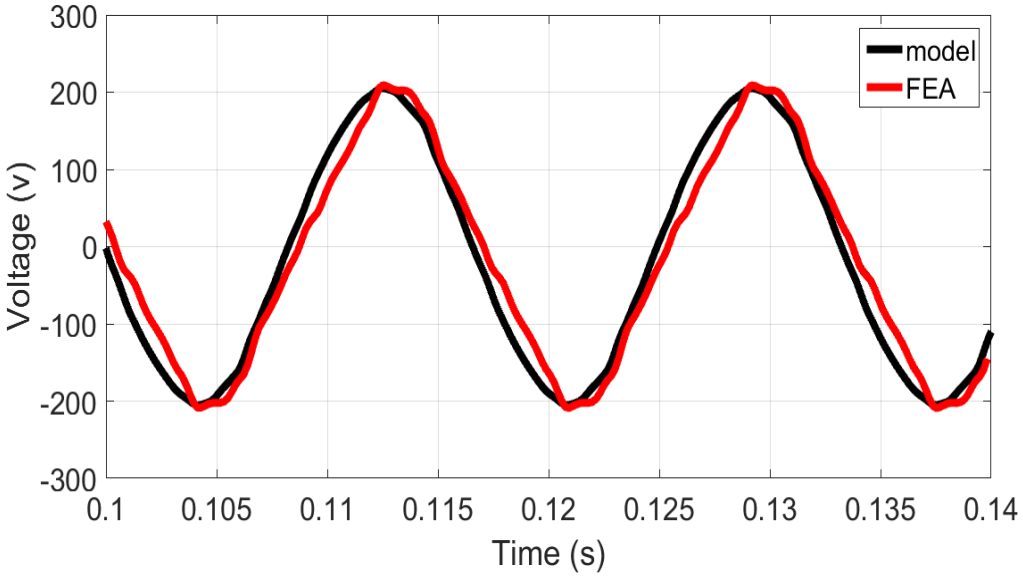

Figure 3.20. Phase b after fault.

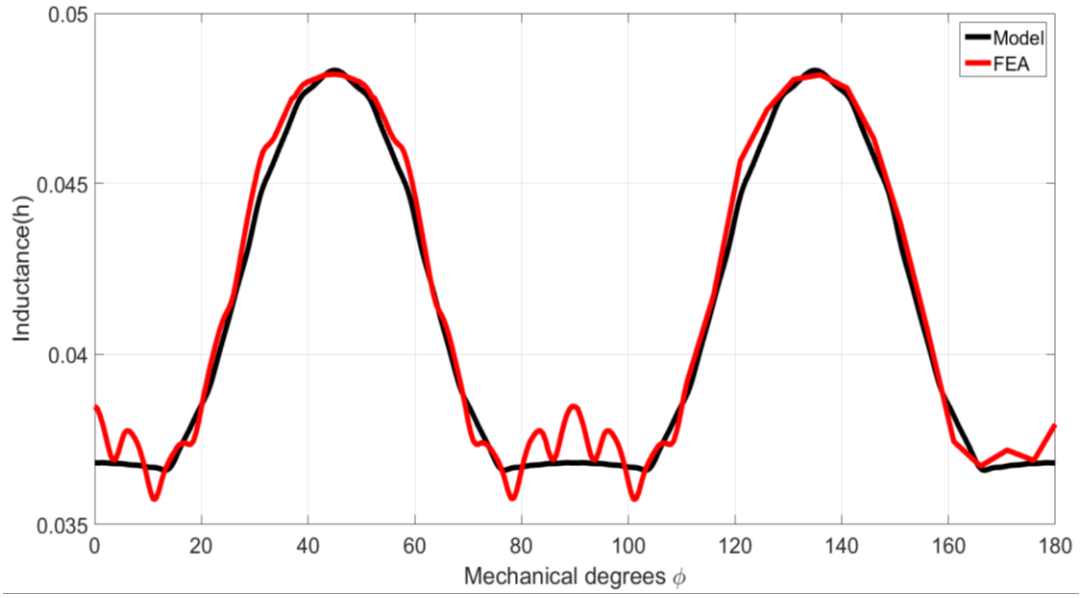

Figure 3.21. Phase a magnetizing inductance obtained from CMC model and FEA.

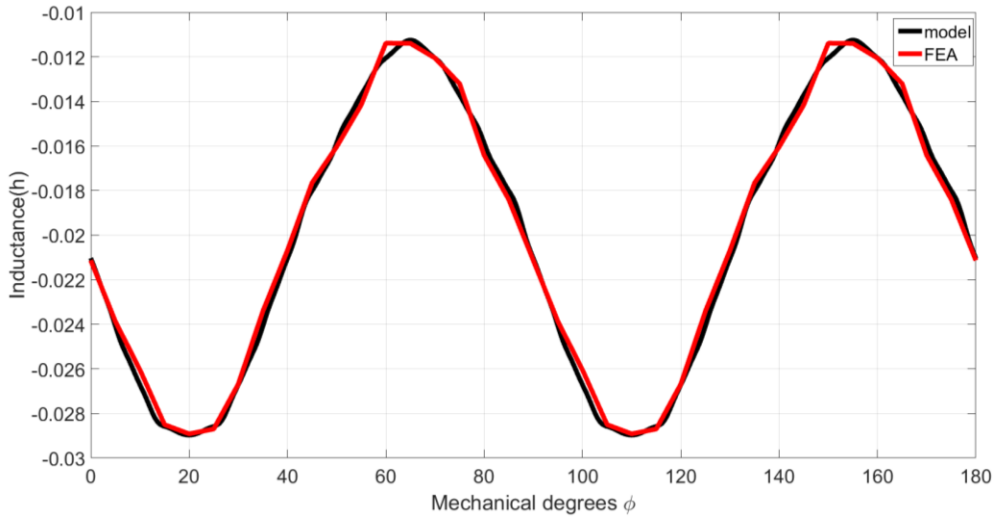

Figure 3.22. Mutual inductance between phase a and c obtained from CMC model and FEA.

3.7 Summary and conclusion

In this Section, a synchronous generator model was developed by considering a coupled magnetic circuits approach instead of a magnetic fields approach. Modified Winding Function (MWF) approach was adopted to calculate the generator inductances during healthy and faulted operation. Based on these inductances, the generator dynamic differential equations were arranged to output the generator voltages. In comparison with the FEA analysis, the results obtained from the model matched the FEA results.

4. AVAILABLE PROTECTION SCHEME ANALYSIS

4.1 Introduction

Stator ground fault is a common type fault in synchronous generators. It occurs because of the stresses and weakening of the stator windings insulation. In industry, many protective schemes have been applied to detect stator ground faults. One of the well-known and wide spread schemes in industry is the 100% stator ground protection scheme which is based on two elements - the neutral over voltage element and the voltage third harmonic ratio element. The neutral over voltage element covers the range 10% to 100% of the windings. The third harmonic ratio element protects the rest of the winding 0 to 5%. However, the third harmonic ratio scheme faces many challenges that cause it to lose reliability. Many incidents of miss-tripping were reported regarding this scheme. These incidents were investigated and reached the conclusion that the machine third harmonic was affected by many other factors besides the stator ground faults. These factors included the machine voltage third harmonic level, the loading of the machine, the operation power factor, and the machine coupling capacitance between the windings and the ground. In this Section, we will shed some light on these factors. In addition, modeling large generators in the lab to test the third harmonic ratio scheme was a big challenge because of those factors. As a result, many adjustments were done to the setup generator to simulate the behavior of large generators under stator winding ground faults.

4.2 Effect of Third harmonic level

The presence of harmonics in AC machines has a negative impact on their performance. Harmonics are the cause of torque pulsation and they increase machine losses. Therefore, current machine design focuses on eliminating harmonics to reduce losses and consequently increase machine efficiency. On the other hand, for the accurate operation of the third harmonic ratio protection scheme, the third harmonic of the machine single phase should be in the range of 2-10% of the phase voltage fundamental [49]. Since the machine design is directed toward eliminating harmonics, this protection will be valuable as long as the old generators are still in operation.

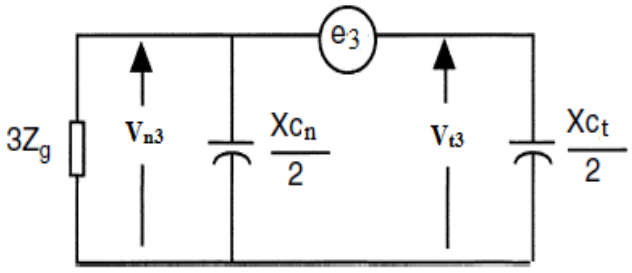

Figure 4.1. Generator third harmonic model.

From the machine third harmonic model shown in Figure 4.1, we can conclude that the third harmonic level of the machine, represented by a voltage source in the model, should be sufficient to produce enough third harmonic current to pass through the winding-ground coupling capacitance. Having the third harmonic current follow through the capacitances will result in having the stator ground fault characteristics which, as

mentioned in Section One, reduce the third harmonic voltage at the fault location and increase the third harmonics voltage in the other side of the winding.

The original windings of the setup generator and winding harmonics spectrum are shown in Figure 4.2.

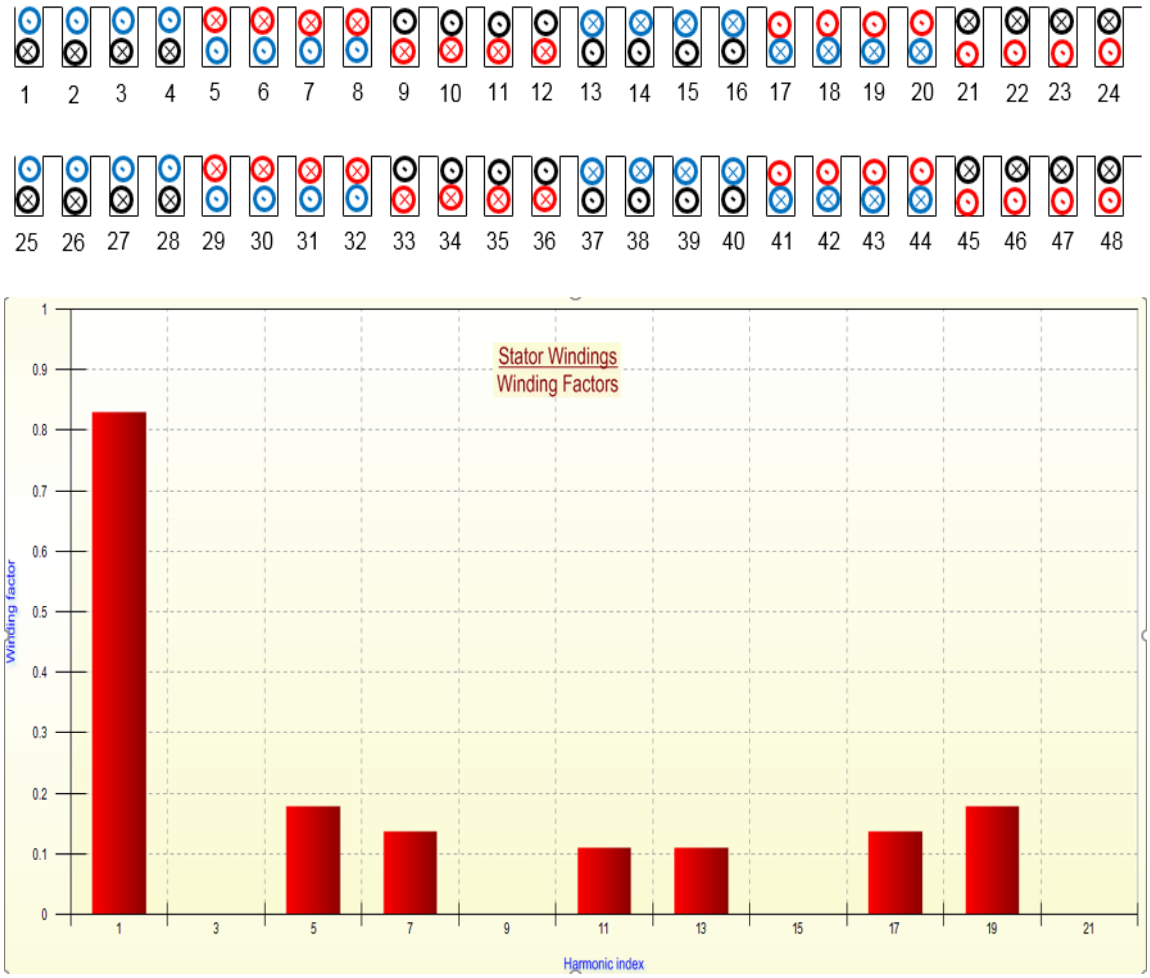

Figure 4.2. Generator original windings and windings factor.

It is clear that this stator windings layout (no overlap) does not have a third harmonic which led to a very low third harmonic in the generator terminals and neutral voltages. Also, the stator ground fault characteristics did not show up when the fault was applied on 6% of the windings. Figures 4.3 and 4.4 show the third harmonics response of 6% fault acquired using LABVIEW. V_p is the sum of all three phases 3rd harmonics and V_n is the neutral 3rd harmonic.

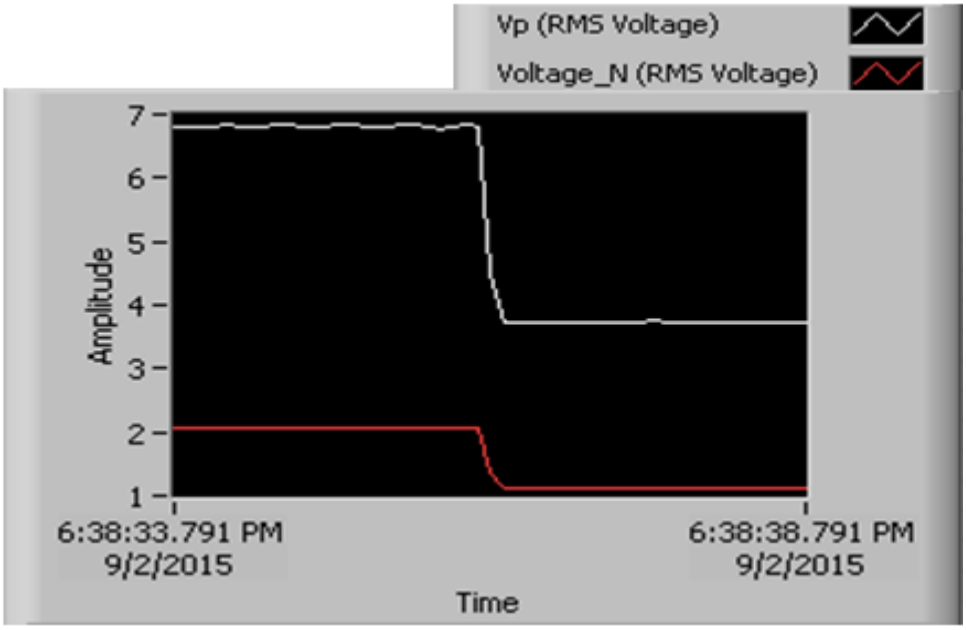

Figure 4.3. Neutral and terminals third harmonic voltage at 6% fault.

The level of phase third harmonic voltage was approximately 2.25V which is 1.4% of the fundamental voltage. The winding to ground coupling capacitance is very small (18 nF) which creates a high impedance path for the third harmonic current. Therefore, we did not observe the fault characteristics easily. One solution for that problem was to increase

the level of the generator's third harmonic voltage by changing the stator winding layout. A new stator winding layout with one slot overlap (shown with green rectangles in Figure 4.4) and higher third harmonic factor was implemented.

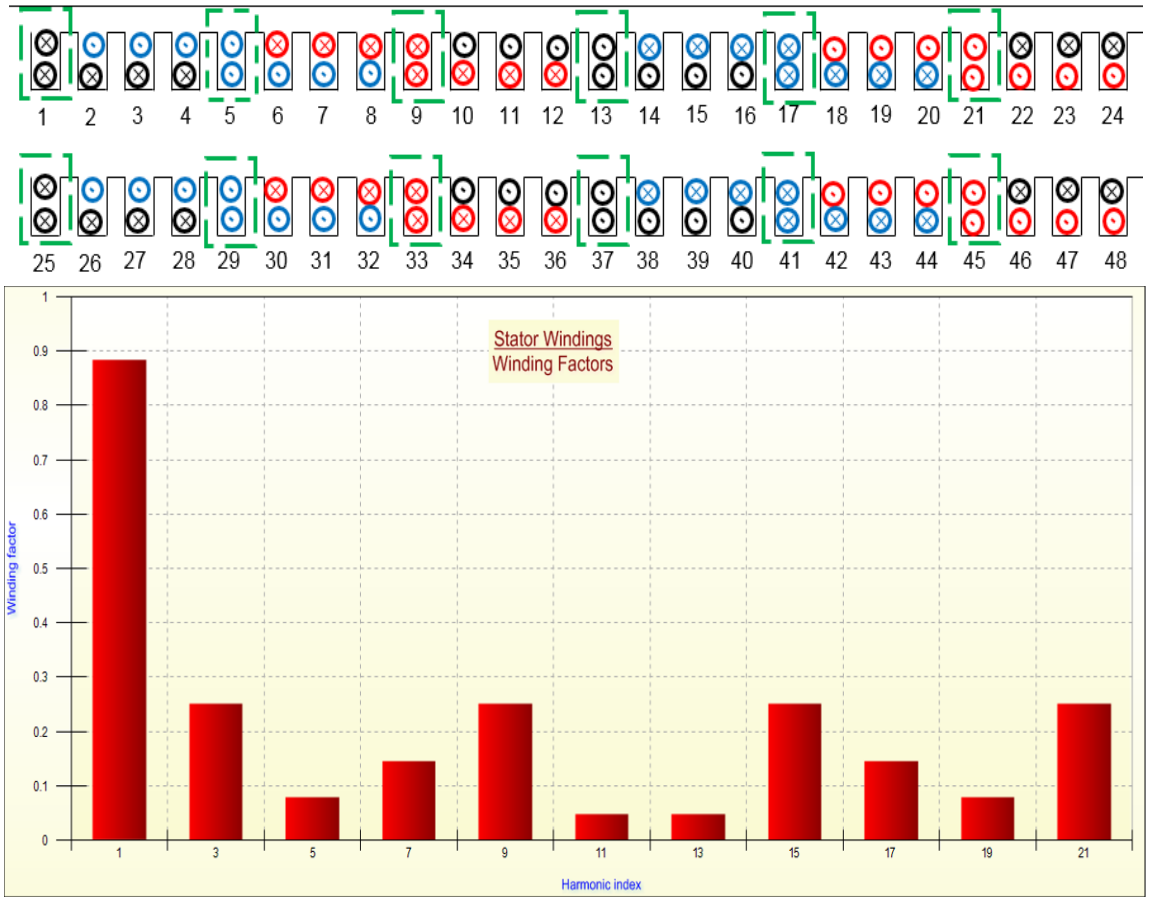

Figure 4.4. New winding layout and winding factor.

Setup results illustrated in Figure 4.5, showed an increase in the third harmonic voltage level from 2.25 V/phase to 8 V/phase which equals 6% of the phase fundamental voltage. In this case, the percentage of the generator's third harmonic voltage matches the requirement for detecting the stator ground fault. Unfortunately, we still did not observe

the fault characteristics. From Figure 4.5 it can be noticed that although the terminal third harmonic voltage increased, the third harmonic voltage in the neutral side was still low. This means that the third harmonic voltage is not distributed evenly between the terminals and neutral. Investigating the setup led to the fact that there was no capacitive current following from the windings to the ground through the coupling capacitance. Despite the increase in the third harmonic voltage level, the coupling capacitance of the winding is still small and creates a high impedance path compared to the neutral path. Adding larger capacitors manually to the winding was implemented. This will be discussed in the next section.

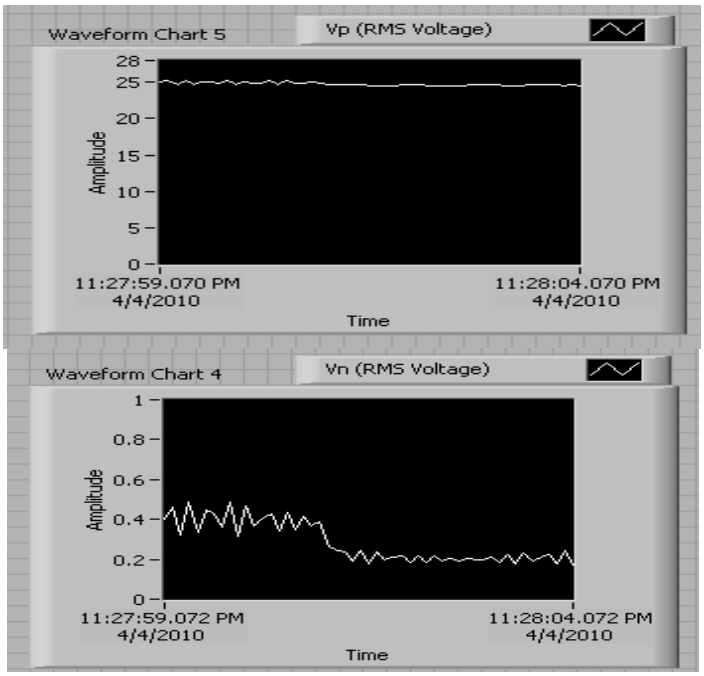

Figure 4.5. Neutral and terminal third harmonic voltages with 6% fault.

4.3 Effect of winding to ground coupling capacitance

Coupling capacitance that we are going to discuss here is the capacitance between the stator winding and the machine body. The electrical field from the winding creates different potentials between the winding and the machine frame. With the existence of the winding insulation the frame stores opposite electric charges like a capacitor. When the machine frame is grounded, capacitive current will flow to ground.

In order to modify the lab generator to act like a large generator, the machine's third harmonic voltage model shown in Figure 4.1 was studied and the voltage transfer function was derived.

$$\frac{V_{n3}}{V_{T3}} = \frac{C_T}{C_N}\left(\frac{s}{s + \frac{1}{R_n C_n}}\right) \tag{4.1}$$

From the transfer function, to increase neutral third harmonic voltage (V_{n3}), we needed to increase terminal capacitance to neutral capacitance ratio. In other words, capacitance should be added at the terminal side. As a result, one large capacitor of value 1μF was added to each phase terminal as shown in Figure 4.6. The new topology was simulated in FEA as shown in Figure 4.7. The change made in topology led to a significant increase in neutral third harmonic voltage and we began to see the stator ground fault characteristics at 6% fault and through 50 Ω fault resistance. The experimental results are also shown in Figure 4.8.

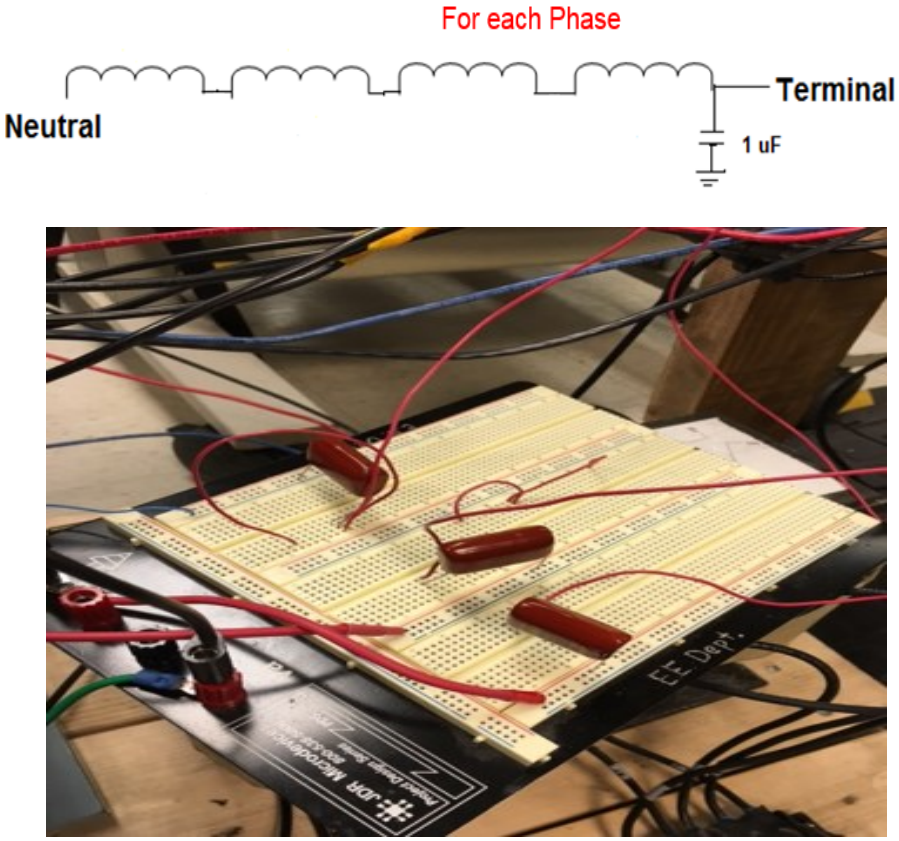

Figure 4.6. Capacitors added to the machine terminals.

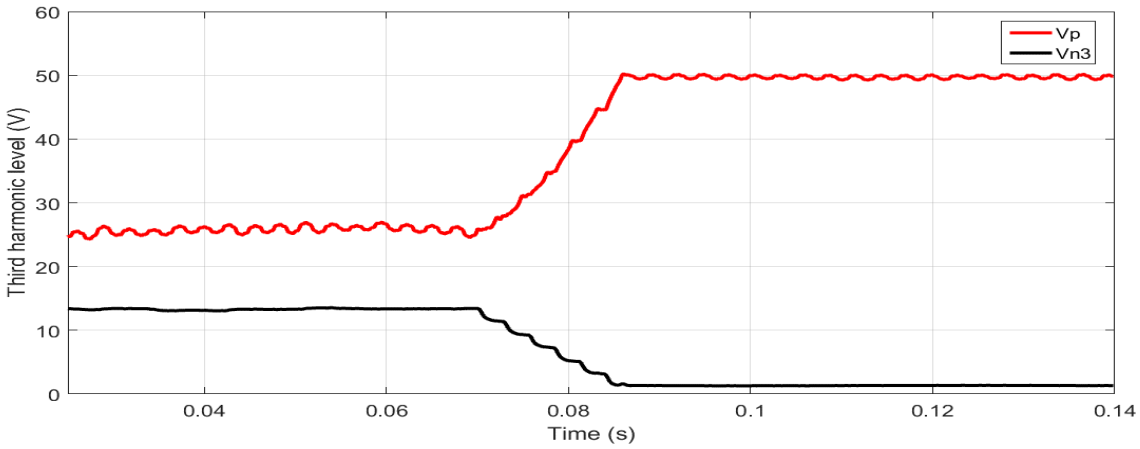

Figure 4.7. 2D FEA simulation for 6% fault.

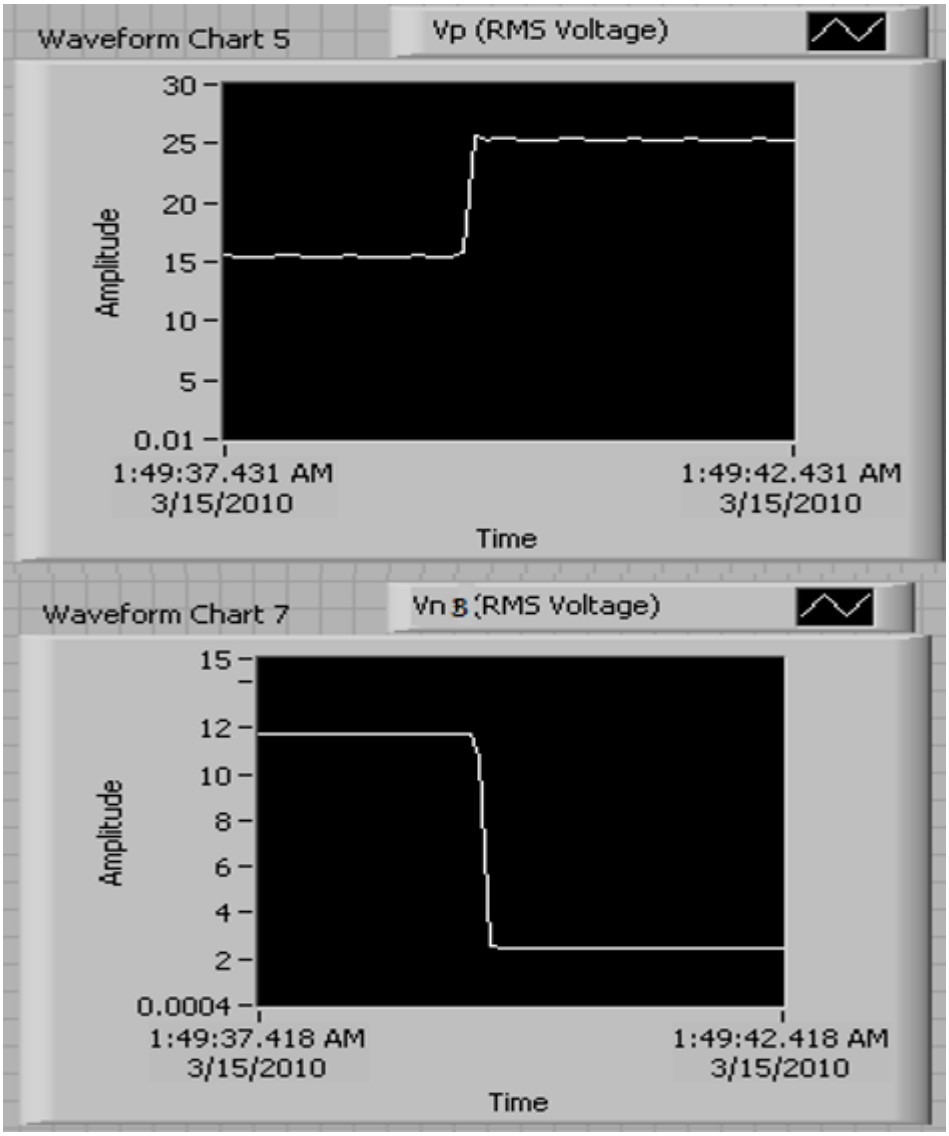

Figure 4.8. Experimental results of 6% fault.

Where V_p is the sum of all three phases third harmonics and V_{n3} is the neutral third harmonic. The difference between the simulated and experimental results is due to 2D FEA errors. 2D simulation does not take account of the end winding effect and rotor skewing.

4.4 Power factor and loading effects

One of the attractive features of synchronous generators is the ability to change the power factor of their output. Synchronous machines sometimes are used as a condenser to correct the power factor of the electrical system. That can be done by adjusting the machine excitation field so they operate in over-excited mode with a leading power factor. However, over-exciting the synchronous generators as well as loading them will saturate the machine which will change the reluctance of the rotor core and increase the harmonics generation in the machine. Therefore, third harmonic amplitude in the machine will be affected by changing the power factor and loading. Figures 4.9 and 4.10 show how the third harmonic levels of the terminal and neutral voltages varies with the variation in the power factor and loading. The data was collected by doing several tests on the generator test bed.

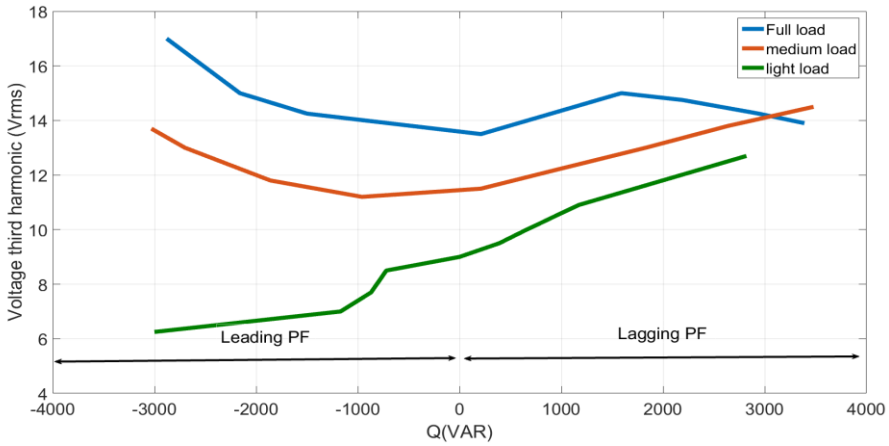

Figure 4.9. Terminal 3rd harmonic voltage with load and power factor variations.

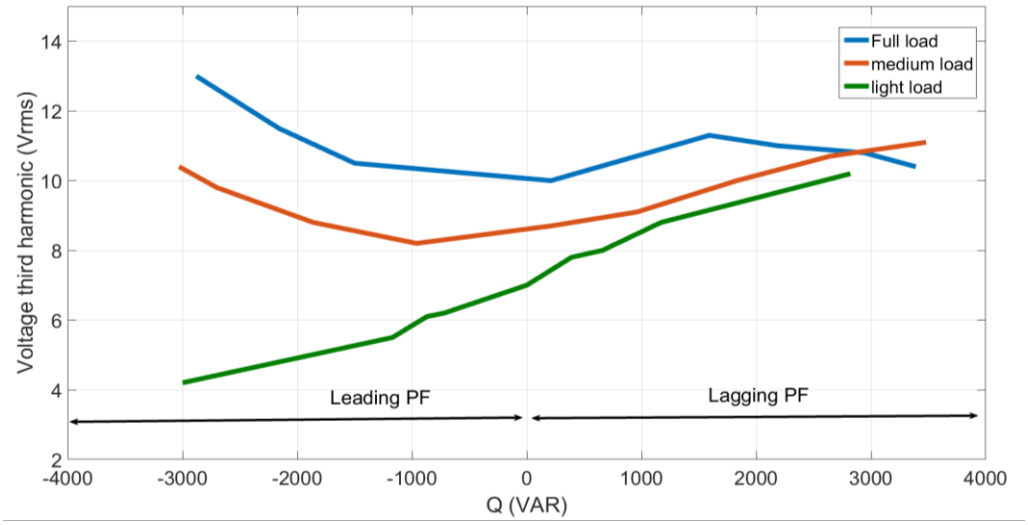

Figure 4.10. Neutral 3rd harmonic voltage with load and power factor variations.

The previous two graphs illustrate that the third harmonics are at maximum when the machine is fully loaded and over-excited (leading PF). In this condition, the machine is highly saturated. On the other hand, the third harmonics do not change much with different loading conditions when the PF is highly lagging. In this case, the generator is consuming reactive power rather than generating it.

4.5 Experimental results

In order to tune the experimental setup, many tests were performed for different fault locations, different load conditions and different power factors. The terminal and neutral third harmonic voltages were collected and applied to third harmonic

ratio protection scheme algorithm used in industry. This algorithm will detect fault [50] if:

$$\left|\widetilde{V_{n3}} - \rho\widetilde{V_{t3}}\right| > 64G2p \tag{4.2}$$

$$\rho = \left[\frac{1}{M}\sum_{i=1}^{M}\widetilde{V_{t3}}\,(i)\right]^{-1}\left[\frac{1}{M}\sum_{i=1}^{M}\widetilde{V_{n3}}\,(i)\right] \tag{4.3}$$

Where 64G2p is the relay restrain value and M is number of samples taken to calculate ρ. The relay manufacturer recommends gathering field data of the third harmonic voltage magnitudes at different generator operation conditions to calculate 64G2p and ρ [50]. The data should be collected for different loading conditions and different power factors. After performing the recommended tests on setup generators the value for 64G2p was set to 5 and ρ to 0.8. The following figures show different faults data recorded and the protection scheme response for such faults. Most of these faults were performed at the neutral point vicinity where the reliability for the scheme is questionable.

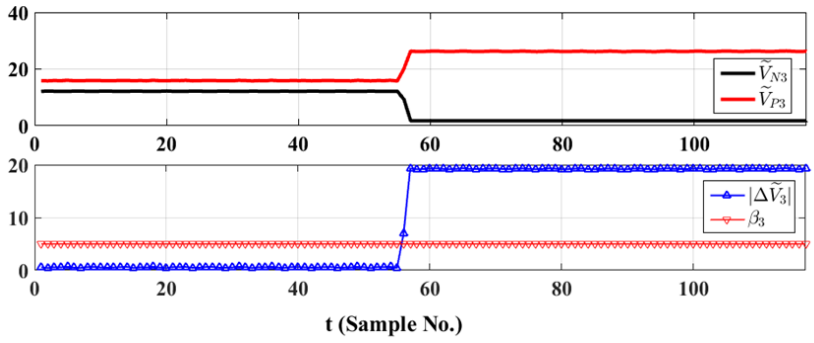

Figure 4.11. Fault at neutral point, PF= 0.85 lagging.

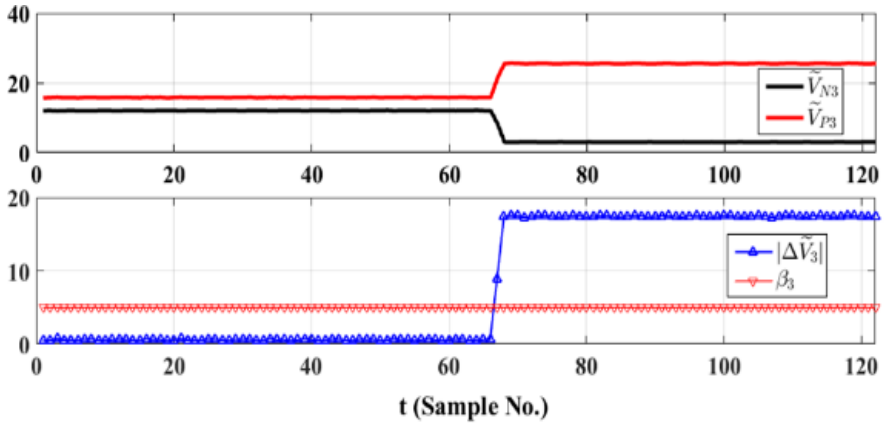

Figure 4.12. Fault at 6%, PF= 0.85 leading.

Where ΔV_3 in the graph is the change in Vn3/Vp3 ratio and β_3 is the restrain value 64G2p. From the previous two graphs it is clear that the protection scheme detects the faults which mean that the change in the neutral third harmonics ratio is sufficient to rise above the restrain value β_3. That proved the availability of the scheme. In order to test the reliability of the scheme, a disturbance in the system was created by reducing the output of the measurement potential transformers to 50% (neutral side) which simulated PT's failure. The response of the scheme was recorded as shown in Figure 4.13.

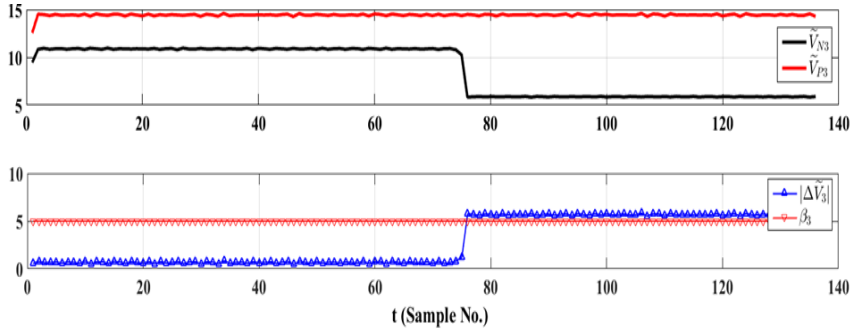

Figure 4.13. Protection scheme response under system disturbance.

Due to the disturbance, the neutral third harmonic voltage was reduced and the terminal third harmonic voltage remained constant. As a result, the third harmonic ratio changed to a value above the restrain value β_3 which triggered the protection scheme. If such a case happened in the real world, a generator would trip leading to unnecessary losses. Such a reliability problem has encouraged many protections companies to look for an option to make the scheme more adaptive or look for other more secure schemes. Many new adaptive schemes have been published but they are still in the verification stage and have not been adopted in industrial relays yet.

4.6 Summary and conclusion

The third harmonic ratio scheme faces many challenges that lead it to lose reliability. The machine third harmonic is affected by many other factors besides stator ground faults. These factors include the machine voltage third harmonic level, the loading of the machine, the operation power factor, and the machine coupling capacitance between the windings and the ground.

The third harmonic level of the machine should be sufficient to produce enough third harmonic current to pass through the winding-ground coupling capacitance. That level depends on the machine design and stator winding layout hence winding factor.

In addition, winding-to-ground coupling capacitance value has a major effect on the stator ground fault. The value of capacitance controls the capacitive current flowing from the winding to ground. The generator third harmonic model transfer function

illustrates that to increase neutral third harmonic voltage, we need to increase the capacitance of the terminal side compared to the neutral side.

Over-exciting the synchronous generators as well as loading them will saturate the machine which will change the reluctance of the rotor core and increase the harmonics generation in the machine. Therefore, third harmonic amplitude in the machine will be affected by changing the power factor and loading.

In lab experiments, the third harmonic ratio protection scheme performed positively in detecting the stator ground fault close to the neutral point. On the other hand, it did not show reliable performance under system disturbances.

5. STATOR GROUND FAULT DETECTION USING WAVELET THEORY

5.1 Introduction and background

Since the eighties, wavelet transform has gone through many stages of development and become a powerful tool in the signals and pattern recognition field. Wavelet has been used in the fields where the Fourier transform doesn't give enough information. Fourier transform works for periodic signals yielding the type and amplitude of frequencies that create that signal without any information about the time aspect. As a result, any transient contribution to the signal will be missed. Fourier transform is defined by [51]:

$$f(\omega) = \int_{\mathbb{R}} f(x) e^{-i\omega x}\, dx \tag{5.1}$$

Unlike the Fourier transform, wavelet transform extracts the time and frequency content of the signal. However, determining frequency and time together at the same instant is not possible because of the Heisenberg uncertainty relation which states that looking at high frequencies will lead to less time resolution and looking at a long period of time will lead to less frequency resolution.

Wavelet breaks a signal down into scaled and shifted functions called mother wavelet. The feature of shifting the mother wavelet along the length of sampled data provides the time information of the original signal. At the same time, scaling (dilations)

the mother wavelet provides the frequency information of the original signal. For each section while shifting and scaling the mother wavelet, correlation coefficients between the mother wavelet and the original signal are calculated. Wavelet transform can be defined by [52]:

$$W_\psi f(a,b) = \int_{\mathbb{R}} f(x) \frac{1}{\sqrt{a}} \psi\left(\frac{x-b}{a}\right) dx \tag{5.2}$$

Where $\psi\left(\frac{x-b}{a}\right)$ is the mother wavelet, a is the scaling parameter, and b is the shifting parameter. Therefore, changing parameter a, changes the mother wavelet scale. Besides, changing parameter b, makes the mother wavelet change its location. Depending on application, there are many different mother wavelets to choose from, as shown in Figure 5.1

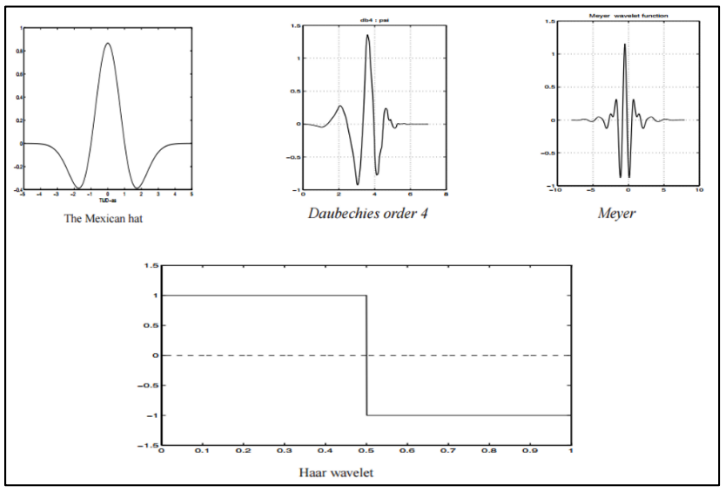

Figure 5.1. Examples of mother wavelet functions.

5.2 Application to synchronous generator stator winding ground fault

As discussed previously, stator ground fault characteristic are affected by many factors. The variation in these factors gives the voltage waveforms irregularity which makes it harder to find unique parameters that can define stator ground fault in comparison with other system transients. Since the wavelet transform has the capability to provide a time frequency representation of the signal, it would be a good choice to decompose the voltage signal and extract the unique features of the stator ground fault that discriminate it from normal transient operations. It has the ability to capture the dynamic features of the fault using its shifting and scaling characteristics.

Generally, relays algorithms are based on detecting the faults and after that classifying the type of fault. Stator ground fault detection is done by obtaining two main factors- the wavelet transform's coefficients (signal decomposition), and the fault unique features (feature extraction). After that comes the classification stage to determine if the features belong to a healthy or faulty case. We will talk about these stages in detail in the upcoming three sections.

5.2.1 Signal decomposition

Synchronous Generator voltage signals are affected by many factors such as machine design, the loading of the machine, and the operation power factor. That makes the different time-domain signals not sufficient. Then, the wavelet transform is used to

change the time signals to time-frequency domain signals. When the fault occurs the wavelet will show distinct coefficients values in different frequency bands [53]. For decomposition of the generator voltage signal, Harr wavelet mother function (db1) at three decomposition levels shown in Figure 5.2 was chosen.

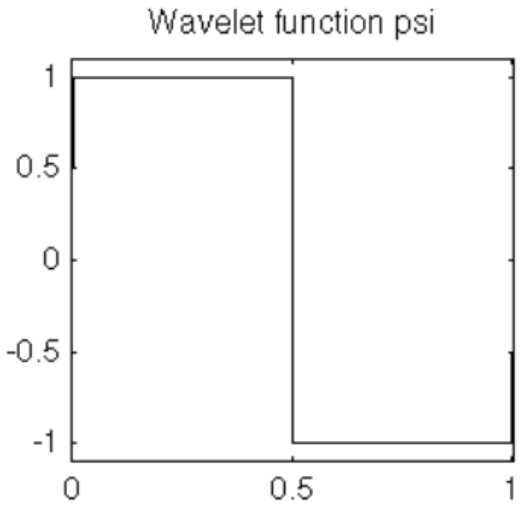

Figure 5.2. Harr wavelet mother function.

The decomposition process depends on four main factors; sampling frequency, window length, the levels of decomposition, and wavelet mother function [53]. For the test setup, 20 kHz was chosen to include higher harmonics in the voltage signal. A 3 level of decomposition was enough to get discriminated coefficients. Going for a higher level would increase simulation time without any additional benefits. Harr mother wavelet is one of Daubechies waveforms which is known for its accuracy of detection for low amplitude signals, short duration and fast decay [53].

5.2.2 Feature extraction

The idea behind the feature extraction stage is finding the unique signal features which, in this case, include the faulted voltage signal in comparison with the healthy case. Also, this stage helps to reduce the amount of data obtained from the signal decomposition stage hence less time and effort is necessary to distinguish the change in signal parameters.

After trying many feature extraction methods, Shannon Entropy method was chosen. Shannon Entropy is used to calculate the signal energy content and can be defined by:

$$F(d) = -\sum_{i=1}^{n} d_i^2 \log(d_i^2) \tag{5.3}$$

Where d is the wavelet coefficient vector of length n. The energy content of the generator terminal and neutral voltages will be calculated and compared before and after stator ground fault.

5.2.3 Classification

Classification is used here to categorize the output of the feature extraction stage to faulted or un-faulted. In order to achieve that, the classification algorithm should be trained first to isolate the faulted and non-faulted signals. The fault condition is defined

based on a number of experiments. The experiment data are fed into the algorithm for training and testing. This will allow the classification algorithm to determine the stator ground fault energy characteristics and improve its ability to distinguish between the healthy and faulted energy data.

5.3 Experimental results

5.3.1 Wavelet transform fault response

The wavelet transform three stages were applied to the generator voltage signals. The signals examined in the test were the generator terminal and neutral voltages at healthy condition and faulty condition. The faults were initially applied to different locations of the winding close to neutral point 3-9% and then applied to the rest of the windings. Also, the fault resistances varied at the different fault locations. The data samples fed to the algorithm were divided into groups of 334 samples which represent one period of the voltage waveforms. The energy of each group was calculated and plotted. Figure 5.3 show how the energy plot of the voltage signals change when applying fault on 6% of phase 'c' winding after the 5^{th} sampling window. Figure 5.4 show the neutral voltage energy curve before and after fault. From those two graphs, the energy of the signal had significant change after the fault, especially the faulted phase. The faulted phase energy was reduced and the other phases and neutral's energy increased in a behavior similar to the fundamental voltage behavior under winding fault. The generator was

further tested by applying stator ground faults in different locations (0-9% of stator winding) with different fault resistance. The fault energy characteristics were the same. Although the faults are close to the neutral point, the change in energy is observable.

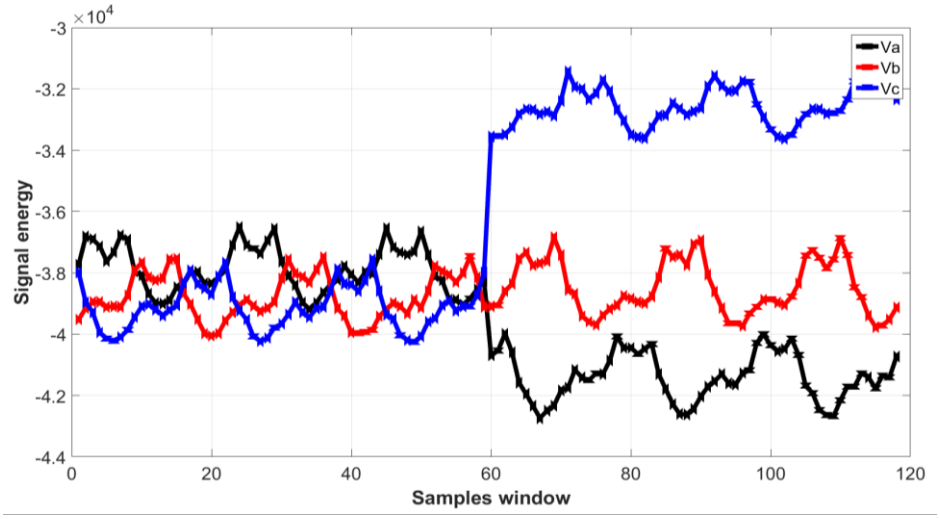

Figure 5.3. Terminals voltage signals energy before and after stator fault.

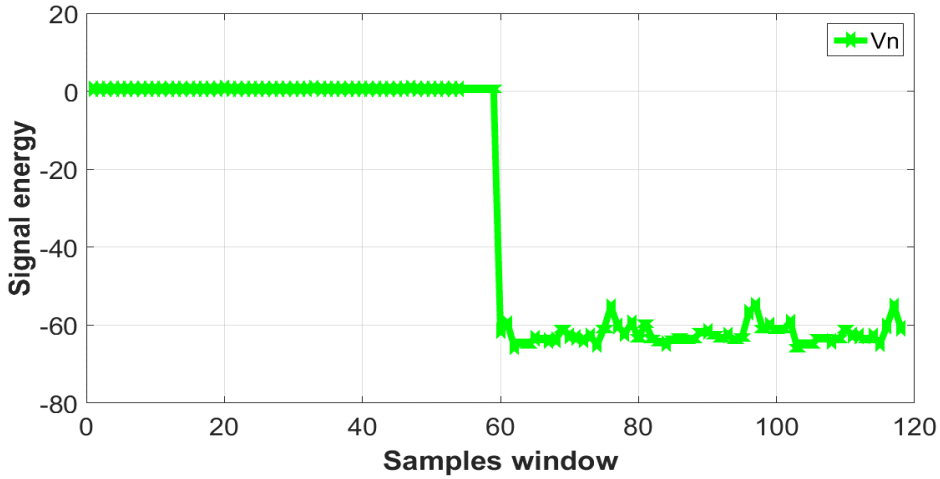

Figure 5.4. Neutral voltage signal energy before and after stator fault.

Since the faults at the neutral vicinity had unique characteristics, it is reasonable to apply the algorithm to faults located in the other parts of the windings (10-100%). Therefore, two faults were applied at the middle point of phase ‘c’ windings and at the terminal of phase ‘c’. The algorithm responses were recorded and are shown in Figures 5.5 to 5.8.

Both faults reflect the stator ground fault characteristics, where the faulted phase voltage energy was reduced and the other un-faulted phases voltages energy increased. All of these tests results are proof that by using wavelet transform theory 100% of the stator windings can be protected from stator ground faults. The change patterns of the energy of the generator voltage signals are a very good indication of faults at the stator windings.

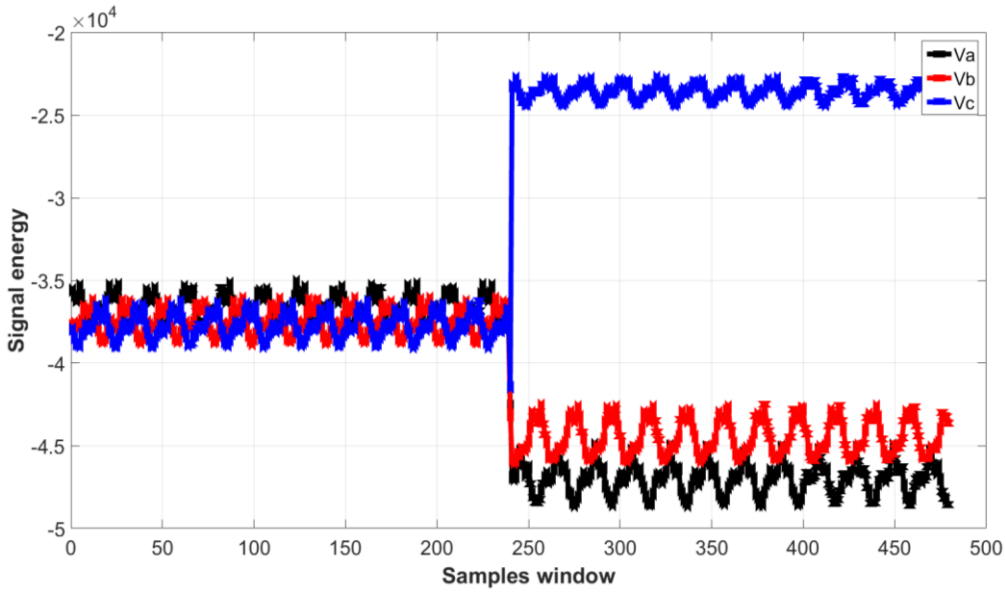

Figure 5.5. Phases voltage energy response for 50% fault in phase 'c'.

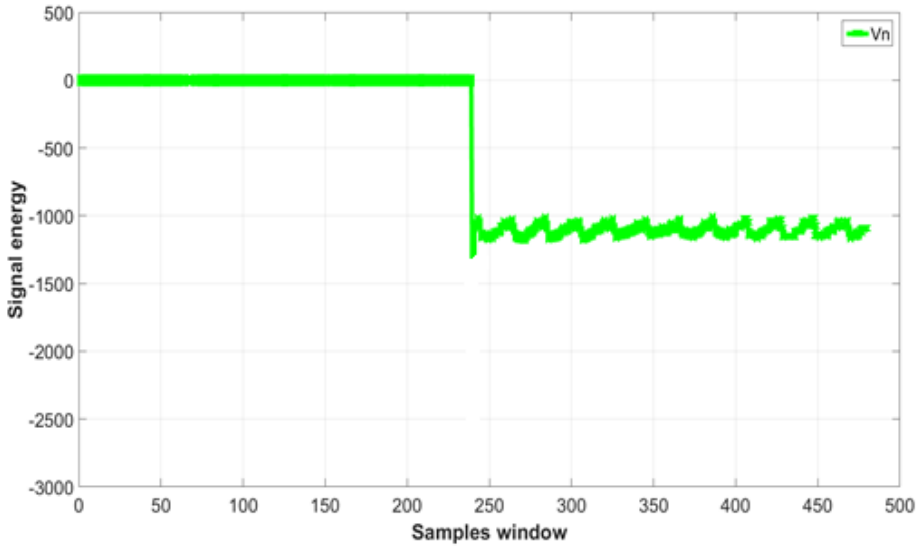

Figure 5.6. Neutral voltage energy response for 50% fault in phase 'c'.

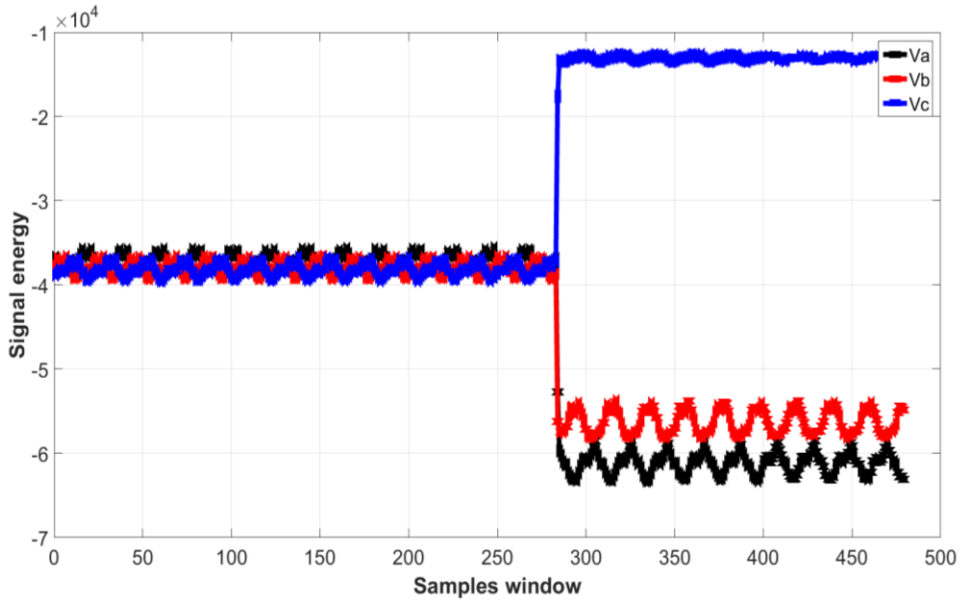

Figure 5.7. Phases voltage energy response for 100% fault in phase 'c'.

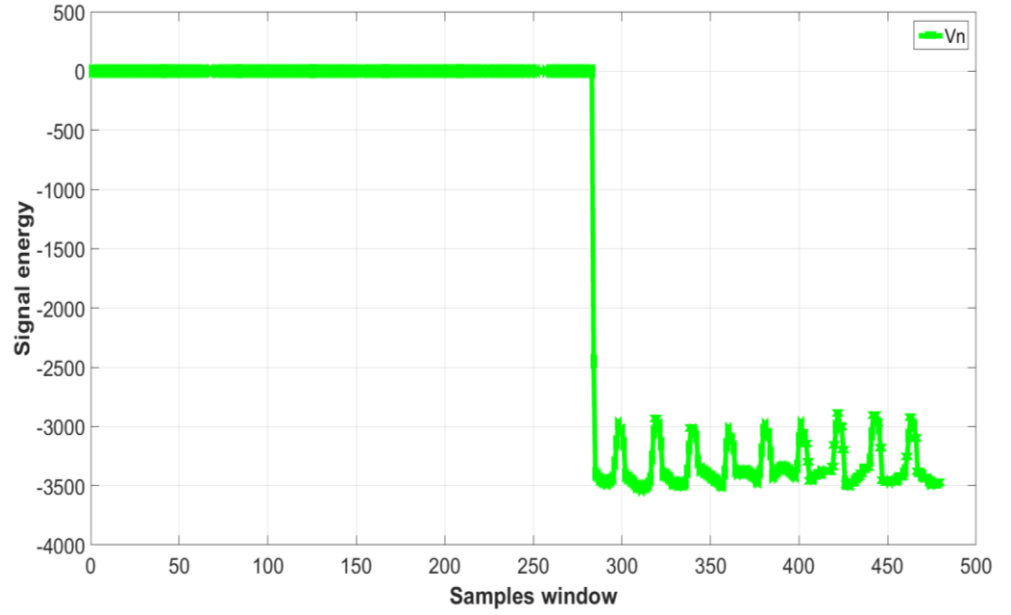

Figure 5.8. Neutral voltage energy response for 100% fault in phase 'c'.

5.3.2 Loading change effects

In Section 4 we discussed how the loading changes the generator performance by changing the level of saturation inside the machine. These changes challenged the reliability of the available protection schemes and exposed their weaknesses. Therefore, in order to test the wavelet protection algorithm reliability, loading disturbance tests were performed on the generator. The generator loading was reduced suddenly from full load (13 A) to very light load (1 A). The excitation was adjusted to keep the generator voltages at rated value and the power factor was kept at unity. The voltage signals energy data were calculated and the results are shown in Figures 5.9 and 5.10.

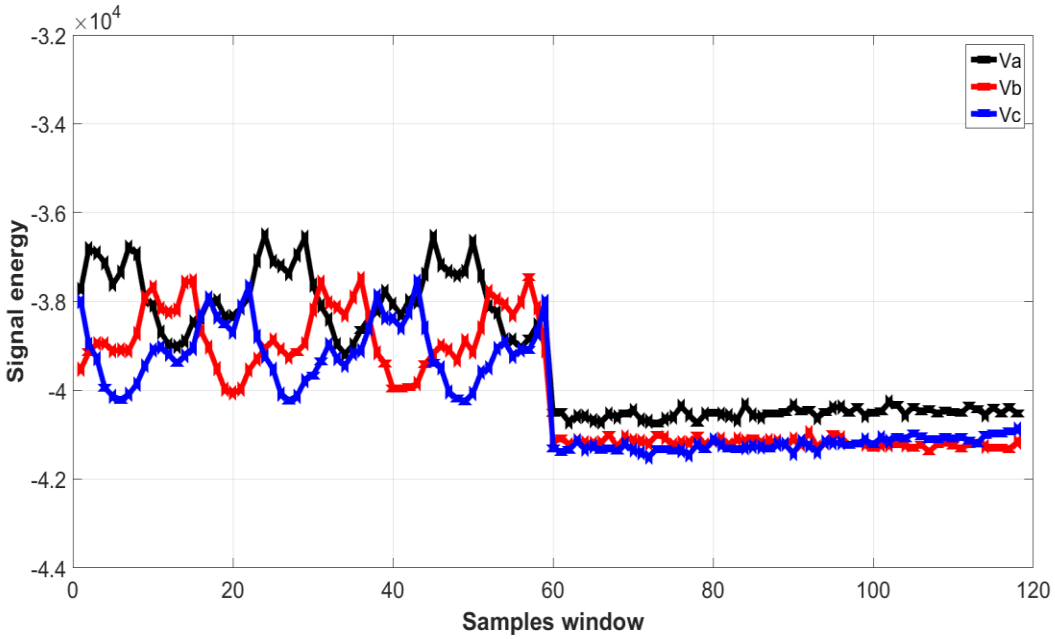

Figure 5.9. Loading effect on voltage signal energy.

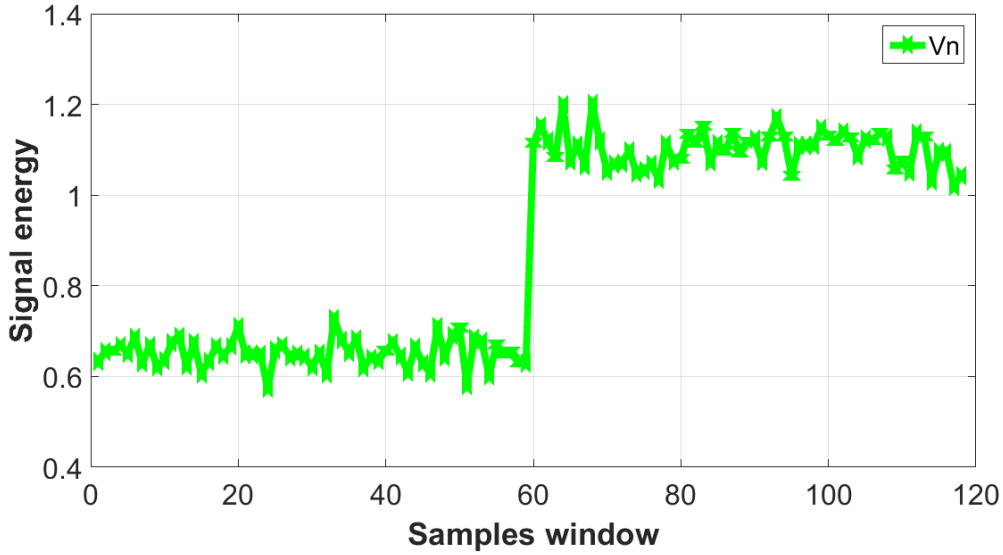

Figure 5.10. Effect of loading on neutral voltage signal energy curve.

The energy curves for the voltages show a drop in the energy content of the machine's phase voltage signals and an increase in neutral voltage energy. However, the drop for all three phases signals energy is the same and the energy values are still close to each other. That is because the three phases are still symmetrical even after the load drop. On the other hand, the energy curves become more stable at small load. That is because the harmonic content of the voltage signals is smaller in small loads, hence more symmetrical. The more symmetric the three phases voltage waves get, the closer the energy components become. Since the energy curve behavior at load change is different from their behavior at fault, it cannot be confused with the fault response. That reflects the wavelet method robustness against load change. However, this response by itself can be utilized to be an indication of load loss.

5.3.3 Power factor change effects

Power factor changes are a normal feature of a power system. These changes are imposed by the system loads changes. However, sometimes power factor change is a source of failure for the available protection scheme. As a result, the generator was tested under different values of power factor. The generator voltages data at 0.84 lagging power factor and 0.84 leading power factor were collected and fed to the wavelet algorithm. The excitation was adjusted to keep the generator voltages at rated value and the power factor was changed from unity to 0.84 lagging and then from unity to 0.84 leading. The outcome of the algorithm is shown below in Figures 5.11-5.14.

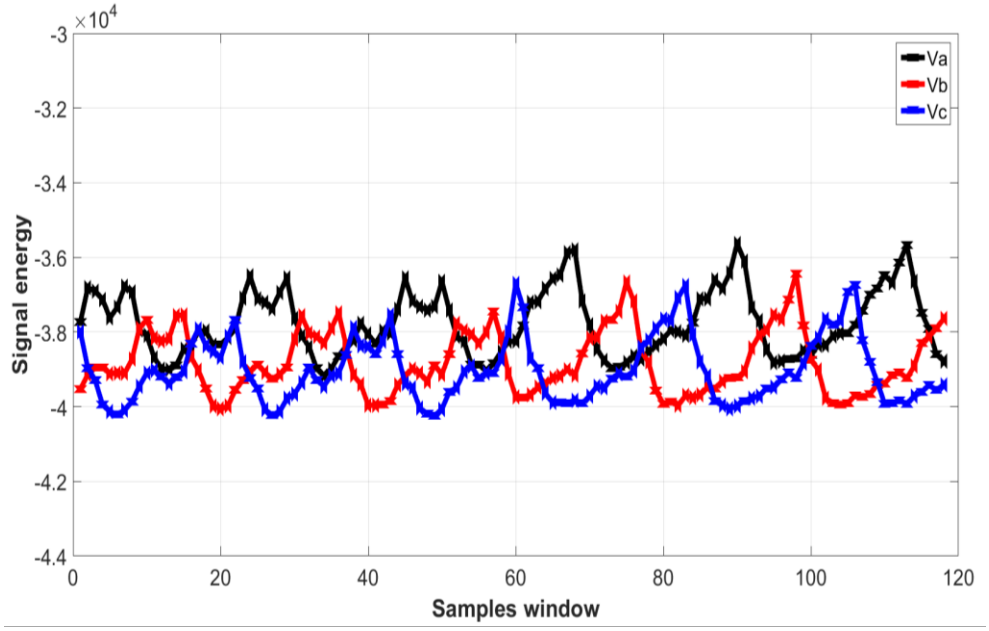

Figure 5.11. Power factor change (1to 0.84 lagging) effect on phase energy.

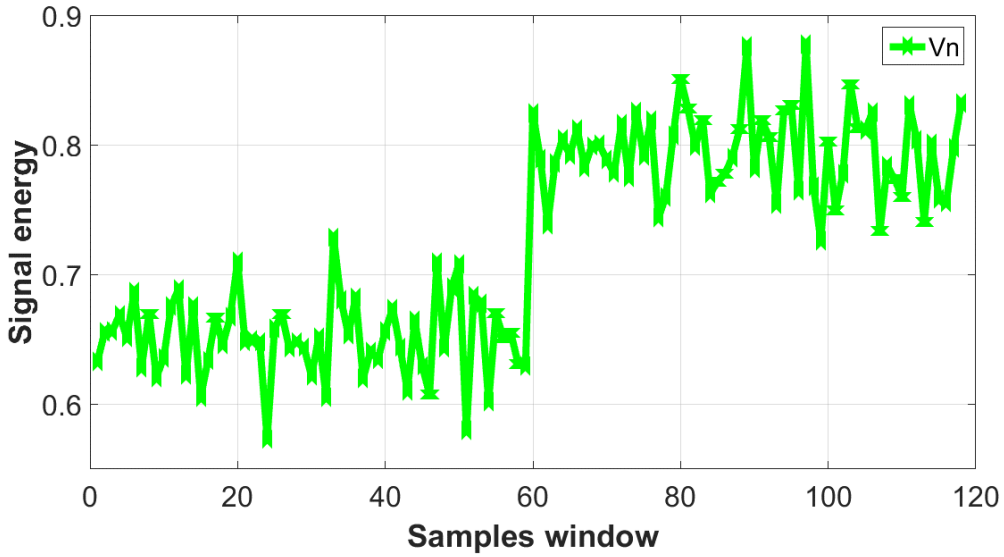

Figure 5.12. Power factor change (1to 0.84 lagging) effect on neutral energy.

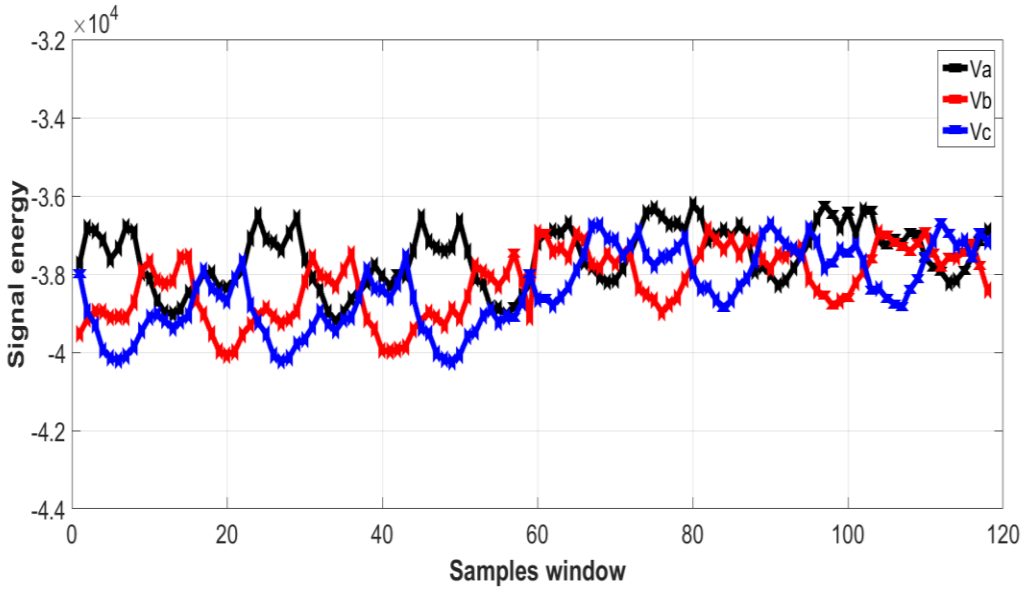

Figure 5.13. Power factor change (1to 0.84 leading) effect on phase energy.

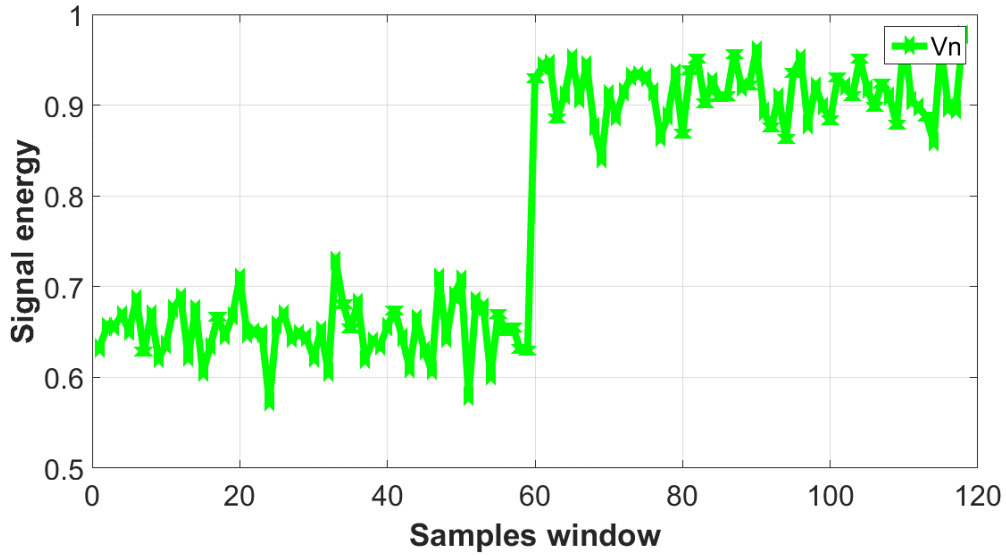

Figure 5.14. Power factor change (1to 0.84 leading) effect on neutral energy.

Changing the power factor from unity to 0.84 lagging enlarged the 3 phases signal energy equally by a factor of 1.03. Besides, changing the power factor from unity

to 0.84 leading reduced the 3 phases signal energy equally by a factor of 1.01 with a small upward shift while the neutral voltage signal energy increased in both cases. All the energy changes due to power factor change affected the entire three phases at the same level. The previous figures illustrate the relation between the power factor value and the magnitude of the signal energy. The simultaneous effect on the three phases energy curve is a reflection of the fact that the changing power factor in the machine is affecting the three phase voltages in the same manner. Since the changes in the three phases are the same and the neutral voltage energy is increased, we can conclude that the behavior of the power factor change is different from the behavior in the fault condition. Thus, detecting faults using wavelet transform is robust against changes in the power factor.

5.3.4 Disturbance effects

Power systems are known for their instability. Some of this instability occurs due to transient disturbances which decay with time. However, sometimes this transient disturbance alters some features that are monitored by protection relays. If these transients remain longer than the relay's waiting time it will be translated as a fault in the system and lead to unnecessary trips, hence unnecessary loss of power. One of the tests performed to check the reliability of the wavelet transform method is the disturbance test. A disturbance was created similar to the disturbance applied to the third harmonic ratio scheme in Section 4 where the neutral transformer was shorted at 50% of its primary

winding. The disturbance was applied at the 470th sampling window. The response of the algorithm is shown in Figures 5.15 and 5.16.

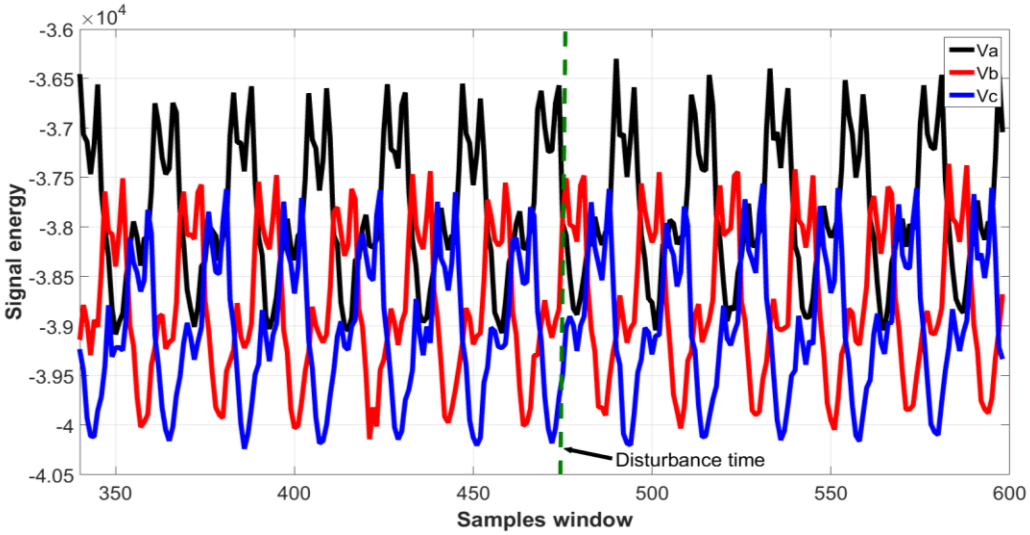

Figure 5.15. Phases energy curve response to neutral disturbance.

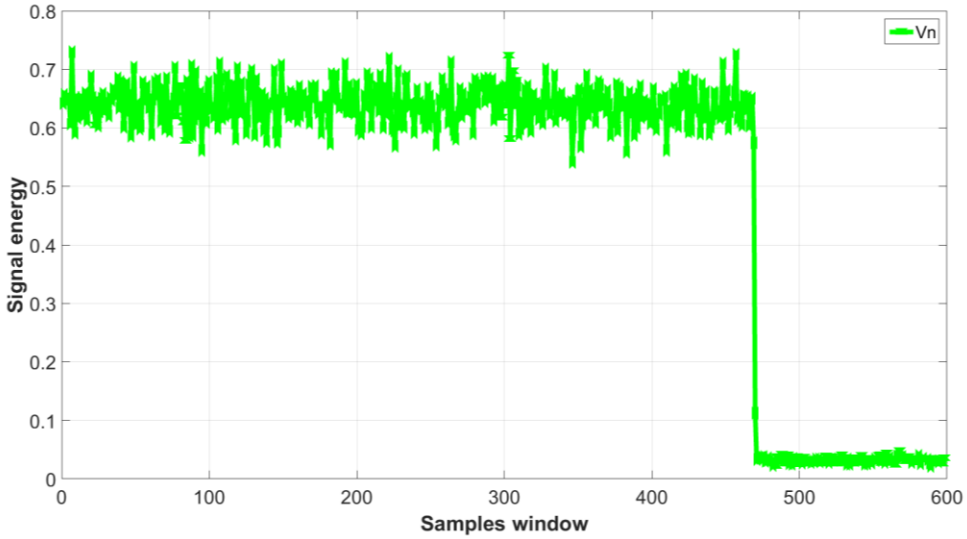

Figure 5.16. Neutral energy curve response to neutral disturbance.

In response to the disturbances the energy curve of neutral voltage signal was reduced and the three phases' voltages energy curves experienced a very small gain (about 1.004). The gain was equal in all the three phases while the neutral voltage energy was reduced to almost zero due to the reduction in the neutral voltage waveform's magnitude. Again, the change happened equally in the three phases voltage energy which is different from the winding ground fault characteristics. The algorithm showed robustness against the system disturbance. The reduction in the energy of the neutral voltage signal and the simultaneous rise in the three phases voltages signals can be considered as indications of a fault at the neutral transformer.

5.4 Summary and conclusion

The wavelet transform became a powerful tool in the signals and pattern recognition field. Unlike the Fourier transform, the wavelet transform extracts the time and frequency content of the signal. It breaks signals down into scaled and shifted functions called mother wavelets.

Since, wavelet transform has the capability to provide a time frequency representation of the signal, it would be a good choice to decompose the voltage signal and extract the unique features of the stator ground fault that discriminates it from normal transient operations. Wavelet transform fault detection is based on finding the wavelet transform's coefficients (signal decomposition), and finding the fault unique features (feature extraction).

Tests were applied on a synchronous generator focusing on terminal and neutral voltages at healthy condition and faulty condition. The faults were applied to different locations of the winding close to neutral point 3-9% initially and then applied to the rest of the windings. All faults reflected the stator ground fault characteristics, where faulted phase voltage energy was reduced and the other un-faulted phase voltages energy increased. All of these test results are proof that by using wavelet transform theory 100% of the stator windings can be protected from stator ground faults.

It has been proved that the energy curves behavior at system disturbances, like load change, power factor changes, and other types of faults, are different from their behavior at stator ground fault. As a result, it cannot be confused with the fault response which reflects the wavelet method robustness against these disturbances.

6. CONCLUSION AND FUTURE WORK

6.1 Conclusion

In this dissertation, a lab synchronous generator was adapted to model large generators in power systems. A small power system was created in the lab to mimic a real power system. The generator stator windings were adjusted to insert tabs in different locations close to the neutral point. Windings tabs were connected through switches to resistors that represent fault resistance to simulate stator winding ground faults. Using a LABVIEW platform, the generator voltages were measured and exported to carry out different analysis on these data.

A new linear coupled magnetic circuit model was developed for salient pole synchronous generator with the generator voltages as outputs. A modified winding function approach was implemented to use the geometry and the physical layout of the generator windings in calculating the different generators inductances during healthy and faulted operations. Based on these inductances, the generator dynamic differential equations were arranged to output the generator voltages. The outputs of the developed model were compared with the FEA analysis and we found that the model results matched the FEA results.

The challenges that face the third harmonic ratio scheme were discussed. These include the third harmonic level of the machine which should be sufficient to produce enough third harmonic current to pass through the winding-ground coupling capacitance.

In addition, winding to ground coupling capacitance value has a major effect on stator ground fault. The value of capacitance controls the capacitive current flowing from the winding to ground. On the other hand, over-exciting the synchronous generators as well as loading them will saturate the machine which changes the reluctance of the rotor core and increases the harmonics generation in the machine. Therefore, third harmonic amplitude in the machine will be affected by changing the power factor and loading. In lab experiments, the third harmonic ratio protection scheme performed positively in detecting stator ground fault close to neutral point. On the other hand, it did not show reliable performance under system disturbances.

Finally, wavelet transform application in stator ground faults protection was presented. A fault detection algorithm using wavelet was applied to a synchronous generator focusing on terminal and neutral voltages at healthy and faulty conditions. The faults were applied to different locations of the winding close to neutral point 3-9% initially and then were applied on the rest of the windings. All faults reflected stator ground fault characteristics where faulted phase voltage energy was reduced and the other un-faulted phases voltages energy increased. All of these test results are proof that by using wavelet transform theory 100% of the stator windings can be protected from stator ground faults. It was proved that the energy curves behavior at system disturbances, like load change, power factor changes, and other types of faults, are different from their behavior at stator ground fault. As a result, it cannot be confused with the fault response that reflected the wavelet method robustness against these disturbances.

6.2 Future work

As for future work, the following problems are worth investigation:

1. Extending the generator model to include leakage inductances and the damper windings.
2. Using the wavelet transform method to detect the location of the fault inside the machine windings.
3. Testing the wavelet protection method response in case of parallel generators.
4. Use the artificial intelligent method such as neural network for the fault type and fault location classification.

REFERENCES

[1] L. J. Powell, "The impact of system grounding practices on generator fault damage," in *IEEE Transactions on Industry Applications*, vol. 34, no. 5, pp. 923-927, Sep/Oct 1998.

[2] I. Megahed and O. P. Malik, "Synchronous generator internal fault computation and experimental verification," in *IEE Proceedings - Generation, Transmission and Distribution*, vol. 145, no. 5, pp. 604-610, Sep 1998.

[3] J. C. Das and E. Perich, "13.8-kV Selective High-Resistance Grounding System for a Geothermal Generating Plant—A Case Study," in *IEEE Transactions on Industry Applications*, vol. 49, no. 3, pp. 1234-1243, May-June 2013.

[4] H. Yang, B. Jiang, V. Cocquempot, Y. Zhang, and H. Gong, "Tolerance of intermittent controller faults via hybrid system approach," *8th IFAC Symposium on Fault Detection, Supervision and Safety of Technical Processes*, Mexico, August 2012, pp. 836-841.

[5] S. Muller, M. Deicke and R. W. De Doncker, "Doubly fed induction generator systems for wind turbines," in *IEEE Industry Applications Magazine*, vol. 8, no. 3, pp. 26-33, May/Jun 2002.

[6] I. Boldea, L. Tutelea and C. I. Pitic, "PM-assisted reluctance synchronous motor/generator (PM-RSM) for mild hybrid vehicles: electromagnetic design," in *IEEE Transactions on Industry Applications*, vol. 40, no. 2, pp. 492-498, March-April 2004.

[7] R. S. Muñoz-Aguilar, P. Rodríguez, A. Dòria-Cerezo, I. Candela and A. Luna, "Sensor-less Sliding Mode Control of a stand-alone wound rotor synchronous generator with unbalanced load," *IECON 2011 - 37th Annual Conference on IEEE Industrial Electronics Society*, Melbourne, VIC, 2011, pp. 3982-3987.

[8] I. Tamrakar, L. B. Shilpakar, B. G. Fernandes and R. Nilsen, "Voltage and frequency control of parallel operated synchronous generator and induction generator with STATCOM in micro hydro scheme," in *IET Generation, Transmission & Distribution*, vol. 1, no. 5, pp. 743-750, September 2007.

[9] U. Amin, G. Ahmad, S. Zahoor, and F. Durrani, "Implementation of parallel synchronization method of generators for power & cost saving in University of Gujarat," in *Energy and Power Engineering*, vol. 6, pp. 317-332, 2014.

[10] J. Driesen and F. Katiraei, "Design for distributed energy resources," in *IEEE Power and Energy Magazine*, vol. 6, no. 3, pp. 30-40, May-June 2008.

[11] G. Didier and J. Lévêque, "Influence of fault type on the optimal location of superconducting fault current limiter in electrical power grid," in *International Journal of Electrical Power & Energy Systems*, vol. 56, pp. 279-285, March 2014.

[12] C. J. Mozina, "Impact of Smart Grids and Green Power Generation on Distribution Systems," in *IEEE Transactions on Industry Applications*, vol. 49, no. 3, pp. 1079-1090, May-June 2013.

[13] S. Udoetok and A. N. Nguyen, "Grounding resistance for control of static electricity ignition hazards," in *Journal of Electrostatics*, vol. 69, Issue 1, pp. 23-29, February 2011.

[14] N. Luo, H. Li, and H. Zhang, "Research on grounding of shore-to-ship power supply system," in *Journal of Power and Energy Engineering*, vol. 2, pp. 612-615, 2014.

[15] Planas, J. Andreu, J. I. Gárate, I. M. de Alegría, and E. Ibarra, "AC and DC technology in microgrids: A review," in *Renewable and Sustainable Energy Reviews*, vol. 43, pp. 726-749, March 2015.

[16] Z. Fu, N. Wang, L. Huang and R. Zhang, "Study on Neutral Point Grounding Modes in Medium-Voltage Distribution Network," *Computer, Consumer and Control (IS3C), 2014 International Symposium on*, Taichung, 2014, pp. 154-157.

[17] S. A. Saleh, A. S. Aljankawey, R. Meng, C. P. Diduch, L. Chang and J. Meng, "Impacts of grounding configurations on responses of ground protective relays for DFIG-based WECSs," *2014 IEEE/IAS 50th Industrial & Commercial Power Systems Technical Conference*, Fort Worth, TX, 2014, pp. 1-8.

[18] Almasoud and M. Al-Solami, "Jeddah soil resistivity and grounding resistance," in *Journal of American Science*, vol. 10, no. 7, pp. 49-55, 2014.

[19] N. K. Gouvalas, I. F. Gonos, and I. A. Stathopulos, "Impact study of short-circuit calculation methods on the design of a wind farm's grounding system," in *Renewable Energy*, vol. 66, pp. 25-32, June 2014.

[20] M. Polikarpova, P. Lindh, C. Gerada, M. Rilla, V. Naumanen, and J. Pyrhönen, "Thermal effects of stator potting in an axial-flux permanent magnet synchronous generator," in *Applied Thermal Engineering*, vol. 75, pp. 421-429, January 2015.

[21] L. Wang, Y. Zhao, W. Jia, B. Han, Y. Liu, T. Tanaka, et al., "Fault diagnosis based on current signature analysis for stator winding of Doubly Fed Induction Generator in wind turbine," *Electrical Insulating Materials (ISEIM), Proceedings of 2014 International Symposium on*, Niigata, 2014, pp. 233-236.

[22] R. Benabid, M. Zellagui, A. Chaghi, and M. Boudour, "Application of Firefly Algorithm for optimal directional overcurrent relays coordination in the presence of IFCL," in *International Journal of Intelligent Systems and Applications*, vol. 6, no. 2, pp. 44-53, 2014.

[23] R. Caldon, M. Coppo and R. Turri, "Coordinated voltage control in MV and LV distribution networks with inverter-interfaced users," *PowerTech, 2013 IEEE Grenoble*, Grenoble, 2013, pp. 1-5.

[24] W. Zhi, X. Wendong, L. Gang and H. Yongqiang, "Design of data acquisition module based on Compact-RIO," *Information Science, Electronics and Electrical Engineering (ISEEE), 2014 International Conference on*, Sapporo, 2014, pp. 1480-1483.

[25] J. Brown and R. Schaerer, "Parametric analysis and simplified calculations of fault current split for wind power plant grounding system safety design," *2014 IEEE PES T&D Conference and Exposition*, Chicago, IL, USA, 2014, pp. 1-5.

[26] H. Sharma, P. Keebler, F. Sharp, M. Josef and J. Price, "Handling excessive third harmonics in utility systems due to proliferation of non-linear loads," *2012 IEEE Power and Energy Society General Meeting*, San Diego, CA, 2012, pp. 1-7.

[27] L. Wei, Z. Liu, R. J. Kerkman and G. L. Skibinski, "Identifying ground-fault locations: Using adjustable speed drives in high-resistance grounded systems," in *IEEE Industry Applications Magazine*, vol. 19, no. 2, pp. 47-55, March-April 2013.

[28] L. J. Kingrey, R. D. Painter and A. S. Locker, "Applying High-Resistance Neutral Grounding in Medium-Voltage Systems," in *IEEE Transactions on Industry Applications*, vol. 47, no. 3, pp. 1220-1231, May-June 2011.

[29] Qi Li and Guangyu Zhou, "Studies of components configuration of intelligent transformer," *Electricity Distribution (CICED), 2012 China International Conference on*, Shanghai, 2012, pp. 1-5.

[30] Y. Y. Wang, X. J. Zeng, J. B. Jian, Z. Y. Dong, Z. W. Li and Y. Huang, "Studies on the Stator Single-Phase-to-Ground Fault Protection for a High-Voltage Cable-Wound Generator," in *IEEE Transactions on Energy Conversion*, vol. 28, no. 2, pp. 344-352, June 2013.

[31] F. Costa, O. Luukkonen, C. R. Simovski, A. Monorchio, S. A. Tretyakov and P. M. de Maagt, "TE Surface Wave Resonances on High-Impedance Surface Based Antennas: Analysis and Modeling," in *IEEE Transactions on Antennas and Propagation*, vol. 59, no. 10, pp. 3588-3596, Oct. 2011.

[32] K. J. Sagastabeitia, I. Zamora, A. J. Mazon, Z. Aginako and G. Buigues, "Low-current fault detection in high impedance grounded distribution networks, using residual variations of asymmetries," in *IET Generation, Transmission & Distribution*, vol. 6, no. 12, pp. 1252-1261, December 2012.

[33] H. Alatrash, A. Mensah, E. Mark, R. Amarin and J. Enslin, "Generator Emulation Controls for photovoltaic inverters," *Power Electronics and Applications (EPE 2011), Proceedings of the 2011-14th European Conference on*, Birmingham, 2011, pp. 1-10.

[34] P. Pillai, A. Pierce, B. Bailey, B. Douglas, C. Mozina, C. Normand, et al., "Grounding and ground fault protection of multiple generator installations on medium-voltage industrial and commercial power systems II. Grounding methods," *Pulp and Paper Industry Technical Conference, 2003. Conference Record of the 2003 Annual*, Charleston, SC, USA, 2003, pp. 63-70.

[35] X. G. Yin, O. P. Malik, G. S. Hope and D. S. Chen, "Adaptive ground fault protection schemes for turbogenerator based on third harmonic voltages," in *IEEE Transactions on Power Delivery*, vol. 5, no. 2, pp. 595-603, Apr 1990.

[36] D. J. Love and N. Hashemi, "Considerations for ground fault protection in medium-voltage industrial and cogeneration systems," in *IEEE Transactions on Industry Applications*, vol. 24, no. 4, pp. 548-553, Jul/Aug 1988.

[37] T. Nengling, H. Zhijian, Y. Xianggen, L. Xiaohua, and C. Deshu, "Wavelet-based ground fault protection scheme for generator stator winding," *Electric Power Systems Research*, vol. 62, Issue 1, pp. 21-28, 28 May 2002.

[38] D. Reimert, *Protective relaying for power generation systems*. Boca Raton, FL: CRC/Taylor & Francis, 2006.

[39] C. J. Mozina, "Experience with 100% stator ground fault protection schemes," *Conference Record 2009 IEEE Industrial & Commercial Power Systems Technical Conference*, Calgary, AB, 2009, pp. 1-8.

[40] J. P. Nelson, "System grounding and ground-fault protection in the petrochemical industry: a need for a better understanding," in *IEEE Transactions on Industry Applications*, vol. 38, no. 6, pp. 1633-1640, Nov/Dec 2002.

[41] J. P. Nelson and P. K. Sen, "High resistance grounding of low voltage systems: a standard for the petroleum and chemical industry," *Petroleum and Chemical Industry Conference, 1996, Record of Conference Papers. The Institute of Electrical and Electronics Engineers Incorporated Industry Applications Society 43rd Annual*, Philadelphia, PA, 1996, pp. 19-26.

[42] N. A. Al-Nuaim and H. Toliyat, "A novel method for modeling dynamic air-gap eccentricity in synchronous machines based on modified winding function theory," in *IEEE Transactions on Energy Conversion*, vol. 13, no. 2, pp. 156-162, Jun 1998.

[43] J. C. Moreira and T. A. Lipo, "Modeling of saturated AC machines including air gap flux harmonic components," in *IEEE Transactions on Industry Applications*, vol. 28, no. 2, pp. 343-349, Mar/Apr 1992.

[44] M. Babaei, J. Faiz, B. M. Ebrahimi, S. Amini and J. Nazarzadeh, "A Detailed Analytical Model of a Salient-Pole Synchronous Generator Under Dynamic Eccentricity Fault," in *IEEE Transactions on Magnetics*, vol. 47, no. 4, pp. 764-771, April 2011.

[45] S. Nandi, "A detailed model of induction machines with saturation extendable for fault analysis," in *IEEE Transactions on Industry Applications*, vol. 40, no. 5, pp. 1302-1309, Sept.-Oct. 2004.

[46] S. Nandi, "Modeling of Induction Machines Including Stator and Rotor Slot Effects", *IEEE Transactions on Industry Applications*, vol. 40, no. 4, pp. 1058-1065, 2004.

[47] B. Heller and C. Hamata, *Harmonic field effects in induction machines*. New York: Elsevier, 1976.

[48] H. Jiang, R. Aggarwal, G. Weller, S. Ball and L. Denning, "A new approach to synchronous generator internal fault simulation using combined winding function theory and direct phase quantities," *Electrical Machines and Drives, 1999. Ninth International Conference on (Conf. Publ. No. 468)*, Canterbury, 1999, pp. 105-111.

[49] C. Griffin and J. Pope, "Generator Ground Fault Protection Using Overcurrent, Overvoltage, and Undervoltage Relays", *IEEE Transactions on Power Apparatus and System*, vol. -101, no. 12, pp. 4490-4501, 1982.

[50] *SEL-300G Multifunction Generator Relay Instruction Manual*, Schweitzer Engineering Laboratories Inc., Pullman, WA, 2015.

[51] G. Bachman, L. Narici and E. Beckenstein, *Fourier and wavelet analysis*. New York: Springer, 2000.

[52] M. Holschneider, *Wavelets. an analysis toll*. Oxford: Clarendon Press, 1995.

[53] I. Baqui, I. Zamora, J. Mazón and G. Buigues, "High impedance fault detection methodology using wavelet transform and artificial neural networks", *Electric Power Systems Research*, vol. 81, no. 7, pp. 1325-1333, 2011.

APPENDIX

I. Synchronous generator specifications:

Manufacturer	General Electric
Model	5SJ4254Y2Y2
Serial	MF7493B07
Frame	254Z
Rated speed	1800 RPM
Frequency	60 Hz
Rated power	5 kVA
Power factor	0.8
Rated voltage	120/240 V
Phases	3
Rated current	27/13.5 A
Field maximum current	1.2 A
Field rated voltage	125 V
Number of poles	4 Poles
Number of stator slots	48 Slots
Stator slot pitch	7.5^{o}
Stator windings resistance	0.6 Ω/phase
Stator outer diameter	266 mm
Stator inner diameter	175 mm
Stack length	97.35 mm
Rotor windings number of turns	560 turns/pole
Rotor windings connections	Series
Rotor windings total resistance	28 Ω
Rotor outer diameter	174 mm
Shaft diameter	47.5 mm

Rotor Dimensions:

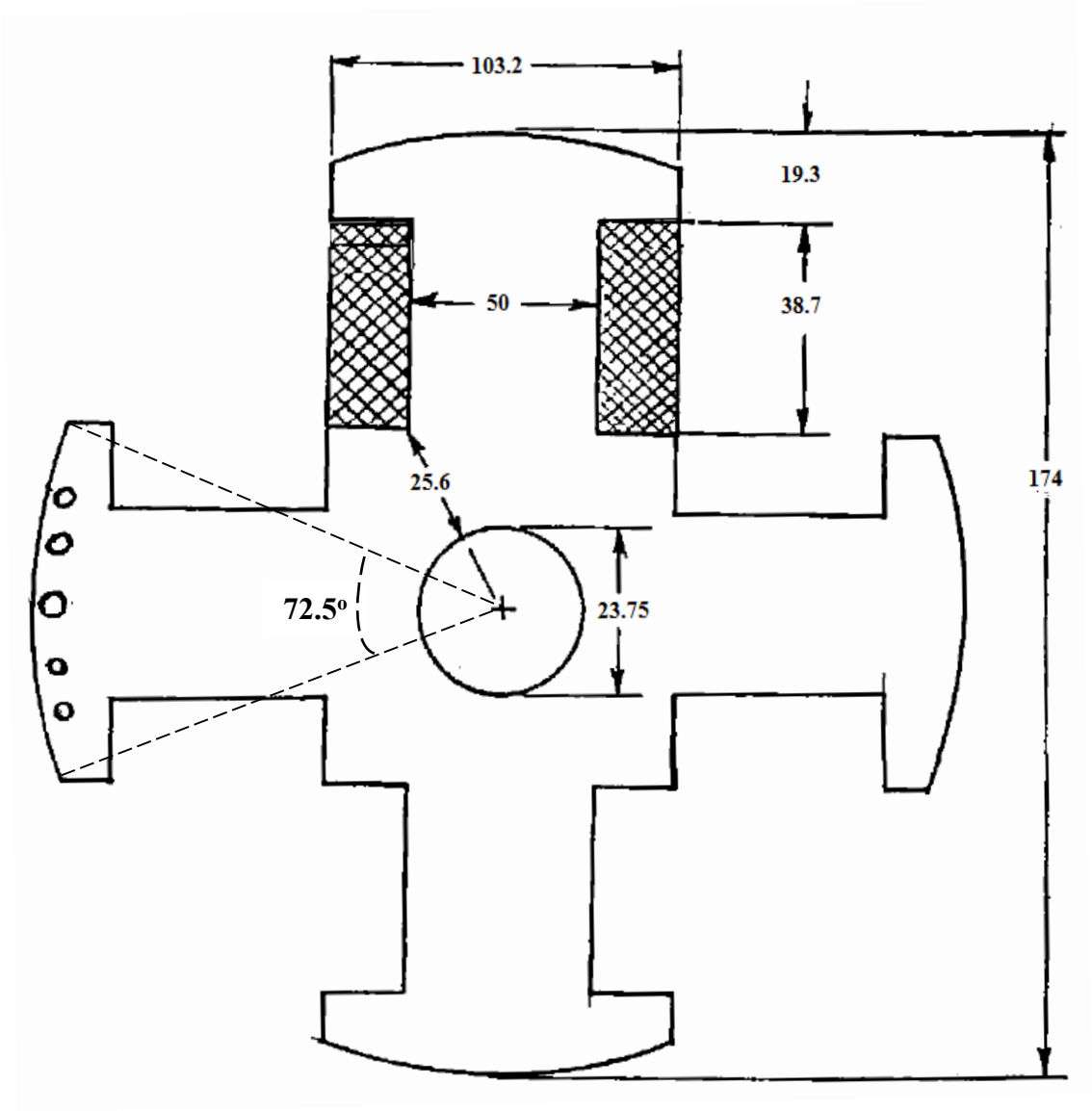

❖ Dimensions are in millimeters.

Stator Slot Dimensions:

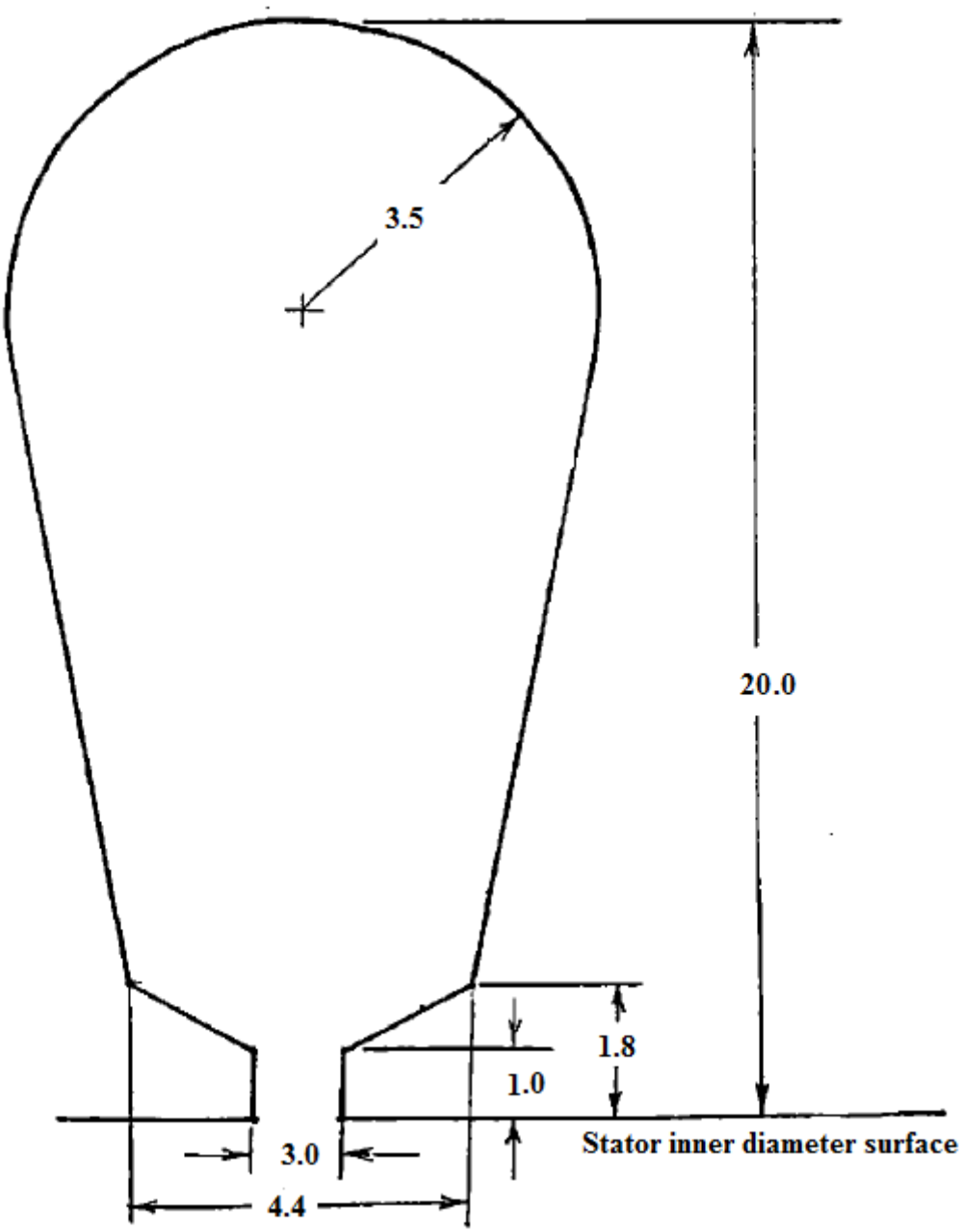

- Dimensions are in millimeters.

II. Power transformers specifications:

Step up transformer:

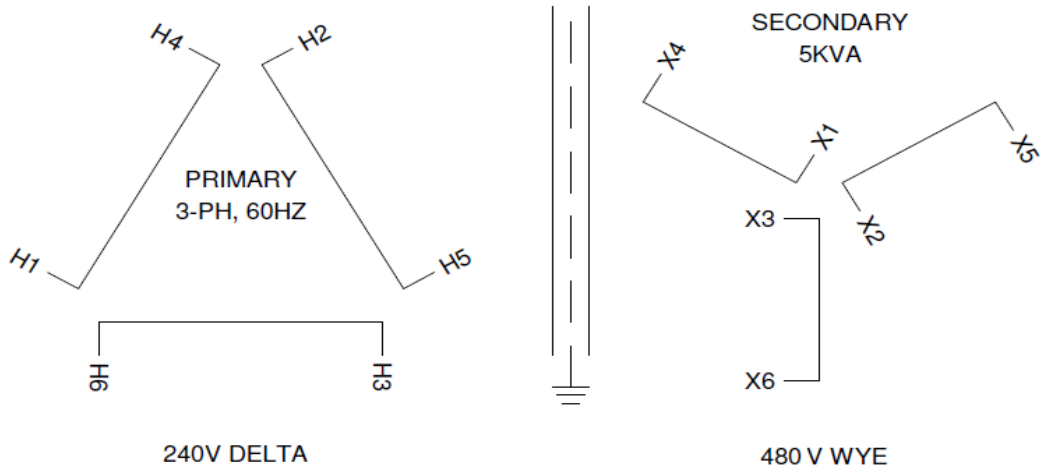

3∅ Isolation Transformer 60HZ

Input: 240 Volts Delta

Output: 480/277 Volts Wye with Accessible Neutral with Static Shield

Terminations: 12” Flexible Leads

Temperature Class: 200° C UL Recognized Insulation System

Approximate Size: 8.13” H x 11.00” W x 6.63” D

Mounting Dimensions: 5.00” W x 5.13” D

Primary resistance: 0.333 Ω

Secondary resistance: 0.576 Ω

Leakage Inductance: 0.462 mH

Step down transformer:

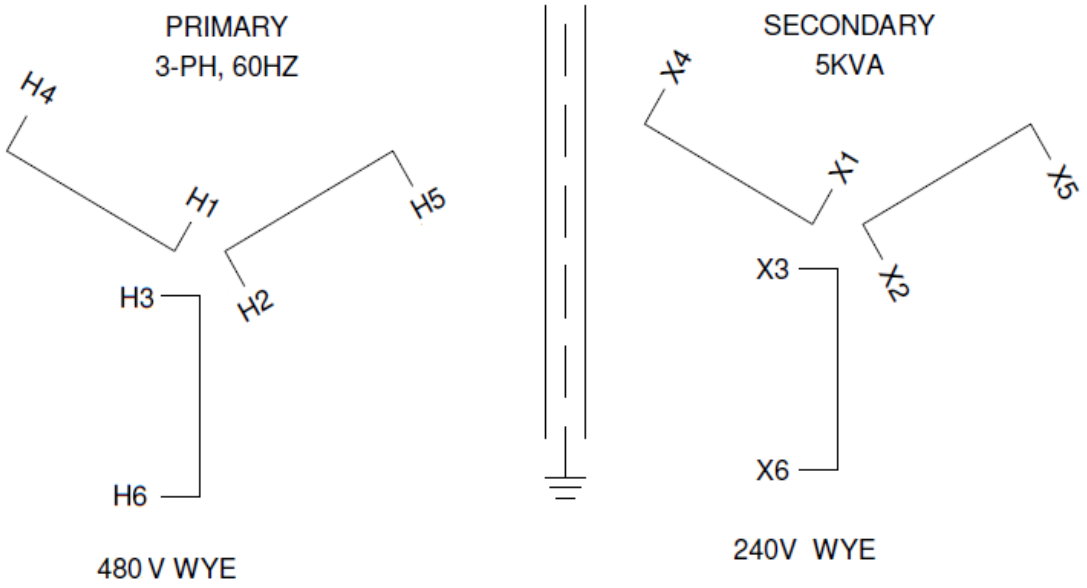

3∅ Isolation Transformer 60HZ

Input: 480/277 Volts Wye with Accessible Neutral

Output: 240/139 Volts Wye with Accessible Neutral with Static Shield

Terminations: 12” Flexible Leads

Temperature Class: 200° C UL Recognized Insulation System

Approximate Size: 8.13” H x 11.00” W x 6.75” D

Mounting Dimensions: 5.00” W x 5.25” D

Primary resistance: 0.474 Ω

Secondary resistance: 0.143 Ω

Leakage Inductance: 0.624 mH